UNIVERSITY OF OKLAHOMA

GRADUATE COLLEGE

# A NEW PARADIGM FOR PROACTIVE SELF-HEALING IN FUTURE SELF-ORGANIZING MOBILE CELLULAR NETWORKS

A DISSERTATION

SUBMITTED TO THE GRADUATE FACULTY

in partial fulfillment of the requirements for the

Degree of

DOCTOR OF PHILOSOPHY

BY

DHRUV SHARMA
Norman, Oklahoma
2019

A NEW PARADIGM FOR PROACTIVE SELF-HEALING IN FUTURE SELF-ORGANIZING MOBILE CELLULAR NETWORKS

A THESIS APPROVED FOR THE
SCHOOL OF ELECTRICAL AND COMPUTER ENGINEERING

BY

Dr. John N. Jiang, Chair

Dr. Theodore Trafalis, Outside Member

Dr. Paul S. Moses, Member

Dr. Ronald Barnes, Member

Dr. Krishnaiyan Thulasiraman, Member

# Acknowledgments

In the name of Allah, the most merciful, the most beneficent.

I thank Almighty Allah for his blessings upon me, for letting me pursue my passion and for surrounding me with people who care about me and who help get the best out of me. This dissertation would not have been possible without His mercy and the sacrifices my family made for me and the support they gave. I am here because my mother sacrificed her own safety and comfort to allow me to pursue my passion. I am here because my wife gave up her life in California to move to Oklahoma for me. I am here because my sisters Madiha, Urooj and Sarah never let me get away without making me finish my schoolwork, always showed me the utmost affection, always shared a laugh with me and always gave me an outlet for venting. And most importantly, I am here because my father, the first Ph.D. I ever knew, gave up his health and comfort to help me achieve my potential.

I would like to thank my advisor, Dr. Ali Imran who gave me the opportunity to come to the University of Oklahoma to pursue my passion. He guided me all these years through my work and helped me develop my research and writing skills while also imparting in me the strong work ethic required to write a doctoral dissertation. His support and leadership has been the primary contributing factor in my becoming the researcher that I am today. I would also like to thank my committee members Dr. Thordur Runolfsson, Dr. Timothy Ford, Dr. Samuel Cheng and Dr. Cliff Chan whose advice was instrumental in my completing my doctoral studies. I would also like to extend my thanks to all of my lab members, past and present with special mention for Dr. Hasan Farooq, who helped me understand and work through my research problems while also creating a great environment for research and collaboration.

Finally, this dissertation is dedicated to everyone who is currently working on completing or has in the past completed their doctoral studies.

# Table of Contents

## List of Figures

# List of Tables

# Abstract

Mobile cellular network operators spend nearly a quarter of their revenue on network management and maintenance. Remarkably, a significant proportion of that budget is spent on resolving outages that degrade or disrupt cellular services. Historically, operators have mainly relied on human expertise to identify, diagnose and resolve such outages while also compensating for them in the short-term. However, with ambitious quality of experience expectations from 5th generation and beyond mobile cellular networks spurring research towards technologies such as ultra-dense heterogeneous networks and millimeter wave spectrum utilization, discovering and compensating coverage lapses in future networks will be a major challenge. Numerous studies have explored heuristic, analytical and machine learning-based solutions to autonomously detect, diagnose and compensate cell outages in legacy mobile cellular networks, a branch of research known as self-healing. This dissertation focuses on self-healing techniques for future mobile cellular networks, with special focus on outage detection and avoidance components of self-healing.

Network outages can be classified into two primary types: 1) *full* and 2) *partial*. Full outages result from failed soft or hard components of network entities while partial outages are generally a consequence of parametric misconfiguration. To this end, chapter 2 of this dissertation is dedicated to a detailed survey of research on detecting, diagnosing and compensating full outages as well as a detailed analysis of studies on proactive outage avoidance schemes and their challenges.

A key observation from the analysis of the state-of-the-art outage detection techniques is their dependence on full network coverage data, susceptibility to noise or randomness in the data and inability to characterize outages in both spacial domain and temporal domain. To overcome these limitations, chapters 3 and 4 present two unique and novel outage detection techniques. Chapter 3 presents an outage detection technique based on entropy field decomposition which combines information field theory and entropy

spectrum pathways theory and is robust to noise variance. Chapter 4 presents a deep learning neural network algorithm which is robust to data sparsity and compares it with entropy field decomposition and other state-of-the-art machine learning-based outage detection algorithms including support vector machines, K-means clustering, independent component analysis and deep auto-encoders.

Based on the insights obtained regarding the impact of partial outages, chapter 5 presents a complete framework for 5th generation and beyond mobile cellular networks that is designed to avoid partial outages caused by parametric misconfiguration. The power of the proposed framework is demonstrated by leveraging it to design a solution that tackles one of the most common problems associated with ultra-dense heterogeneous networks, namely imbalanced load among small and macro cells, and poor resource utilization as a consequence. The optimization problem is formulated as a function of two hard parameters namely antenna tilt and transmit power, and a soft parameter, cell individual offset, that affect the coverage, capacity and load directly. The resulting solution is a combination of the otherwise conflicting coverage and capacity optimization and load balancing self-organizing network functions.

# CHAPTER 1

## Introduction

# CHAPTER 2

## Literature Survey of Self-Healing Techniques

### *2.0.1 Summary and Insights*

A review of techniques for outage compensation in self-healing mobile cellular networks suggests four basic metrics are targeted in the event of an outage. These are: 1) *coverage area*, 2) *SINR*, 3) *cell capacity/load*, and 4) *spectral efficiency*. The optimization of these metrics is suitable for legacy mobile cellular networks. However, future 5th generation cellular networks will be more complex and quality of experience-focused. This means that outage compensation solutions of the future will have to focus on more than just these basic metrics. Some examples of potential metrics which will be important in 5th generation cellular networks include energy efficiency, service latency, and throughput fluctuations [**?** ].

Ensuring service latency by itself will be a major challenge for network operators in 5th generation mobile cellular networks due to the complex nature of these networks. A review of outage compensation studies suggests that the most popular techniques for outage compensation are convex and non-convex optimization. Both of these techniques are computationally tedious and require far more time than would be acceptable in a 5th generation network. Furthermore, as these networks become denser, and the number of tunable parameters increases, the optimization process will get slower and more complex. Thus, one of the foremost challenges for future outage compensation solutions will be to reduce the time it takes for an optimization algorithm to reach its solution. Exploring trade-offs between different metrics for outage compensation in 5th generation networks will also be an interesting future area of study.

Another important research area in terms of outage compensation solutions is their integration into the larger SON framework. The SON framework includes technique for self-optimization which oftentimes use the same parameters as outage compensation techniques. For example, coverage and capacity optimization solutions use transmit powers, antenna tilts and beam-forming parameters which are also key for outage compensation techniques, as evidenced by the review of studies above. To avoid this issue, network operators will need to incorporate a self-coordination entity to resolve such conflicts. Additionally, coordination will be important to avoid the triggering of self-optimization as a result of some outage compensation action. For example, changing the azimuth of a cell to provide coverage to subscribers of a cell affected by a full outage might trigger coverage and capacity optimization in a neighboring cell. This could, in turn, trigger a cascade of changes in neighboring cells. While some studies have proposed the use of exclusion zones to reduce the impact of outage compensation on other cells [? ], this area needs further research.

Finally, like existing outage detection and outage diagnosis techniques, outage compensation techniques do not incorporate technologies such as massive multi-input multi-output antennas and millimeter spectrum utilization. To enable self-healing in 5th generation networks, more solutions must be explored which focus on these technologies, making this a key area of research.

## 2.1 Challenges and Future Prospects in Self-healing for 5G and beyond

In order for future 5G mobile cellular networks to achieve the desired gains laid out by the research and standardization community [? ], SON solutions must play a far greater role than ever before [? ]. This means that future mobile cellular networks must be intelligent, proactive, knowledge-rich and interactive at the same time. To achieve this goal, researchers must develop solutions which enable the network to achieve self-reliance, and harness the power of vast quantities of data generated by the users and network nodes to empower such solutions. However, Self-healing in future mobile cellular networks must cope with several research challenges which have been discussed below.

***Challenge 1: Coping with increased outages due to increased network density***

Network densification, driven by the need to meet capacity and data rate requirements of 5G mobile cellular networks, means that future mobile cellular networks will have to handle far more network nodes than before. Higher cell densities coupled with technologies such as millimeter wave spectrum utilization, and more configurable parameters will result in frequent network outages driven by both parametric misconfigurations and routine equipment failures as demonstrated in Figs. **??** and **??**.

***Possible Solution and Future Direction***

A number of research areas have been highlighted in recent studies that can aid in dealing with network outages quickly and efficiently, especially in the context of dense and ultra-dense HetNets. One such approach is the control-data separation architecture (CDSA) [? ] where the control functionality lies with macro cells while data transmission is handled by small cells. This adds redundancy to the network architecture. For example, in the event of a small cell failure, the macro cell can handle both control and data transmissions to the affected users.

Furthermore, with the development of UAV technology for enabling 5G mobile cellular networks, UAV based outage compensation techniques, such as the one presented in [? ], can become ubiquitous. Additionally, decreasing cost of small cell deployment will mean network densification itself can be used to create redundancies within the network such that the UE-to-cell ratio becomes less than 1. This will mean that in the event of a small cell failure, there will be additional small cells ready to serve the users without effecting their quality of experience. Network densification will play an especially significant role in the context of millimeter wave cells where coverage will be limited to line of sight links and outages due to link obstruction will be frequent.

***Challenge 2: Coping with sparsity of data due to smaller number of users per cell***

With network densification, another challenge arises in the form of data sparsity due to fewer users per cell. This will make full outage detection and partial outage detection extremely difficult since there will not be enough measurements to accurately distinguish between cell edge users and outage scenarios. Moreover, even though the expected throughput per user will increase, decreasing user density per cell will mean fewer users will consume more data, hence data sparsity will stay an issue for Self-healing in 5G mobile cellular networks.

***Possible Solution and Research Direction***

As was shown in section 2.2, the overwhelming majority of full outage detection and partial outage detection solutions relied on machine learning techniques. However, unlike analytical or heuristic techniques, learning based algorithms are overwhelmingly dependent on data from the network, which can be sparse especially in the case of ultra-dense small cell deployment. To improve the accuracy of learning based outage detection solutions and to counter data sparsity in future mobile cellular networks, measurement prediction techniques can be used. Predictive techniques such as Grey prediction model [? ], and smoothing techniques such as Witten-Bell smoothing [? ] and Good-Turing smoothing [? ] can be used to remove knowledge gaps in the measurement data.

***Challenge 3: Meeting 5G latency requirements in self-healing***

5G mobile cellular networks are expected to have end-to-end data latency of 1 ms. This means that any Self-healing solution deployed in the network must be able to detect, diagnose and compensate any outage in far less time than state-of-the-art solutions.

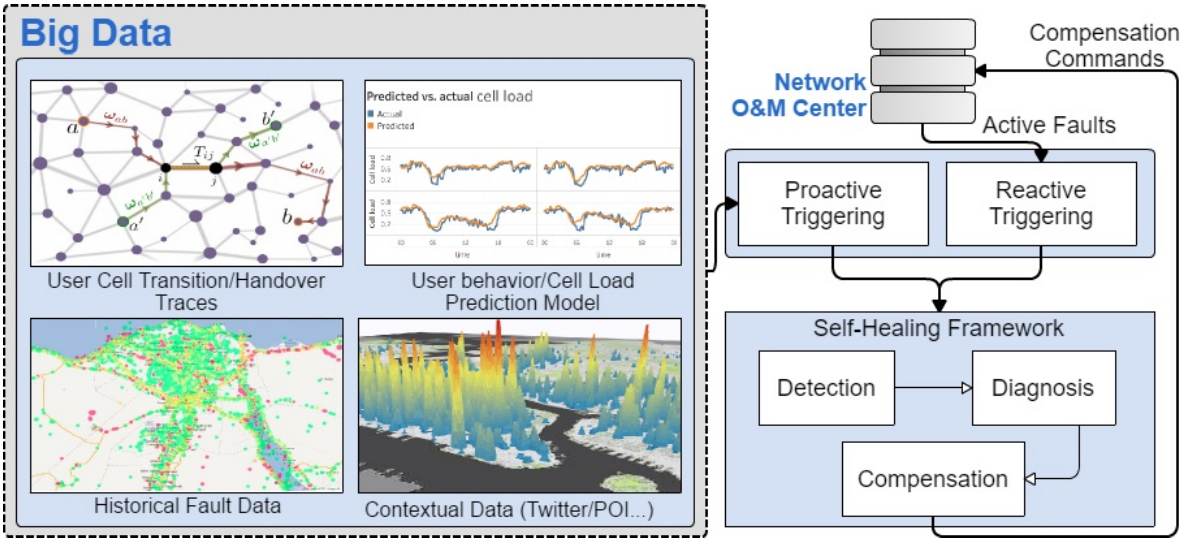


**Fig. 2.1:** Proactive Self-Healing Framework for Future Cellular Networks

***Possible Solution and Research Direction***

While solutions to proactively avoid outages due to parametric misconfiguration have been discussed extensively in section 2.5, future self-healing solutions must be fully proactive in nature. This implies that the self-healing framework will predict when and where an outage might occur with some probability, and execute changes in neighboring cells proactively. Despite the seemingly random nature of outages, especially full outages, outage prediction is possible and has been demonstrated by **?** ] who have used different machine learning techniques such as neural networks, NBC and SVM to predict the next fault from real network data. Similarly, **?** ] have predicted fault occurrences by collecting the past data and calculating maximum likelihood of next fault location using Bayesian Network prediction models.

All of the above-mentioned techniques rely on exploitation of big data [**?** ] to identify key patterns in cell and user performance data and associating the information with previous outage information and data. This will allow the proactive self-healing algorithms to identify changes in network performance that lead to a failure or an outage. Fig. 2.1 illustrates the concept of exploiting big data resources for prediction of faults in a future mobile cellular network. The definition of big data in the context of Self-healing framework includes historical fault data, user transition and handover data, network traffic and cell load data, and contextual data mined from sources such as social media. A more comprehensive solution for proactive outage prevention in also discussed in chapter 5 of this dissertation.

#### *Challenge 4: Meeting quality of experience requirements in self-healing*

The combination of requirements for 5G mobile cellular networks including low latency, high capacity, high throughput and low energy consumption means 5G networks will be user quality of experience centric compared to legacy networks which were user quality of service centric. This implies that meeting user quality of experience requirements will be the utmost priority in future mobile cellular networks, even in the event of an outage. Given that outages due to failures and parameter misconfigurations are likely to increase, meeting user quality of experience will be a key challenge for Self-healing solutions.

#### *Possible Solution and Research Direction*

The solution to meeting user quality of experience requirements despite outages is to deploy intelligence-rich proactive Self-healing framework such as the one shown in Fig. 2.1. The user-centricity of the framework will be driven by spatio-temporal user activity models. These include user mobility models derived from user transition data in the form of MDT reports [? ] along with user location information which can easily be harvested from the positioning sensors inside modern cell phones. Additionally, user behavior load prediction models can be generated using machine learning techniques shown in Fig. 2.2 while contextual data from social media sources such as Twitter and Facebook can be mapped to network topology which would help to identify potential traffic hotspots and failures. Historical fault data collection can be done by setting up databases that would include network failure records as well the KPI data immediately

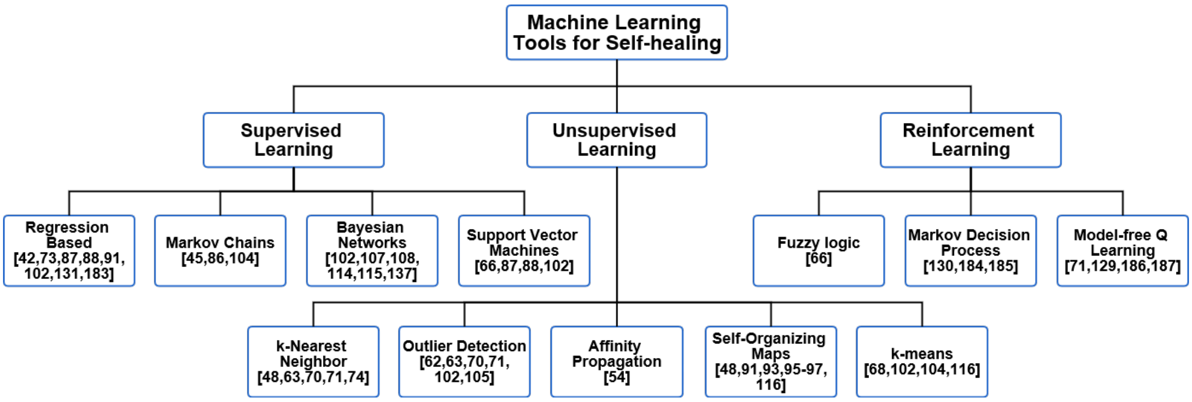


**Fig. 2.2:** Machine Learning Tools to Enable Proactive Self-Healing Framework for Future Cellular Networks

preceding the failure. All this information will be fed to the proactive fault prediction algorithms which would sit alongside a reactive Self-healing triggering algorithm which monitors fault data from live network.

### *Challenge 5: Coping with bandwidth constraints for Self-healing*

Bandwidth constraints are one of the greatest limiting factors for mobile cellular network capacity. Limited bandwidth means extra capacity can only be added by adding more cells into the network. However, as discussed previously, network densification can lead to a rise in network outages itself. Furthermore, bandwidth limitation becomes even more acute in the event of an outage when already strained neighboring cell resources can become completely choked causing partial outages.

### *Possible Solution and Research Direction*

While millimeter wave spectrum utilization has been promoted as the primary solution to bandwidth limitation [? ], it is still in exploratory phases. In addition, the limited range of millimeter wave cells does not make them the ideal candidates for outage compensation solutions unless they are deployed in very high densities. One possible solution to the issue of bandwidth limitation for Self-healing is to deploy spectrum sensing or cognitive radio solutions [? ? ]. Some outage compensation solutions based on spectrum splitting have been proposed in [? ? ? ? ] but these solutions propose to reserve HCs specifically for outage compensation. Given that mobile cellular networks are already facing bandwidth shortage, this approach may not be suitable especially when there are no outages. To avoid dedicating bandwidth for outage compensation, cognitive radio technologies can be explored to split the spectrum between HCs and normal bandwidth specifically in the event of an outage. Not only would this improve radio resource utilization under normal circumstances, it can also improve the service provided to outage-affected users by assigning them low interference resources.

## 2.2 Conclusion

Self-healing is potentially the most powerful SON component in terms of reducing mobile cellular network operational expenses, especially for future 5th generation and beyond networks. This chapter explores the full breadth of studies pertaining to self-healing techniques for mobile cellular networks. The studies on self-healing have been broken down by the area of self-healing framework they belong to in addition to their methodologies, topologies, design metrics and control mechanisms. Additionally, the survey includes the studies for avoiding outages due to SON function conflicts, also known as self-coordination which has been discussed under the umbrella of self-healing. This is done in order to consolidate the work done on outage prevention, detection, diagnosis and compensation under into a comprehensive survey on mobile cellular network outages.

In addition to the review of existing literature supporting self-healing for mobile cellular networks, this chapter presents and elaborates the challenges faced by self-healing functions in terms of future 5th generation and beyond mobile cellular networks while also presenting possible solutions and future research directions. This literature survey and the insights gained from it pave the way for solutions presented for outage detection and prevention in the proceeding chapters.

# CHAPTER 3

## Distance from networks perspective

The concept of graph distance, also known as geodesic distance, in simple connected graphs (introduced in [2]), is defined in [3] and further used in [4, 5, 6] and has two variants: the simple one considering only the number of edges, while the weighted one having a "length" for each edge. Distance $d_G(u, v)$ between two vertices $u$, $v$ of a graph $G$ is defined as the length of the shortest path between $u$ and $v$ in $G$. A path in a graph is a sequence of distinct vertices, such that adjacent vertices in the sequence are adjacent in the graph. For an unweighted graph, the length of a path is the number of edges on the path. For an (edge) weighted graph, the length of a path is the sum of the weights of the edges on the path. The distance function is a metric on the vertex set of a (weighted) graph $G$. In particular, it satisfies the triangle inequality:

$$d_G(u, v) \leq d_G(u, w) + d_G(w, v)$$

for all vertices $u$, $v$, $w$ of $G$. This follows from the fact that, if we want to get from $u$ to $v$, then one possibility is to go via vertex $w$.

The average distance of a graph $G = (V, E)$ of order $n$, denoted by $\mu(G)$, is the expected distance between a randomly chosen pair of distinct vertices given by

$$\mu(G) = \frac{1}{\binom{n}{2}} \sum_{u,v \subset V} d(u, v) \tag{3.1}$$

Further, considering finite directed graph $G$ with a directed edge $e$ having an associated length $w(e)$, the authors in [7] consider the measure of distance between two vertices $v_i$ and $v_j$ defined by (3.2).

$$d_{ij} = \min_{P(v_i, v_j)} w(P(v_i, v_j)) \tag{3.2}$$

where $P(v_i, v_j)$ ranges over all directed paths from $v_i$ to $v_j$ and $w(P(v_i, v_j))$ represents the sum of all edge-lengths in $P(v_i, v_j)$. This is while given the condition that the graph $G$ is strongly connected or $d_{i,j}$ always exists where $d_{i,j}$ is the $(i, j)th$ entry of the distance matrix $D(G)$ of $G$.

Considering strongly connected graph $G$ which is divided into various blocks $G_i$. The authors introduce a relation in (3.3) between the ratio of determinant and cofactors of graph $G$ and sum of corresponding determinants and sum of cofactors of the blocks of graph $G$. This is given as

$$\frac{detD(G)}{cofD(G)} = \sum_i \frac{detD(G_i)}{cofD(G_i)} \tag{3.3}$$

where $detD(G)$ and $detD(G_i)$ are the determinants of graph $G$ and block $G_i$ respectively while $cofD(G)$ and $cofD(G_i)$ represent the respective cofactors of graph $G$ and block $G_i$ of the graph.

### 3.1 Network Perspective

The resistance or Kirchoff Index, because of its structural meaning, has become a useful tool to analyze structural properties of graphs, or more generally of networks. In this context, a network is a connected graph in which each edge has been assigned a positive value, named the conductance of the edge. In contrast with the standard geodesic distance, defined as the length of the shortest path between vertices, the resistance distance takes into account all paths between vertices. The high sensibility of this metric with respect to small perturbations, makes it suitable to compare different network structures.

The identification of effective resistance as distances is done in [8]. The resistance distance $R(G)$, of a connected undirected graph $G = (V, E)$ with vertex set $V = 1, 2, \cdots, N$ and edge set $E$, was defined by Klein *et.al.* [8] as

$$R(G) = \sum_{i<j} R_{ij} \tag{3.4}$$

where $R_{ij}$ is the effective resistance between vertices $i$ and $j$ as computed with Ohm's law when all the edges of $G$ are considered to be unit resistors. The quantity $R_{ij}$ is shown in [8] to be a distance function on the set of vertices, and it is introduced together with the index $R(G)$ as an alternative to the usual graph theoretical distance. The indexing is so done that the resistance distance can be compared with that of conventional graphical distance.

The properties of resistance distance are discussed in [9] and further [10, 11, 12] present the applications of resistance distance in a network along with various indices such as Kirchoff index and wiener index.

### 3.2 Topological Perspective

#### *3.2.1 Centrality measure-based Index*

The authors in [13] builds the resistor networks, at each node placing a $1\Omega$ resistor and representing each link by a $1\Omega$ resistor. For each network, the resistance matrix is calculated, which is essentially equivalent to the admittance matrix for an equivalent electrical network. The resistance matrix R, defines a relationship between voltages and currents, as shown in eq. below.

$$\Delta V = R\Delta I \tag{3.5}$$

From this, the ratio of different elements in $R$ matrix can be calculated and assessed. The ratio can be defined as

$$S_{kl} = \frac{R_{kl}}{R_{kk}} \tag{3.6}$$

The elements of $S$, describe the extent to which a state change at location $k$ will affect a similar change at location $l$. Essentially this matrix tells the extent to which information flowing through the system will propagate through each network, or conversely, the extent to which information can be contained within a small area.

The weighted degree distributions along the topology of a network is discussed in [14] where the weights are based on the physical capacity constraints of the paths for a system. The degree distrbution is a centrality measure used in various domains ranging from nonlinear science, mechanics, medicine, social networks, engineering etc. [15, 16].

### *3.2.2 Connectivity Distance-based Index*

While electrical distance does not perfectly represent all of the ways in which components in a network connect, it is a useful starting point for structural analysis. There are numerous variant measures of electrical distance, but one of the simplest is the absolute value of the inverse of the system admittance matrix as described in [17] and shown below.

$$E = |Y^{-1}| \tag{3.7}$$

This electrical distance matrix, $E$ with elements $e_{ab}$, gives the a relation between voltage and current changes for every node pair. $e_{ab}$ is used to define the measure of connectivity distance for each node a.

$$e_a = \sum_{b=1;b\neq a}^{n} \frac{e_{ab}}{n-1} \tag{3.8}$$

Given the electrical distance matrix $E$, it is possible to rank nodes by the amount of load/demand that is within a given electrical distance threshold. Such a measure of distance to load enables additional insight to the electrical network structure. A similar measure has been discussed in [13] while the concept of electrical distance has been used in [18].

## 3.3 Summary - Distance from Networks Perspective

The representation of distance from a networks perspective provides a unique insight on the sensitivity of different structure-based variables. The distance as seen from a networks perspective has been broadly divided into categories defining the proximity of a bus on the basis of topology of the network and on the basis of actual resistance distance.

The resistance distance is based on the electrical network theory, wherein a fixed resistor is imagined on each edge connecting the nodes. The resistance function is defined as a distance function. On the other hand, from a topological perspective, the aim is to simplify the network to demonstrate the structure of the network. The ratio matrix adds an information regarding the validity of state change across the network. The connectivity distance is possibly the simplest measure of electrical distance based on the admittance matrix of the network.

The distances from networks and topological perspective are studied and various indices defining the measurements are mentioned. From the networks perspective, [8] identifies the distance as effective resistance as shown in (3.4) which is calculated using Ohm's law where resistance can be defined as a sensitivity parameter. Further, from a topological perspective, authors in [13], defines the resistance matrix in (3.5) and the ratio in (3.6). Finally in [17], the elements $e_{ab}$ gives the sensitivity between current and voltage changes in (3.8). Hence it can be seen that the distance described by various methods is actually the sensitivity depending on different parameter changes in the network.

### 3.4 Conclusion

In this chapter, several key issues present in the state-of-the-art coverage hole and outage detection algorithms have been presented. These issues include: 1) sensitivity to shadowing, 2) considering instantaneous spatial network coverage profile only, and 3) making assumptions regarding data and noise distributions. To overcome these limitations, a novel entropy field decomposition based solution has been proposed here which detects outages and coverage holes in spatio-temporal coverage data. The results presented in this chapter compare the efficacy of the proposed entropy field decomposi-

**Table 3.1:** Distance from a Networks Perspective

| | | Topological Perspective | |
|---|---|---|---|
| | Network Resistance Perspective | Centrality measure-based Index | Connectivity Distance-based Index |
| Measure/Index | Effective resistance or Kirchoff Index | Resistance matrix | System Admittance matrix |
| Equation | $R(G) = \sum_{i<j} R_{ij}$ | $S_{kl} = \frac{R_{kl}}{R_{kk}}$ | $e_a = \sum_{b=1;b\neq a}^{n} \frac{e_{ab}}{n-1}$ |
| Similarities | 1. Gives the sensitivity index of a network<br>2. All are based on the equivalent network impedance | | |
| Differences | Takes into account all the paths between vertices. | Defines the effective proximity of a state change across the network | Retains the links representing strong electrical connections irrespective of direct physical connection |
| Applications | Simplifies the network by "multiple-route distance diminishment" feature | Gives a new dimension to scale-free networks and defines the effective boundaries of any state change | Used in creating synthetic electrical network topologies |

tion based outage detection method with the state-of-the-art outage detection methods including independent component analysis and k-means clustering in a dense urban mmWave-small cell UDHN over a range of shadowing values. Results show that proposed entropy filed decomposition based solution is a powerful tool in combating the effects of shadowing on coverage hole and outage detection while also demonstrating its efficiency at extracting spatio-temporal information flows from coverage data. However, entropy field decomposition is a computationally complex solution with exponential computation time with respect to input coverage data. Therefore, for practical implementation, a distributed execution where the network is divided into small spatial units is advisable.

# CHAPTER 4

## Distance from power systems perspective

It is a well-known empirical evidence that electric power grids are inherently prone to frequent disturbances of different sizes. In [19], it follows a different approach based on the development of the science of complex networks i.e. the details of the electromagnetic processes were neglected and focused only on the topological properties of the grid. The aim was to demonstrate that the structure of an electric power grid highlights important information on the vulnerability of the system. However in order to get a more accurate measure with the changing system dynamics, the concept of distance is discussed from a power systems perspective.

### 4.1 Electro-mechanical Perspective

With the expansion and heavy interconnections, power systems can no longer be studied in isolation. The concept of electro-mechanical distance (EMD) into area division of dynamic equivalence for transient stability in power systems was introduced. In order to reduce the complex analysis and computation, the precise mathematical models are adopted within the studying system, but for the external systems, each coherent sub-system is subjected to dynamic equivalence which simplifies it into small quantities of aggregate generators. EMD is a concept of evaluating the electro-mechanical disturbance propagation between generators.

#### *4.1.1 Reflection Distance-based Index*

The definitions of subsystems within the interconnected network based on electrical equivalencing and electro-mechanical equivalencing was introduced in 1971 by J.M. Undrill *et.al.* [20]. However the concept of EMD was introduced in 1973 by S.T.Y. Lee *et.al.* [21] and later discussed by Podmore [22] which suggested a method to identify coherent groups without conducting a transient stability study. The study used the concept of a *distance measure* which could be a means of assessing the impacts of generators. It is defined in two ways: from electrical perspective and from electro-mechanical perspective. Electrical perspective gives the simplest distance measure which is the transfer admittance between generators and describes how closely coupled two generators are electrically close to each other. While the admittance based distance is a purely electrical distance, the reflection distance is designed to measure the dynamical effect of a generator on the stability of inner circle generators.

The reflection distance of a generator $k$ which is in the set $\Omega$ measured with respect to the inner circle $\phi$ is defined as follows.

$$R_d(k) = \max_{f \in \phi} \left\{ \max_{i \in \phi} \frac{\Delta P_{ri}}{M_i} \right\}, \qquad k \in \Omega \tag{4.1}$$

where

$$\Delta P_{ri} = \frac{\partial P_{ik}}{\partial \delta_k} \Delta \delta_k \tag{4.2}$$

$\Delta P_{ri}$ in (4.2) is the change in electrical power of a generator $i$ owing to a small change in the angle of generator $k$. Also $R_d(k)$ in (4.1) can be defined as the inverse distance in the sense that the bigger it is, the closer is that generator to the inner circle. $\phi$ is the set of inner circle generators, and $\Omega$ is the set of all generators outside the inner circle. In (4.2), $\Delta\delta_k$ is caused by a fault at one of the inner circle generators for a duration $t_c$ seconds and is given by

$$\Delta \delta_k \approx \frac{1}{2} a_k t_c^2 \tag{4.3}$$

where, $a_k$ is the acceleration of generator $k$ at the instant of fault, however it does not change much during the short duration of fault.

Since the reflection distance measure can be interpreted as the synchronizing force between a generator close to a fault and the generator whose distance is to be measured. Applying this to generators existing in the network, a relative distance can be measured with respect to the location of fault. Generators showing the same response are coherent generators and hence can be grouped together.

### *4.1.2 Coherency-based Index*

The coherency-based technique is introduced in [23] which is based on the property of equal acceleration for coherent machines. The concept of coherency is discussed in various studies such as [22, 24, 25] which focuses on the dynamic equivalence of a network. In an operating condition, two generators are said to be coherent if their angular difference is constant within a certain tolerance limit, $\epsilon$, over a certain time interval. For the two machines $i$ and $j$,

$$|\delta_{ij} - \delta_{ij}^{s}| \leq \epsilon$$

Then the coherency factor can be defined as

$$CF = \frac{max|\delta_{ij}|}{|\delta_{ij}^{s}|} \tag{4.4}$$

For a machine $i$, the dynamic equation (4.5) as

$$M_i \Delta\ddot{\delta}_i = \Delta P_{m,i} - \Delta P_{G,i} \tag{4.5}$$

After simplifying, the relation is of the form

$$[M][\Delta\ddot{\delta}] = [M]^{-1}[Y][\Delta\delta] \tag{4.6}$$

Here $[M]^{-1}[Y]$ is the jacobian matrix $J$. This method compares only the elements of the Jacobian matrix to identify the coherent group. A normalized quantity $\beta$ is defined such that

$$\beta = \frac{|j_{ij} - j_{ji}|}{max(j_{ij}, j_{ji})} \tag{4.7}$$

the term $|j_{ij} - j_{ji}|$ can be taken as a measure to estimate the relative variation between $\Delta\delta_i$ and $\Delta\delta_j$. When the moments of inertias $M_i$ and $M_y$ are equal, then $\beta = 0$, which means that the machines are perfectly coherent.

### *4.1.3 Electro-mechanical distance-based Index*

The EMD between two machines is defined in [26] as a measure of the maximum angular movement between the machines during the transient period. A logical measure of the electromechanical interaction between a pair of machines during the transient period could be the synchronizing power flow or the maximum angular deviation. The EMD between the generator $i$ and the reference generator $n$ is defined as

$$d_{in} = \Big[\sum_{l=1}^{m}(p_{il}^2 + q_{il}^2) + \sum_{l=2m+1}^{2n-1} s_{il}^2\Big]^{1/2} \tag{4.8}$$

The elements $p_{il}$, $q_{il}$ and $s_{il}$ represent the amplitudes of the complex modes and the real modes, respectively in $\delta_{in}$. A measure (the Euclidean norm) of such amplitudes for all the modes is taken and defined as the EMD. Thus the EMD $d_{in}$ reflects the maximum angular excursion between the generator $i$ and the reference generator $n$. Similarly, the EMD between generators $i$ and $j$ is derived from the expression $(\Delta\delta_{in} - \Delta\delta_{jn})$ and is given by

$$d_{ij} = \Big[\sum_{l=1}^{m}[(p_{il} - p_{il})^2 + (q_{il} - q_{jl})^2] + \sum_{l=2m+1}^{2n-1}(s_{il} - s_{jl})^2\Big]^{1/2} \tag{4.9}$$

Based on $d_{ij}$, the coherent generators can be included in a single area depending on the threshold for that network such that the power system is decomposed into several regions. The distance measure under transient conditions is discussed in [21, 23, 27] under different scenarios and assumptions.

### *4.1.4 Composite EMD-based Index*

EMD is a concept of evaluating the electromechanical disturbance propagation between generators. Since EMD is relative index to evaluate the propagation of dynamic phenomenon associated with a given disturbance, its definition is also not completely the same. According to the basic definition of EMD, the concept of composite EMD was presented in [28, 29]. The application scope of EMD was also extended. It could not only deal with some emergent situations under some given operation conditions, but also the stability problems of a special emergent situation under different operation conditions and the degree of influencing the different parts of a power system. [30] highlights the following definitions of EMD and thus combine these to form composite EMD.

1 The absolute value of initial power angle acceleration ($ED_{1i}$).

2 The absolute value of initial acceleration power ($ED_{2i}$).

3 Transfer admittance before disturbance ($ED_{3i}$).

4 Inertia constant ($ED_{4i}$).

Combining the above mentioned definitions of EMD, we get EMD between buses $j$ and $i$ is

$$ED_{ij} = w\sqrt{2M_j/B_{ij}} \tag{4.10}$$

and similarly the EMD between buses $i$ and $j$ is

$$ED_{ji} = w\sqrt{2M_i/B_{ji}} \tag{4.11}$$

where $M_i$ is the inertia constant of the generator at bus $i$ and $B$ is the susceptance matrix which is symmetrical which gives $B_{ij} = B_{ji}$. For a real power system, it is difficult to confirm the direction of electromechanical disturbance propagation, so the algebraic average value of EMD between the generator buses $i$ and $j$ can be obtained as

$$ED_{ij}^{av} = ED_{ji}^{av} = \frac{w}{2}(ED_{ij} + ED_{ji}) \tag{4.12}$$

## 4.2 Voltage Interaction Perspective

A given power system can be separated into some non-overlapping voltage-control areas comprising coherent bus groups. A set of buses can be classified as a voltage-control area if they are sufficiently uncoupled electrically, from its neighboring areas. And the controllable reactive power in the area should be enough to master the voltage changes at the buses in the area.

As mentioned in [18] and later used in [31, 32, 33], electrical distance measures the voltage interactions between different buses of the system. With the usual hypothesis of the active-reactive decoupled system, the reactive model is written as:

$$[\Delta Q] = \left[\frac{\delta Q}{\delta V}\right][\Delta V] \tag{4.13}$$

or

$$[\Delta V] = \left[\frac{\delta V}{\delta Q}\right][\Delta Q] \tag{4.14}$$

where $\left[\frac{\delta Q}{\delta V}\right]$ is part of power flow Jacobian matrix and $\left[\frac{\delta V}{\delta Q}\right]$ is its inverse.

Electrical distance between bus $i$ and bus $j$ is defined as

$$D_{ij} = D_{ji} = -log(\alpha_{ij} \cdot \alpha_{ji}) \tag{4.15}$$

where $\alpha_{ij} = \frac{(\delta V_i/\delta Q_j)}{(\delta V_j/\delta Q_j)}$ represents normalized voltage attenuation on bus $i$ with respect to the perturbation at bus $j$. In practice, the matrix $\left[\frac{\delta V}{\delta Q}\right]$ can be approximated by the inverse of the system susceptance matrix $[B']$, which is with the rows and columns corresponding to $PV$ buses.

## 4.3 Steady State Perspective

### *4.3.1 Reactive Power support capability-based Index*

In [34], an index is proposed to estimate the reactive power support capabilities that load buses can obtain from generation units in a power system by using the reactive power capacities of generation units and the electrical distances between load buses and generation units. The electrical distances between loads and generation units can be derived based on reactive power equations. In a power system with $N_g$ generation units and $N_d$ loads, the reactive power at bus $i$ can be represented as

$$Q_i = V_i \sum_{j=1}^{N_g+N_d} V_j \Big[ G_{ij} sin(\delta_i - \delta_j) - B_{ij} cos(\delta_i - \delta_j) \Big]$$

$$i = 1, \ldots, N_g + N_d$$

where $V_i$ and $\delta_i$ are the voltage magnitude and angle of the $i^{th}$ bus respectively; $G_{ij}$ is the real part of the negative of the branch admittance between buses $i$ and $j$; $G_{ii}$ is the sum of real parts of all branch admittances connected to the $i^{th}$ bus; $B_{ij}$ is the imaginary part of the negative of the branch admittance between buses $i$ and $j$; and $B_{ii}$ is the sum of imaginary parts of all branch admittances connected to the $i^{th}$ bus. Based on the equations of reactive power change at the generator and load buses can be represented as

$$\begin{bmatrix} \Delta Q_G \\ \Delta Q_D \end{bmatrix} = - \begin{bmatrix} B_{GG} & B_{GD} \\ B_{DG} & B_{DD} \end{bmatrix} \begin{bmatrix} \Delta V_G \\ \Delta V_D \end{bmatrix} \tag{4.16}$$

where $B_{GG}$, $B_{GD}$, $B_{DG}$ and $B_{DD}$ are the sub-matrices in the susceptance matrix, which is the imaginary part of the bus admittance matrix.

Therefore the electrical distances between loads and generation units can be presented as

$$\Delta Q_G = D \cdot \Delta Q_D \tag{4.17}$$

where,

$$D = B_{GD} B_{DD}^{-1} \tag{4.18}$$

where the elements $(i, j)$ of $D$ (i.e. $|d_{ij}|$) represents the electrical distance between the $j^{th}$ load and $i^{th}$ generation unit. The larger $|d_{ji}|$ means $j^{th}$ load and $i^{th}$ generation unit are electrically closer. Furthermore, $|d_{ij}|$ is also the reactive power distribution factor, which indicates the reactive power that $i^{th}$ generation unit distributes to the $j^{th}$ load when a unit of reactive power change occurs at the $j^{th}$ load. A larger $|d_{ij}|$ means that the $i^{th}$ generation unit distributes more reactive power to the $j^{th}$ load than the other generation units when a unit of reactive power change occurs at the $j^{th}$ load. Different techniques related to reactive power monitoring and calculations with respect to voltage stability criterion had been investigated in [35, 36, 37, 38].

### *4.3.2 Relative Electrical Distance-based Index*

The method presented by authors in [39] is used for allocating transmission transaction charges among users in transmission services for various combinations of power contracts. The method allocates the transaction charges over the participants/contracts based on the relative electrical distance i.e., the relative locations of load points with respect to the generator points in open access. The method is based on the fundamentals of the impact of transactions in a transmission system which are discussed in [40, 41, 42, 43].

The relative electrical distances (RED) is a representation of the relative locations of load nodes with respect to the generator nodes and is given by $[R_{LG}]$.

$$[R_{LG}] = 1 - abs\{[F_{LG}]\} \tag{4.19}$$

where

$$[F_{LG}] = -[Y_{LL}]^{-1}[Y_{LG}]$$

where, $Y_{LL}$ and $Y_{LG}$ are partitioned portions of network $Y$-bus matrix obtained from the equation given below.

$$\begin{bmatrix} I_G \\ I_L \end{bmatrix} = \begin{bmatrix} Y_{GG} & Y_{GL} \\ Y_{LG} & Y_{LL} \end{bmatrix} \begin{bmatrix} V_G \\ V_L \end{bmatrix} \tag{4.20}$$

The elements of $[F_{LG}]$ matrix are complex and its columns correspond to the generator bus numbers and rows correspond to the load bus numbers. This matrix gives the relation between load bus voltages and source bus voltages. It also gives information about the location of load nodes with respect to generator nodes that is termed as relative electrical distance between load nodes and generator nodes.

### *4.3.3 Generation Shift Factor-based Index*

When performing power market studies, the most accurate approach would be to model the transmission system using a full ac implementation, including the impacts of all germane contingencies. However, for a large network this can be computationally prohibitive for long-term market simulations. The use of DC power flow model reduces the computation drastically. In [44, 45, 46, 47], the authors use the concept of GSF in order to define the proximity of a bus to a tie-line. GSF is defined by the change in power flows on a line due to the change in the injection at a generator bus, and a corresponding withdrawal at slack generator. GSF is based on change in phase angles with respect to bus injections and change in line flows with respect to phase angles. Hence, GSFs can be considered as the impact of bus injections on tie-line flows. The DC load flow model in matrix form is given by

$$P = [B]\delta$$

where, $P$ is the power vector of net injection where each element represents the individual power injection. $[B]$ is the susceptance matrix and $\delta$ is the vector of phase angles of the respective buses.

GSF of tie-line $ab$ with respect to bus $i$ can be calculated using elements of inverse of susceptance matrix as shown in equation below.

$$g_{ab,i} = \frac{\bar{X}_{a,i} - \bar{X}_{b,i}}{x_{ab}} \quad (4.21)$$

where, $g_{ab,i}$ is the GSF of tie-line $ab$ with respect to bus $i$, $\bar{X}_{a,i}$ and $\bar{X}_{b,i}$ are the elements of inverse of susceptance matrix and $x_{ab}$ is the reactance of tie-line $ab$.

### 4.4 Electro-magnetic Transient Perspective

Electro-magnetic Transient Program (EMTP) refers to a group of advanced transient analysis techniques used in power system analysis. EMTP models are characterized based on the structure variables such as reactance, resistances, loads, generator constants, etc. during steady state which are obtainable values provided by the grid operator or common data reports in a power system. Additionally, the initial status for voltages and currents are steady state variables result from the power flow simulation. On the other hand, in the case of extreme and accurate EMTP models which need more than traditional parameters, reduced and equivalent representation illustrates the main electromagnetic behavior of a branch switching.

In the assessment of the time responses of electro-magnetic transients in single or multi-phase networks, Dommel in [48] formulated a method of solving networks by nodal admittance matrix which was pursued later in [49, 50, 51, 52]. The formulation is based on the method of characteristics for distributed parameters and the trapezoidal rule of integration for lumped parameters. The method of characteristics and the trapezoidal rule can easily be combined into a generalized algorithm capable of solving transients in any network with distributed as well as lumped parameters. Numerically this leads to the solution of a system of linear (nodal) equations in each time step.

Starting from initial condition at $t = 0$, the state of the system is found at $t = \Delta t, 2\Delta t, 3\Delta t, \ldots$ until the maximum time $t_{max}$ for the particular case has been reached.

While solving for the state at $t$, the previous states at $t-\Delta t, t-2\Delta t, \ldots$ are known. With a record of this past history, the equations of both methods can be represented by simple equivalent impedance networks. A nodal formulation of the problem is shown below from these networks.

A solution for transients is necessarily a step-by-step procedure that proceeds along the time axis with a variable or fixed step width $\Delta t$. Based on this, equivalent impedance networks are used to describe different elements in the system.

- ***Lossless Line:*** Considering a lossless line with inductance $L'$ and capacitance $C'$ per unit length. Then at a point $x$ along the line voltage and current are related by

$$-\frac{\partial e}{\partial x} = L'\left(\frac{\partial i}{\partial t}\right)$$
$$-\frac{\partial i}{\partial x} = C'\left(\frac{\partial e}{\partial t}\right)$$

Considering the voltage at node $m$ at time $t-\Delta t$ remains same as that at node

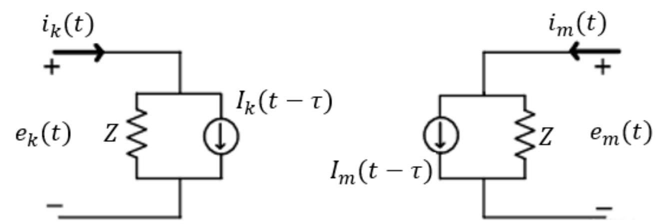


**Fig. 4.1:** Lossless line equivalent impedance network

$k$ at time $t$, the line can be seen as a two-port network. With equivalent current sources $I_k$ and $I_m$ which are known at state $t$ from the past history at time $t-\Delta t$,

$$I_k(t-\Delta t) = -(1/Z)e_m(t-\Delta t) - i_{m,k}(t-\Delta t) \tag{4.22}$$

$$I_m(t-\Delta t) = -(1/Z)e_k(t-\Delta t) - i_{k,m}(t-\Delta t) \tag{4.23}$$

Eq. (4.22) and (4.23) describes the corresponding equivalent impedance network. Topologically the terminals are not connected; the conditions at the other end are only seen indirectly and with a time delay $\Delta t$ through the equivalent current sources $I_k(t-\Delta t)$ and $I_m(t-\Delta t)$.

- ***Inductance:*** For the inductance $L$ of a branch $km$ and consider the equivalent current source $I_{k,m}$ is known for past history, which yields $I_{k,m}(t-\Delta t)$ between the nodes $k$ and $m$ given in (4.24).

$$I_{k,m}(t-\Delta t) = i_{k,m}(t-\Delta t) + (\Delta t/2L)(e_k(t-\Delta t) - e_m(t-\Delta t)) \tag{4.24}$$

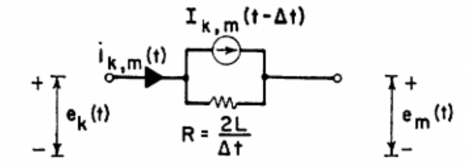


**Fig. 4.2:** Inductance equivalent impedance network

- ***Capacitance:*** Similar relation is derived for capacitance $C$ of branch $km$

$$I_{k,m}(t-\Delta t) = -i_{k,m}(t-\Delta t) - (2C/\Delta t)(e_k(t-\Delta t) - e_m(t-\Delta t)) \tag{4.25}$$

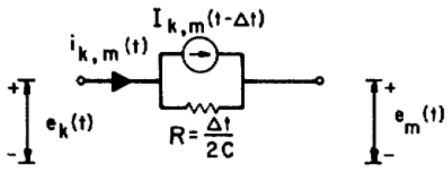


**Fig. 4.3:** Capacitance equivalent impedance network

- ***Resistance:*** For completeness the branch equation for the resistance is also added

$$i_{k,m}(t) = (1/R)(e_k(t) - e_m(t)) \tag{4.26}$$

- ***Nodal Equations:*** With all network elements replaced by equivalent impedance networks, it becomes very simple to establish the nodal equations for any arbitrary system. The result is a system of linear algebraic equations in (4.27) that describes the state of the system at time $t$.

$$[Y][e(t)] = [i(t)] - [I] \tag{4.27}$$

where, $[Y]$ is nodal conductance matrix, $[e(t)]$ is column vector of node voltages at time $t$, $[i(t)]$ is column vector of injected node currents at time $t$, $[I]$ column vector of known equivalent current sources.

The real symmetric conductance matrix $[Y]$ remains unchanged as long as $\Delta t$ remains unchanged. It is, therefore, preferable, to fix the time step width at $\Delta t$. The formation of $[Y]$ follows the rules for forming the nodal admittance matrix in steady-state analysis.

## 4.5 Modeling of load

Stable operation of a power system depends on the ability to continuously match the electrical output of generating units to the electrical load on the system. The modeling of loads is complicated because of composition of each load comprising large number of devices. It is a common practice to represent the composite load characteristics as seen from the bulk power delivery points [53]. The load models are traditionally classified into two major categories: static models and dynamic models.

### *4.5.1 Static Load Models*

A static load model represents the load characteristics as algebraic function of bus voltage magnitude and frequency at an instant [53]. The active and reactive power components can be of the load can be determined on the basis of initial operating conditions by the exponential model as shown in (4.28).

$$P = P_0(\bar{V})^a$$
$$Q = Q_0(\bar{V})^b \tag{4.28}$$
$$\bar{V} = \frac{V}{V_0}$$

where $P_0$, $Q_0$ and $V_0$ represents the initial operating values for each of the variable respectively. The parameters $a$ and $b$ represents whether the load model has constant power, constant current or constant impedance characteristics ranging 0, 1 or 2 respectively. For composite system loads, the voltage dependency is shown through a polynomial model mentioned in (4.29).

$$\begin{aligned} P &= P_0[p_1\bar{V}^2 + p_2\bar{V} + p_3] \\ Q &= Q_0[q_1\bar{V}^2 + q_2\bar{V} + q_3] \end{aligned} \tag{4.29}$$

This models is referred to as *ZIP* model since it is composed of constant impedance, constant current and constant power components.

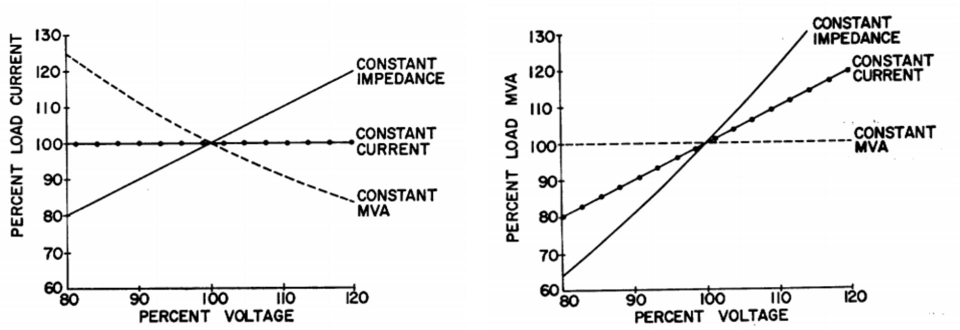


**(a)** Relationship between load current and bus voltage **(b)** Relationship between load MVA and bus voltage

**Fig. 4.4:** ZIP load models [1]

The model for frequency dependency of load characteristics is obtained by including the frequency component in the voltage dependent *ZIP* model and is shown in (4.30).

$$\begin{aligned} P &= P_0[p_1\bar{V}^2 + p_2\bar{V} + p_3](1 + K_{pf}\Delta f) \\ Q &= Q_0[q_1\bar{V}^2 + q_2\bar{V} + q_3](1 + K_{qf}\Delta f) \end{aligned} \tag{4.30}$$

where $\Delta f$ is the frequency deviation $f - f_0$. The bus frequency $f$ is usually not a state variable in the system model used for analysis, therefore it is evaluated by computing the time derivative of the bus voltage angle.

### *4.5.2 Dynamic Load Models*

The response of most composite loads to voltage and frequency changes is fast and the steady state of the response reaches very quickly. Hence the use of static models is justified for such cases. There are, however, many cases which accounts for the dynamics of load components especially the dynamics of motors which is a significant aspect of system loads. Induction motors form the majority of motor loads across the power system network. Since there is no field winding in the induction motor, the cage rotor is modeled by two coils in quadrature while the armature is modeled by $d$- and $q$-axis armature coil. Since it does not rotate at synchronous speed, the teo rotor equations include a rotational emf term proportional to the rotor slip speed $s\omega_s$. These equations are in the form given by (4.31).

$$\begin{aligned} v_d &= 0 = Ri_d + \dot{\Psi}_d - s\omega_s\Psi_q \\ v_q &= 0 = Ri_q + \dot{\Psi}_q + s\omega_s\Psi_d \end{aligned} \tag{4.31}$$

where slip $s = \frac{(\omega_s - \omega)}{\omega_s}$, $\Psi_d$ and $\Psi_q$ are the flux linkages.

### *4.5.3 Impact on Electrical Distance*

The response of nearly all loads to voltage changes can be represented by some combination of constant impedance, constant current, and constant power devices. It is also important to recognize that the total active power of the motor load depends not only on the system frequency, but also on the rate of the frequency change which is evaluated by computing the time derivative of the bus voltage angle. Large induction motor loads can cause relatively severe instability conditions. Contrary to the active power, a major portion of which is consumed by load as systems are so designed and operated, the reactive power characteristics depend not only on component characteristics, but also on the network parameters between major buses and end-use devices.

## 4.6 Modeling of FACTS devices

The typical problems encountered in large interconnected transmission systems are with respect to voltage control, reactive power control, steady state and dynamic stability as well as inter-area oscillations in an interconnected power system [54]. Apart from the steady-state considerations, a sudden change in real power demand in the power system can be observed due to rapid changes in reactive power and the corresponding voltage variations, caused by line switching, faults, load rejection, and various other disturbances. This rapid change in real power demand can cause some power generators to accelerate, and others to decelerate, from their steady-state synchronous speed resulting in transients in frequency and power angle which if gets worse can result in total loss of synchronism between the generators [55].

### *4.6.1 Static Var Systems*

Static var systems are applied by utilities in transmission applications for several purposes. The primary purpose is usually rapid control of voltage at weak points in a network. CIGRE defines a static var system (SVS) as a coordinated combination of a static var compensator (SVC) and switching capacitors and reactors [56, 57]. Components of SVS may include Thyristor-controlled reactors (TCRs), Thyristor-switched reactors (TSRs), Thyristor-switched capacitors (TSCs), Mechanically-switched capacitors (MSCs) or reactors (MSRs).

A typical SVS for transmission application is shown in Fig. 4.5. In the figure, the system is assumed to contain one TCR and two TSCs, along with a MSC. The TCR reactive power rating is typically slightly larger than the discrete TSC and MSC blocks

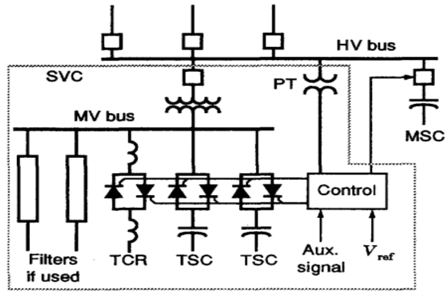


**Fig. 4.5:** Static Var System Structure

which allows continuous (smooth) control over the entire SVS rating. In the active control range, reactive power is varied to regulate voltage according to the required voltage regulation and the requirement of compensating reactive power in the system. At the capacitive limit, the SVC becomes a shunt capacitor while at the inductive limit, it behaves as a shunt reactor [58].

### *4.6.2 Variable Var Generation*

The dynamic reactive compensation in a system can be achieved by addition of supplementary reactive devices attached to the system. The major dynamic reactive requirements are in the areas of, (1) transient stability improvement, (2) power oscillation damping, (3) voltage support. The functional requirements of static var compensators, used for transient stability improvements, power oscillation damping and voltage support, can be stated simply as follows:

1 They must be able to stay in synchronism with the terminal voltage under all conditions, including major disturbances.

2 They must be able to regulate (transient stability improvement and voltage support), or control (power oscillation damping) rapidly the terminal voltage by generating reactive power for, or absorbing it from, the ac power system.

The performance and operating characteristics of current var generators are determined by the major thyristor-controlled devices such as the thyristor-controlled reactor and the thyristor-switched capacitor.

***Thyristor Controlled Reactor***

An elementary single-phase thyristor-controlled reactor (TCR) consists of a fixed reactor of inductance $L$, and a bi-directional thyristor switch. A typical TCR along with its associated waveform output is shown in Fig. 4.6.

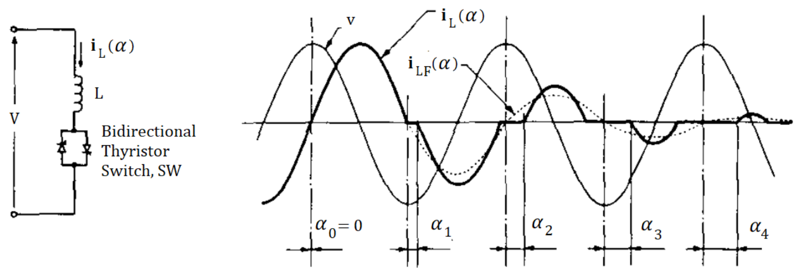


**Fig. 4.6:** Basic Thyristor Controlled Reactor and associated waveforms

The current in the reactor can be controlled and varied from maximum to zero by the function of switching thyristors using the method of firing delay angle control. This method of current control is illustrated in Fig. 4.6, where the reactor current $i_L(\alpha)$ and its fundamental component $i_{FL}(\alpha)$ are shown at various firing delay angles, $\alpha$. The amplitude $I_{FL}(\alpha)$ of the fundamental reactor current $i_{FL}(\alpha)$ can be expressed as a function of angle $\alpha$ and is shown in (4.32).

$$I_{FL}(\alpha) = \frac{V}{\omega L}\Big(1 - \frac{2}{\pi}\alpha - \frac{1}{\pi}\mathrm{sin}2\alpha\Big), \tag{4.32}$$

where, where $V$ i s the amplitude of the applied ac voltage, $L$ is the inductance of the thyristor-controlled reactor, and $\omega$ is the angular frequency of the applied voltage. The conduction angle control results in harmonics in the waveform which can be reduced by multi-pulse or multi-bank circuits [59].

### *Thyristor Switched Capacitor*

A single-phase thyristor-switched capacitor (TSC) is shown in Fig. 4.7. It consists of a capacitor, a bidirectional thyristor valve, and a relatively small surge current limiting reactor. This reactor is needed primarily to limit the surge current in the thyristor valve under abnormal operating conditions and may also be used to avoid resonances with the ac system impedance at particular frequencies.

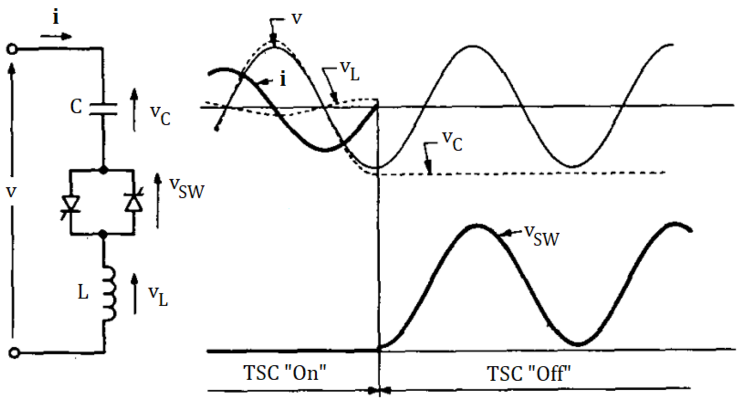


**Fig. 4.7:** Basic Thyristor Switched Capacitor and associated waveforms

Under steady-state conditions, when the thyristor valve is closed and the TSC branch is connected to a sinusoidal ac voltage source, $v = V\sin\omega t$, the current in the branch $i$ is given by

$$i_{ss} = V\frac{n^2}{n^2-1}\omega C\cos\omega t, \tag{4.33}$$

where,

$$n = \frac{1}{\sqrt{\omega^2 LC}} = \sqrt{\frac{X_C}{X_L}} \tag{4.34}$$

The TSC branch can be disconnected at any current zero by prior removal of the signal to the thyristor valve. At the current zero crossing, the capacitor voltage is at its peak value, $V = V_n^2/(n^2-1)$.The disconnected capacitor stays charged to this voltage and, consequently, the voltage across the non-conducting thyristor valve varies between zero and the peak-to-peak value of the applied ac voltage. This is illustrated in Fig. 4.7.

Further, removal and re-connection of the capacitor may induce some transients which can be minimized if the thyristor valve is turned on at those instants at which the voltage across the thyristor is zero.

### *4.6.3 Static Synchronous Compensator*

Static synchronous compensator (STATCOM) can be seen as a controllable reactive power, which can change voltage and current waveform of the inverter through power electronic means, and which also can improve the power quality [60]. STATCOM can be divided into two types of circuits namely: voltage-bridge circuit and current-bridge circuits. As shown in Fig. 4.8, the main circuit of STATCOM is composed of voltage-bridge circuit and the structure is composed of the following parts: the DC side capacitor, which plays a role in providing voltage support; voltage source inverter (VSC), which constitutes self-commutating solid-state electronic switching devices such as GTOs/IGBTs. It uses a pulse width modulation (PWM) technology to control the power electronic switching. The primary objective of STATCOM is to obtain a harmonic free and controllable three-phase AC output voltage waveforms at the point of common interaction (PCI) to regulate reactive current flow by generation and absorption of controllable reactive power by the solid-state switching algorithm .

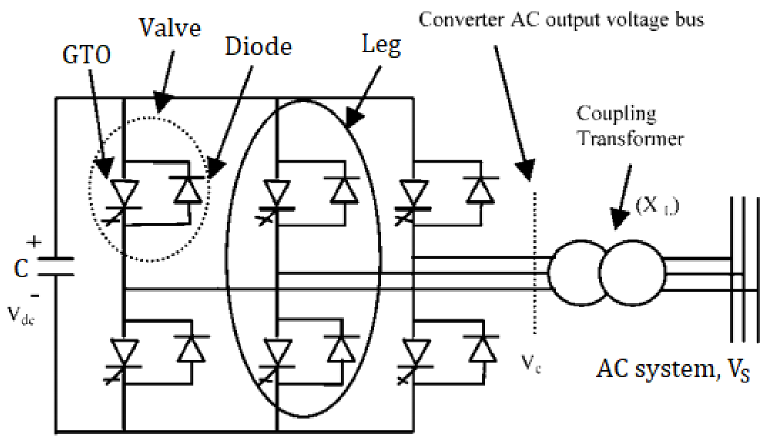


**Fig. 4.8:** Static synchronous compensator (STATCOM)

As STATCOM has inherent characteristics for real power exchange with a support of proper energy storage system, operation of such controller is possible in all four quadrants of $Q˘P$ plane [61] and it is governed by the power flow relation given in (4.35).

$$S = 3\frac{V_sV_c}{X_L}\sin\delta - j3\Big(\frac{V_sV_c}{X_L}\cos\delta - \frac{V_s^2}{X_L}\Big) = P - jQ, \tag{4.35}$$

where, where $S$ is the apparent power flow, $P$ the active power flow, $Q$ the reactive power flow, $V_s$ the main AC phase voltage to neutral (rms), $V_c$ the STATCOM fundamental output AC phase voltage (rms), $X_L$ the leakage reactance, $L$ the leakage inductance, $f$ the system frequency and $\delta$ the phase angle between $V_s$ and $V_c$. The AC voltage output ($V_c$) of STATCOM is governed by DC capacitor voltage ($V_{dc}$) and it can be controlled by varying phase difference ($\delta$) between $V_c$ and $V_s$.

### *4.6.4 Unified Power Flow Controller*

The Unified Power Flow Controller (UPFC) can be described as a combination of a static synchronous compensator (STATCOM) and a static synchronous series compensator (SSSC). It can provide the benefits of both, shunt connected FACTS device as well as that of series connected FACTS device and most of all it can also provide active power flow control. The steady state power flow control using a UPFC is attained by injecting a voltage with controllable magnitude and phase angle in series with the line via series inverter. The UPFC injection model is derived enabling three parameters to be simultaneously controlled namely, shunt reactive power, the magnitude, and the angle, of injected series voltage [62, 63]. Sub-synchronous resonance mitigation in UPFC is carried out by modulating the real power flowing through the DC link capacitor. Figure (4.9) shows the structure of UPFC.

UPFC along with the many benefits has limitations. For example, the real power series voltage injection will be limited when the UPFC is operating in a STATCOM mode. As

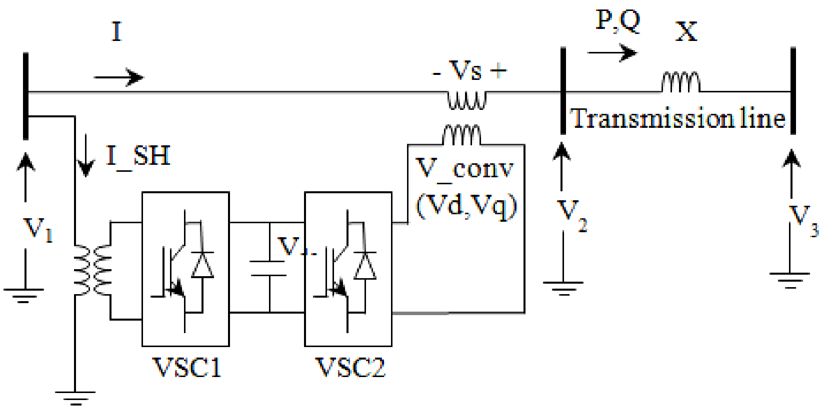


**Fig. 4.9:** Unified Power Flow Controller (UPFC)

the series transformer is in the line, the leakage reactance of the series transformer adds to the series line impedance, which the UPFC is compensating. High and low operating voltage limitations on the bus will limit the effective range of the UPFC.

### *4.6.5 HVDC*

HVDC power transmission systems and technologies associated with the FACTS continue to advance as they make their way to commercial applications [64]. HVDC, like FACTS, were also based initially on thyristor technology and more recently on fully controlled semiconductors and voltage-source converter (VSC) topologies. The ever increasing penetration of the power electronics technologies into the power systems is mainly due to the continuous progress of the high-voltage high power fully controlled semiconductors [65]. The current HVDC installations employ two major technologies, (1) line commutated current source converters (CSCs) that use thyristors, and (2) Forced commutated voltage source converters (VSCs) that use IGBTs.

In a general setting of two ac voltage sources shown in Fig. 4.12 connected via a reactor where one voltage is generated by the VSC and the other one is the voltage of the ac system the active and reactive powers are defined by the relationships given by (4.36) and (4.37). The relationships are based on the fundamental frequency and assuming

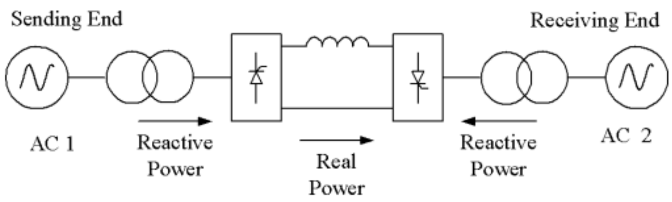


**Fig. 4.10:** HVDC system based on CSC technology with thyristors.

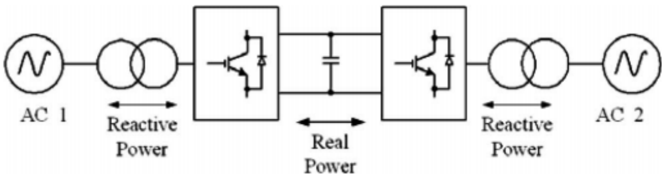


**Fig. 4.11:** HVDC system based on VSC technology built with IGBTs.

that the reactor between the converter and the ac system is ideal (i.e. lossless).

$$P = \frac{V_s \sin \delta}{X_L} V_r, \tag{4.36}$$

$$Q = \frac{V_s \cos \delta - V_r}{X_L} V_r, \tag{4.37}$$

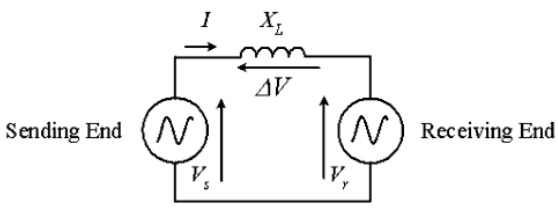


**Fig. 4.12:** General setting of interaction of two sources.

## 4.7 Reduction of Dynamic Model of Power System

As discussed in previous chapters and previous methods of network equivalencing using the concept of electrical distance, a power system can be divided into internal subsystems and external subsystems. The internal subsystem is modeled in detail while remainder of the system is approximated in order to simplify the computational requirements. The model reduction methods can be further divided into three groups: 1) *Physical reduction*, which requires the electrical distance parameter in order to determine the proximity from the area of disturbance; 2) *Topological reduction*, eliminates certain nodes thus reducing the size of the equivalent network; 3) *Modal reduction*, uses linearized models of the external subsystem that neglects the unexcited modes.

The equivalent model is obtained using modal reduction in the form of a reduced set of linear differential equations [66]. This type of technique is rarely used in practice as it is difficult to achieve standardization of the technique in order to apply it to different operating scenarios.

Topological reduction, along with physical reduction, gives an equivalent model that retains the equivalent system elements. The topological reduction gives a good representation of the system static performance as well as the dynamic performance during the short time following a disturbance. The reduced model can therefore be used for load flow analysis and transient stability analysis when disturbances occur in the internal system.

### *4.7.1 Network Transformation*

Topological reduction is achieved by transforming a large network into an equivalent smaller network by either elimination or by aggregation of nodes.

#### *Elimination of Nodes*

It is evident from the basis of analysis of structure of power network that the elimination of nodes from the network model must be done in such a way that currents and nodal voltages at the retained nodes are unchanged. The network is defined by nodal equation shown in (4.38).

$$\begin{bmatrix} I_R \\ I_E \end{bmatrix} = \begin{bmatrix} Y_{RR} & Y_{RE} \\ Y_{ER} & Y_{EE} \end{bmatrix} \begin{bmatrix} V_R \\ V_E \end{bmatrix} \tag{4.38}$$

The equation shown above considers all the nodes with classification such as set of eliminated nodes given by {E} and set of retained nodes given by {R}. The eliminated voltages and currents in (4.38) can be swapped to modify it to (4.39).

$$\begin{bmatrix} I_R \\ V_E \end{bmatrix} = \begin{bmatrix} Y_R & K_I \\ K_V & Y_{EE}^{-1} \end{bmatrix} \begin{bmatrix} V_R \\ I_E \end{bmatrix} \tag{4.39}$$

where, $Y_R = Y_{RR} - Y_{RE}Y_{EE}^{-1}Y_{ER}$, $K_I = Y_{RE}Y_{EE}^{-1}$, $K_V = -Y_{EE}^{-1}Y_{ER}$.

The nodal currents in the set {R} are given by

$$I_R = Y_R V_R + \Delta I_R \tag{4.40}$$

where, $\Delta I_R = K_I I_E$.

Eq. (4.40) refers to the relationship between the currents and voltages of the retained nodes in the reduced network. The matrix $Y_R$ corresponds to a reduced equivalent network that consists of the retained nodes and equivalent branches linking them. This network is often referred to as the transfer network and the matrix describing it as the transfer impedance matrix. $K_I$ gives a relation between the nodal currents from the eliminated nodes to the retained nodes and is known as distribution matrix. The method is illustrated in Fig. 4.13.

***Sparse Matrix Techniques***

Sparse matrix techniques are used in order to reduce the complexity of elimination algorithm shown in (4.40) [67, 68]. This form is equivalent to Gauss elimination of a corresponding row and column from the admittance matrix.

For each eliminating node, $k$, of set {E}, the matrix $Y_R$ is updated. This is given in

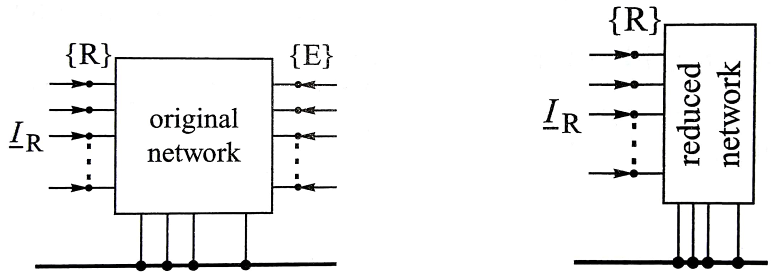


**(a)** Network before elimination **(b)** Network after elimination

**Fig. 4.13:** Elimination of nodes

(4.41) for each element $Y_{ij}^{new}$ of matrix $Y_R$.

$$Y_{ij}^{new} = Y_{ij}^{old} - \frac{Y_{ik}Y_{kj}}{Y_{kk}}, \qquad \text{for } i \neq k, j \neq k, \tag{4.41}$$

where $Y_{ij}^{old}$ is an element of matrix $Y_{RR}$.

It is worth noting that if nodes $i$ and $j$ are not adjacent to node $k$, then elimination of $k$ does not modify the admittance matrix $Y_{ij}$. Also, self admittances of all the nodes adjacent to $k$ are modified with the elimination of $k$. Therefore, while using sparse matrix techniques the order in which the rows/columns of a matrix are processed is important. Simple heuristic methods [69, 68] are used to carry out the node elimination techniques based on the following rules: 1) Nodes with least number of adjacent nodes are eliminated; 2) Nodes which introduce the least number of new connections are eliminated. Following these rules ensure that the elimination have a minimum impact on the structure of the power system and hence the equivalent network can be a closer representation to the full complex network.

#### *Aggregation of Nodes using Dimo's Method*

This method works on the principle of replacing a group of nodes by a single equivalent node, illustrated in Fig. 4.14. The author in [70] introduced this method by considering an aggregated node set {A} and assuming the presence of fictitious branches to the aggregated node set. The branch admittances to each node is chosen in such a way as to make the terminal voltage of all the branches equal. Subsequently, the terminal equipotential nodes are connected with a fictitious auxiliary node. The voltage at this fictitious node is zero, hence a negative admittance is added to the node which is given by

$$Y_{fa} = -\frac{S_a^*}{V_a^2}, \qquad \text{where } S_a = \sum_{i \in \{A\}} S_i, \tag{4.42}$$

and where $f$ is the fictitious node and $Y_{fa}$ is the negative admittance between node $f$ and node $a$ which is the equivalent node replacing the aggregated node set {A}. Eq. (4.42) makes the voltage $V_a$ at the equivalent node equal to the weighted average of the voltages at aggregated nodes $V_i$ for $i \in \{A\}$. This weighted average is determined as shown in (4.43).

$$V_a = \frac{S_a}{I_a} = \frac{\sum_{i\in\{A\}} S_i}{\sum_{i\in\{A\}} \left(\frac{S_i}{V_i}\right)^*}. \tag{4.43}$$

This method produces a large number of fictitious branches and also the aggregation

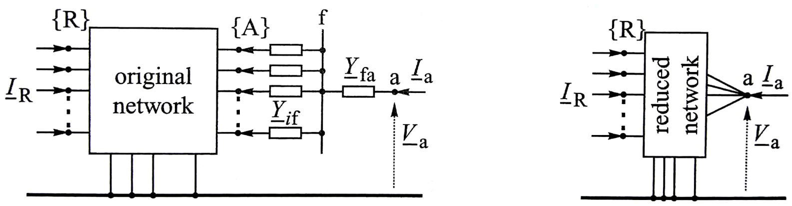


**(a)** Network with fictitious branches **(b)** Network after elimination/aggregation

**Fig. 4.14:** Node aggregation using Dimo's Method

introduces a branch with negative impedance, these parameters if exist in a network after reduction may cause convergence problems. These discrepancies were eliminated by Zhukov's method.

***Aggregation of Nodes using Zhukov's Method***

This method of aggregation considers impact of voltage angle at the equivalent node which is a function of power injection at the aggregated node $i$ and the inertia coefficient of the unit placed at aggregated node $i$. In this method, there is no change in admittances of the network branches hence it is not required to introduce fictitious branches as was the case in previous method. However, it does introduce fictitious shunt branches at the retained nodes.

As it is convenient to have equivalent branches of low resistances, the voltage angle $\delta_a$ at the equivalent node is assumed to be equal to the weighted average of voltage angles at the aggregated nodes. This gives a following relation,

$$\delta_a = \frac{\sum_{i\in\{A\}} S_i\delta_i}{\sum_{i\in\{A\}} S_i}, \tag{4.44}$$

or

$$\delta'_a = \frac{\sum_{i\in\{A\}} M_i\delta'_i}{\sum_{i\in\{A\}} M_i}, \tag{4.45}$$

where $S_i$ is the apparent power injection at the aggregated node $i$ and $M_i = \frac{T_{mi}S_{ni}}{\omega_s}$ is the inertia coefficient of the unit installed at aggregated node $i$. Further since it introduces the shunt branches between the retained nodes, the diagonal element of $Y_{RR}$ which is the sum of all the series and shunt branch admittances is given by

$$Y_{ii} = y_{i0} + \sum_{j\in\{R\}} y_{ij} + \sum_{k\in\{A\}} y_{ik} \quad \text{for } i \in \{\text{R}\}, \tag{4.46}$$

where $y_{i0}$ is the sum of admittances of all shunt branches connected to $i$ and $y_{ij}$ is the admittance of a branch linking nodes $i$ and $j$. Hence it can be seen that Zhukov's method introduces some equivalent shunt admittances at the retained nodes {R}.

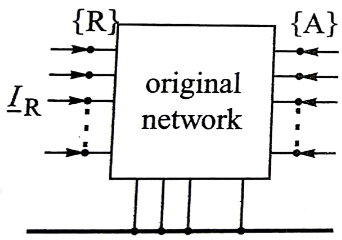


**(a)** Network before elimination

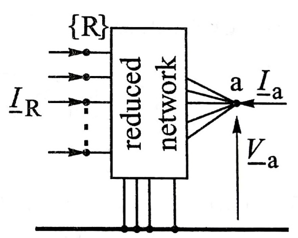


**(b)** Network after aggregation

**Fig. 4.15:** Node aggregation using Zhukov's method

*Coherency*

The prime reason for the dependence of admittances on voltage angle is due to the voltage transformation ratio $\vartheta = \frac{V_i}{V_a}$ between the aggregated nodes $i \in \{A\}$ and the equivalent node $a$. For any two nodes $i, j \in \{A\}$, the equivalent network obtained for an initial state is valid for other states only if the transformation ratio can be assumed to remain constant, this is given by

$$\frac{V_i(t)}{V_j(t)} e^{j[\delta_i(t)-\delta_i(t)]} = \text{constant} \quad \text{for } i, j \in \{\text{A}\} \tag{4.47}$$

Nodes satisfying the condition in (4.47) are referred to as electrically coherent nodes. If the voltage magnitudes of the aggregated nodes are considered to be constant, the above condition simplifies to

$$\delta_i(t) - \delta_j(t) = \delta_{ij} \quad \text{for } i, j \in \{\text{A}\}, \tag{4.48}$$

For generator nodes the coherency condition can be expressed in a similar fashion as shown in (4.49).

$$\delta'_{ij}(t) = \delta'_i(t) - \delta'_j(t) \quad \text{for } i, j \in \{\text{A}\}, \tag{4.49}$$

where $\delta_i$ refers to the rotor angle of the generator connected to node $i$.

In an operating condition, two generators are said to be coherent if their angular difference is constant within a certain tolerance limit, $\epsilon$, over a certain time interval. As discussed earlier, the coherency-based technique which is based on the property of equal acceleration for coherent machines and focuses on the dynamic equivalence of a network. For the two machines $i$ and $j$,

$$|\delta_{ij} - \delta_{ij}^0| \leq \epsilon$$

where $\delta_{ij}$ and $\delta_{ij}^0$ are the angular differences between the machines at nodes $i$ and $j$ at any time and at initial time respectively. Then the coherency factor can be defined as

$$CF = \frac{max|\delta_{ij}|}{|\delta_{ij}^s|} \tag{4.50}$$

For a machine $i$, the dynamic equation (4.51) as

$$M_i \Delta \ddot{\delta}_i = \Delta P_{m,i} - \Delta P_{G,i} \tag{4.51}$$

After simplifying, the relation is of the form

$$[M][\Delta \ddot{\delta}] = [M]^{-1}[Y][\Delta \delta] \tag{4.52}$$

Here $[M]^{-1}[Y]$ is the jacobian matrix $J$. This method compares only the elements of the Jacobian matrix to identify the coherent group. A normalized quantity $\beta$ is defined such that

$$\beta = \frac{|j_{ij} - j_{ji}|}{\max(j_{ij}, j_{ji})} \tag{4.53}$$

the term $|j_{ij} - j_{ji}|$ can be taken as a measure to estimate the relative variation between $\Delta\delta_i$ and $\Delta\delta_j$. When the moments of inertias $M_i$ and $M_y$ are equal, then $\beta = 0$, which means that the machines are perfectly coherent.

Also, from the DC model in matrix form, the network power flow can be simplified and represented as

$$P = [B]\delta$$

where, $P$ is the power vector of net injection where each element represents the individual power injection. $[B]$ is the susceptance matrix and $\delta$ is the vector of phase angles of the respective buses.

Hence, it can be clearly seen that the sensitivity is given by the elements of the Jacobian matrix $J$ and the coherency is observed on the basis of factors such as moment of inertias of the machines as well as on the network admittance.

### *4.7.2 Equivalent Model of External Subsystem*

The process of forming an equivalent model of the external subsystem involves the reduction of the number of nodes. The number of load nodes are either completely eliminated or aggregated to equivalent nodes while generator nodes are aggregated into small groups represented by equivalent nodes based on the coherency of the generators connected to those nodes. The elimination/aggregation is done using the methods described in previous section. In summary, there are certain assumptions that are needed to create dynamic equivalent model which are as follows:

1 Elimination of the load nodes in the external subsystem.

2 Identification of coherent groups of generators in the external subsystem.

3 Aggregation of the coherent groups.

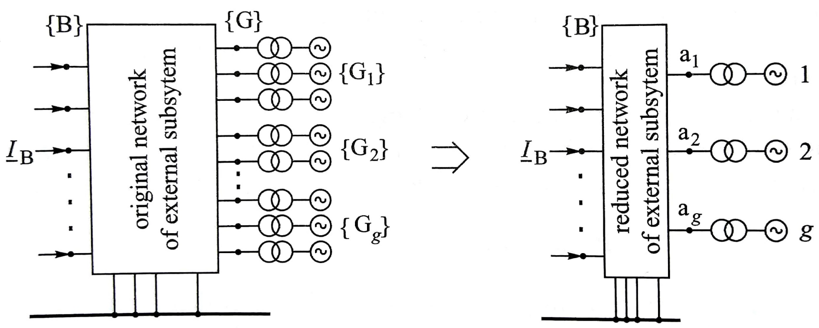


**Fig. 4.16:** Model reduction of the external system

Fig. 4.16 shows the aggregation of coherent group of generator nodes and illustrates the whole process of forming an equivalent model of the external subsystem.

### 4.8 Summary - Distance from Power Systems Perspective

Distance from a power systems perspective is discussed on the basis of various parameters and sensitivities of those parameters with respect to the varying operating conditions. As discussed, EMD is a concept of evaluating the electromechanical disturbance propagation between generators which considers the dynamic properties of the machines and their behavior during transient period. Their dynamic behavior with respect to other generators in the network give a relative measure of proximity as described in (??) and (??), and also defines the coherency of the generators using the coherency factor in (??) and EMD measure in (??) and (??). Coherency of buses is also investigated on the basis of voltage interactions between different buses of the system which reactive power controlled and is shown in (??). From the steady-state operation perspective, the representation of proximity of loads from the generation units on the basis of reactive power supply is discussed using (??). Proximity of load nodes from the generator nodes is also shown using relative electrical distance in (4.19) but the basis of this measure is the sensible allocation of transmission charges across the network. Apart from these measures, GSFs and AEDs presents unique measure of impact of a bus on a tie-line, these are shown in (??) and (??). Further electro-magnetic transient perspective of the system is based on structure variables and the initial status of the network. For each element, an equivalent network is setup on the basis of steady state operating conditions. Load modeling on the basis of static and dynamic models are also based on the initial operating conditions and uses an exponential model.

The reduction of dynamic model of power system highlights the significance of electrical distance in order for reduction/aggregation of nodes in the network and hence the structure of the network. Further, the coherency of various generators can be seen as a relation between the angular difference of the machines and electrical distance between them. This ensures the recognition of coherent generators that can be aggregated together to be represented by a single unit.

## 4.9 Conclusion

This chapter has explored

**Table 4.1:** Electrical Distance from a Power Systems Perspective

| | Electro-Mechanical Distance Perspective | Voltage Interaction Perspective | Steady State Perspective |
|---|---|---|---|
| Measure/ Index | Reflection distance, Coherency Factor, EMD, C-EMD | Voltage Interaction | RPSC, RED, GSF, AED |
| Similarities | 1. Gives the sensitivity index of a network<br>2. The proximity of the buses across the network is based on various operating parameters and not entirely on the network structure | | |
| Differences | Takes into account the dynamical effect of a generator apart from the electrical perspective when a network is subject to any disturbance | Based on the voltage changes dependent on the controllable reactive power in the area | Defines the proximity of buses relative to other elements in the network in a steady state operation condition |
| Applications | The development of dynamic electro-mechanical equivalents had been applied to transient stability programs | This finds its application in determining optimum location of installing voltage control facilities to allow better control of voltage profile and segregating areas voltage-control areas by controlling the prices of reactive power services | Most of the electrical distance concepts are used to aggregate the network and reduce the computational load in making decisions on a day-to-day basis such market analysis, generation redispatch, load shedding etc. |

# CHAPTER 5

## Power Systems based Analysis

The analysis of distance from different perspectives for networks and operating power systems is done by evaluation of different scenarios from a networks perspective which essentially gives the sensitivity of different network parameters.

### 5.1 Electrical Distance Calculations

#### *5.1.1 General Description*

***Steady State***

Electrical distance metric in steady state operating conditions can be defined as an intuitive measure where the distance between two nodes is the equivalent Thevenin impedance between them which is the parallel combination of all impedance paths connecting them.

1 *Thevenin Impedance*:

Electrical Distance can be calculated directly from the system's $Z_{bus}$ matrix, which is simply the matrix inverse of the system's $Y_{bus}$ matrix, which describes the fundamental topology of the electrical system connections, corresponding to the Laplacian matrix for general networks. As defined in (**??**), the electrical distance between two buses $a$ and $i$ is given by

$$Z_{ai}^{th} = Z_{aa} + Z_{ai} - 2Z_{ii} \tag{5.1}$$

where, $Z_{ai}$ denotes the element in the $a^{th}$ row and $i^{th}$ column of the $Z_{bus}$ matrix and is the mutual impedance between buses $a$ and $i$.

While thevenin impedance defines the distance between two buses, Average Electrical Distance in [? ] defined in (??) gives a perspective of electrical distance from a bus to a tie-line.

$$d_{ab,i} = \frac{|Z_{th,ai} - Z_{th,bi}|}{2} \tag{5.2}$$

The equation (??) comprises of thevenin impedances, which are elements from the Laplacian matrix which defines the structure of the system. Note that the $Z^{th}$ distance is independent of system loading and can be calculated without power flow techniques. Crucially, it properly accounts for all the available current paths between two nodes. In networks, the impedance between nodes is approximated by summing impedances along the topologically shortest path.

2 *Power injection sensitivity*:

With power transfer being a significant part of any power system, it becomes imperative to analyze the impact of power injection and withdrawal with respect to the associated distance. Based on the load flow model, the GSF of tie-line $ab$ with respect to bus $i$ given in [? ] by $g_{ab,i}$ in (??).

$$g_{ab,i} = \frac{\bar{X}_{a,i} - \bar{X}_{b,i}}{x_{ab}} \tag{5.3}$$

where $\bar{X}_{a,i}$ and $\bar{X}_{b,i}$ are the elements of inverse susceptance matrix and $x_{ab}$ is the reactance of line $ab$. The power injection at a bus has an impact on power flow in a tie-line which can be observed as sensitivity of power flow in a tie-line. There is a correlation between the impact and the electrical distance between the bus and the tie-line which is given by (??). The correlation refers to the increase in impact when a line and a bus are electrically closer to each other and hence an increase in impact can be seen as a decrease in net impedance between the two.

3 *Load Points*:

Another method that specifically considers the location of load points with respect to generation nodes is mentioned in [? ]. For a system, (??) defines the relation between the currents and voltages at respective generator and load nodes.

$$\begin{bmatrix} I_G \\ I_L \end{bmatrix} = \begin{bmatrix} Y_{GG} & Y_{GL} \\ Y_{LG} & Y_{LL} \end{bmatrix} \begin{bmatrix} V_G \\ V_L \end{bmatrix} \tag{5.4}$$

$I_G$, $I_L$ and $V_G$, $V_L$ represent complex current and voltage vectors at the generator nodes and load nodes respectively. The matrix is the admittance matrix rearranged in the order of generation and load nodes. The location of load nodes with respect to the generator nodes is given by $[F_{LG}] = -[Y_{LL}]^{-1}[Y_{LG}]$. This gives a voltage relation perspective between load and generator nodes and thus voltage stability index is also defined which gives a relation of voltage level with respect to the loading in the system.

4 *Shunt-Reactive Power Handling*:

A similar measure but with respect to the reactive power handling capability is defined in [**?** ] where an index is proposed that load buses can obtain from generation units in a power system by using the reactive power capacities of generation units and the electrical distances between load buses and generation units. This is given by (**??**).

$$\begin{bmatrix} \Delta Q_G \\ \Delta Q_D \end{bmatrix} = - \begin{bmatrix} B_{GG} & B_{GD} \\ B_{DG} & B_{DD} \end{bmatrix} \begin{bmatrix} \Delta V_G \\ \Delta V_D \end{bmatrix}$$

This equation gives a relation between the reactive power change ($\Delta Q_G$ and $\Delta Q_D$) and the voltage change ($\Delta V_G$ and $\Delta V_D$) at generation and load nodes respectively. Hence there is a direct correlation between these operating parameters, however these reactive power and voltage vectors are correlated through susceptance matrix which defines the system structurally. Hence the structure also has an impact on the reactive support capabilities of generation units. From the susceptance matrix, the distance relation shown in (**??**) can be seen as similar to the electrical distance in a system with current and voltage relation, this relation can also be defined the distance as the ratio of reactive power change at generator and load nodes.

***Electro-mechanical Dynamics***

The concept of electro-mechanical distance measure reflects the interaction between machines during a disturbance occurrence in the system. In order to take into account the electro-mechanical effect of machines apart from electrical parameters, it is important to define the impact of machines with linear differential equations.

1 *Line Admittances*:

For an electro-dynamical system, the electrical distance comprises of two elements; admittance distance which is the maximum of magnitudes of transfer admittance between two generators, and reflection distance which accounts for the dynamical effect of a generator onto the other generators. The admittance distance $Y_d(k)$ of generator $k \in \Omega$ with respect to a group of generators $i \in \Phi$ is given in (5.5).

$$Y_d(k) = \max |Y_{ki}| \tag{5.5}$$

where $Y_{ki}$ represents the magnitude of the transfer admittance between generator $k$ and generator $i$.

2 *Power-angle sensitivity*:

The definition of electrical distance directly takes into account the structure of the network by utilizing the admittance matrix, but the electrical distance from the electro-mechanical dynamical perspective must also utilize the dynamic behavior of machines which is captured by reflection distance between the machines and is presented in (5.6) and (5.7).

$$R_d(k) = \max_{f \in \phi} \left\{ \max_{i \in \phi} \frac{\Delta P_{ri}}{M_i} \right\} \qquad k \in \Omega \tag{5.6}$$

where

$$\Delta P_{ri} = \frac{\partial P_{ik}}{\partial \delta_k} \Delta \delta_k \tag{5.7}$$

In the formulation of reflection distance is a function of sensitivity of the electrical power of generator $i$ with respect to the angle change in generator $k$ and the angular momentum $M_i$ of generator $i$ which is a key in determining the impact of any change in angle of a generator in the network. In (5.6), the change in power $\Delta P_{ri}$ is limited by the change in angle of another generator. Further, the distance is defined as the ratio of change in power to angular momentum of the generator which gives a similar impact as we see with admittance in electrical networks.

The measure of maximum angular movement between two machines during a transient period is the EMD between the two machines [**?** ]. The EMD is the measure of electromechanical interaction between the pair of machines. This interaction is defined by the Euclidean norm of change in power with respect to the angles.

3 *Inertia*:

Two generators with constant angular difference are said to be coherent and for these machines, the coherency factor is given as in (5.8).

$$CF = \frac{max|\delta_{ij}|}{|\delta_{ij}^s|} \tag{5.8}$$

The elements of Jacobian matrix $J$ given in 5.9 as $J = [M]^{-1}[Y]$.

$$[M][\Delta\ddot{\delta}] = [M]^{-1}[Y][\Delta\delta] \tag{5.9}$$

The sensitivity is given by the elements of Jacobian matrix $J$ and is dependent on the moment of inertias and the admittance across the structure of the network.

#### Voltage Interaction

The voltage variations in different buses $i$, $j$ of the system defines the magnitude of interaction between them and hence the electrical distance. From (5.10), the voltage variations $\Delta V_i$, $\Delta V_j$ of the buses $i$, $j$ respectively are related as

$$\Delta V_i = \alpha_{ij}\Delta V_j \tag{5.10}$$

where $\alpha_{ij} = (\delta V_i/\delta Q_j)/(\delta V_j/\delta Q_j)$ represents normalized voltage attenuation on bus $i$ with respect to the perturbation at bus $j$. The ratios $\delta V_i/\delta Q_j$ and $\delta V_j/\delta Q_j$ are elements of sensitivity matrix of the system.

Further the electrical distance between the buses is defined in (5.11).

$$D_{ij} = D_{ji} = -log(\alpha_{ij} \cdot \alpha_{ji}) \tag{5.11}$$

Here, the electrical distance is the ratio of voltage attenuations due to the impact of buses onto the other buses.

#### *Electro-magnetic Transients*

The network defined for electro-magnetic transient states consists of line elements such as resistances, capacitances and inductances. Although lossless lines are also defined. In a transient state, the resistance is independent of changing variables such as frequency thus the resistance can be used as it is. However, with changing frequency, the reactances of inductors and capacitors change and it is recommended to represent these elements with a constant equivalent resistance. The equivalent resistance in both the cases is represented in 5.12.

$$R = \frac{2L}{\Delta t} \text{ and } R = \frac{\Delta t}{2C} \tag{5.12}$$

The electrical distance here in such operating conditions can be determined by considering the initial state condition and thus representing the network elements by equivalent resistance.

### *5.1.2 Characterization of Impact Variable*

#### *Circuit-based*

1 *Actual Variables:*

The impact variables for a system operating in steady-state condition are the variables that exhibit the true state of the system. These variables include components of impedance such as resistance and inductor-or capacitor-based reactances. In transient conditions, the frequency of the system changes which may not have any impact on the resistance as it is independent of the operating frequency. However, any change in frequency brings a greater impact on the reactances, $X_L$ or $X_C$ based on inductor or capacitor respectively, although the value of inductor ($L$) or capacitor ($C$) does not change.

2 **Approximate Variables:**

During a short-circuit, the steady-state reactance ($X_d$) is temporarily reduced due to the interaction of the magnetic flux between the damper windings and the armature windings in a generator. The complex magnetic flux interactions created by the small resistances and inductances (self and mutual) between the various elements (damper windings, field windings and rotor body) during a transient condition ultimately act to dramatically and suddenly reduce the machine's reactance. This reactance reduction is temporary, but its sudden drop allows much higher instantaneous short-circuit currents to form during the first few cycles of a fault. The reduced reactance is classified as transient reactance ($X'_d$) and sub-transient reactance ($X''_d$).

***Mechanical-based***

The impact variables for a system with electro-mechanical dynamics are power-angle and inertia and generator swing equations describe the dynamics of synchronous machines driven by the relationship between mechanical system (i.e. governor/turbine) and electric system. Consider three-phase synchronous alternator that is driven by a prime mover. The equation of motion of the machine rotor is given by

$$J\frac{d^2\theta}{dt^2} = T_m - T_e \tag{5.13}$$

where $J$ is the total moment of inertia of the rotor mass, $T_m$ is the mechanical torque supplied by the prime mover, $T_e$ is the electrical torque output of the alternator and $\theta$ is the angular position of the rotor.

In steady state, the machine angular speed is equal to the synchronous speed and we get

$$\frac{2H}{\omega_s}\frac{d^2\theta}{dt^2} = P_m - P_e \tag{5.14}$$

Equation (5.14) describes the behavior of the rotor dynamics and hence is known as the swing equation. The angle $\delta$ is the angle of the internal emf of the generator and it dictates the amount of power that can be transferred. This angle is also called the load angle.

## 5.2 Structure - Interpretation of Electrical Distance

The interpretation of electrical distance in different settings and perspectives is shown in Fig. 5.1.

## 5.3 Remarks

The distance as seen from a networks perspective has been broadly divided into categories defining the proximity of a bus on the basis of topology of the network and on the basis of actual resistance distance. Further we investigate the distance measure from power systems perspective in order to understand the structure of the network on the basis of impact of various operating conditions on parameters defining the network. In the wake of such analysis, we analyze electro-mechanical distance perspective of a power system which takes into account the dynamical effect of a generator due to any change in another generator with in the proximity when a network is subject to any disturbance which is demonstrated in (**??**), (**??**), (**??**) and (**??**). Each definition of electrical distance

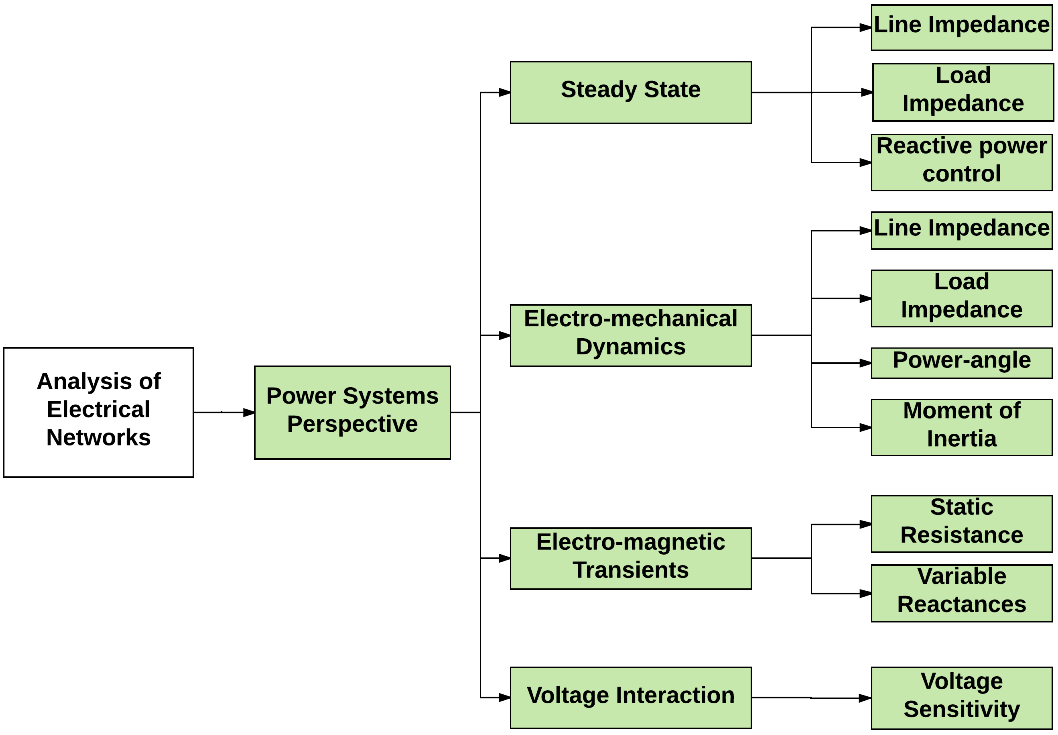


**Fig. 5.1:** Interpretation of Electrical Distance

represents the coherency of generators which can be simply seen as the sensitivity of one generator with respect to the other. This in turn defines the structure of the network and enables us to identify the valid proximity of impact of each generator.

Electrical distance between different buses can be defined on the basis of voltage control capability of the buses in a network by controlling the reactive power. The rate of change of voltage with respect to reactive power, shown in (**??**), is the inverse of power flow jacobian matrix and can be approximated by impedance matrix which defines the structure of the network in terms of electrical distance from a networks perspective which is defined in (**??**). Distance from the steady-state operation perspective, in a similar fashion, can be concluded as the sensitivity with respect to various parameters in the operating system. Hence this can be correlated to the topological perspective of a network which employs electrical distance on the basis of network structure.

Electromagnetic transients studies often require detailed modeling of complex transmission networks. EMTP models are based on structure variables as obtained during steady state operation and are taken as initial status of the network. Since transients require a step-by-step procedure starting at the initial condition and solving for the state at a certain time. This requires various parameters to be defined in a steady state form using respective equivalent networks. The system is represented as linear algebraic equations in (??). The nodal conductance matrix is the same as the nodal admittance matrix in steady state analysis which strikes a similarity to the admittance matrix defined in the networks perspective as electrical distance measure for the nodes. Thus for EMTP models, it becomes imperative to make the process iterative as the time progresses but uses the same concept of electrical distance as used in steady-state perspective.

As far as transient studies are concerned, there has always been a need for a correct representation of electrical loads in studies. Load characteristics affect the dynamic behavior of a power system, thus can have significant effects on the rates of acceleration or deceleration of individual generators during the fault, and therefore, on eventual stability of the system. Voltage dependency is shown to affect the real and reactive power in (??) and (??) such that the sensitivity associated with the operating variables provide a case to differentiate the operating nodes with a perspective of effective distance from a generation point. A study made in [? ] shows cases in which decreasing the sensitivity of load to voltage in one area increased the tie-line power limit when the area was exporting power, but decreased it when the area was importing power [? ]. Stability limits often decrease when active power changes from constant-impedance type toward constant-power type, especially in the cases where loads are at major load centers remote from generation. The impact of frequency decreases as the impedance increases between the generators. This shows a relation between the characteristics of electrical loads and the correlation with the structure of the network and associated electrical distance.

The reduction of dynamic model of power system is based on the concept of electrical distance. This is achieved by elimination of nodes on the basis of impact on the network.

The reduction/aggergation is done in such a way that currents and nodal voltages at the retained nodes remain unaltered. Further, the sparse matrix technique in (4.41) is used to reduce the complexity which utilizes the admittance matrix to assess the impact of each node. The reduction is based on the sensitivity of angular difference of the machines and electrical distance between them. This ensures the identification of coherent generators that can be aggregated together to be represented by a single unit and hence resulting in efficient aggregation. This highlights the significance of electrical distance in reducing the network and even aggregating the coherent generators.

It is seen that port-Hamiltonian system framework is open dynamical system and is a representation of the energy in a particular network. From the analysis of the matrix $\hat{D}\hat{D}^T$, it is obtained that matrix $DL^{-1}D^T$ is the Laplacian matrix corresponding to the weighted graph of the network. The elements of the Laplacian matrix serve as a parameter to define the electrical distance of the network nodes in terms of the graph energy of the underlying network.

The study of the existing power system analysis techniques done from a different perspective sheds light on the dependency of parameters sensitivities on the structure of the network and measures associated with it. Analyzing the power system from different perspective gives an insight on different sensitivities and associated relation to the concept of electrical distance. Specifically, EMT studies and modeling of load under transients require a completely different perspective of electrical distance which may not be very obvious. In conclusion, the concept of electrical distance can be correlated with sensitivity of different parameters under varying operating conditions of a power system.

# CHAPTER 6

# Electric Circuit Foundation of Structural Analysis for Power Systems from a Network Perspective

## 6.1 Introduction

## 6.2 Analysis of structure feature of major types of models

## 6.3 Overview to Analysis of structure

## 6.4 Conclusion

# CHAPTER 7

## A network science based $k$-means++ clustering method for power systems network equivalence

The last few decades have witnessed a new movement of interest and research in the study of complex networks, i.e. networks whose structure is irregular, complex and dynamically evolving in time such as power grids, communication networks, biological networks, social networks, etc. Investigating dynamics in such complex networks requires an understanding of the interaction between network topology and specific domain constraints. For example, the study of power grids requires basic circuit laws, relating voltages and currents, to be incorporated along with the network topology. In this paper, we explore this interaction in the context of deriving simplified equivalent networks as representations of large power grids. In this paper, the terms power systems, power system network and power network are used interchangeably. Power network equivalencing has been studied in the literature with different objectives. Our objective is to study the equivalents appropriate for electrical market analysis.

Electrical market analysis involving power exchange is becoming more and more complex due to the size and degree of interconnections in modern power systems due to economic, political and environmental reasons [? ]. With such inherent complexities and information deficiency, it is difficult for participants to make operational and market decisions at buses that are sensitive to the condition of transmission lines. For these reasons, it is necessary to develop an enhanced method to support decisions, particularly, those sensitive to major and critical transmission lines. The analysis can be computationally challenging, especially, when a full AC implementation approach is used [? ]. As compared to the full AC analysis, a simplified analysis of the network can be done by using full network DC power flow model [? ]. Although the full AC analysis would be the most accurate approach, the DC approach allows network operators to make informed dispatch decisions thereby saving time and effort required. The enormous size of power system networks makes full network DC analysis computationally taxing. To reduce the computational burden and to simplify the analysis of electricity markets, several network equivalence models have been used [? ? ? ? ].

Various approaches for network equivalencing have been presented in [? ? ? ? ? ? ]. These approaches follow the traditional method of eliminating less important elements from the system on the basis of geographical and electrical parameters. Such elimination results in partitioning of the network into three clusters of buses: a cluster of internal buses, a cluster of external buses, and a cluster of boundary buses that divide the external buses from the internal buses. Due to their trivial impact on the internal system, remote generators and transmission lines connected to the boundary buses may be eliminated with minor impact on decisions. However, irrespective of the bus demarcation, market analysis of large power system networks requires retaining the desired buyer/seller pairs corresponding to operating zones in order to understand the impact of power flows on transmission lines from the buyer/seller pairs at various buses. Hence, in this study we do not eliminate the external buses but rather focus on the line flows between various operating areas. These line flows are called tie-line flows.

In this paper, the metric developed for the study has properties similar to resistance distance which has been widely used since the early days of electrical circuit theory. There are several books on the basics of circuit analysis that deal with resistance distance and topological formula for resistance distance, for example [? ]. However, recently this concept gained increased importance in view of its applications in areas outside electrical circuit theory [? ? ? ? ? ? ? ].

In recent studies, network equivalencing has been done using Generation Shift Factor (GSF)-based methods [? ? ? ? ]. In these methods, buses with similar impact on the interconnecting tie-line flows evaluated using GSFs are grouped together. In order to improve the efficiency and accuracy of bus clustering, [? ] uses $k$-means algorithm based on GSF to cluster the buses. However, GSFs are sensitive to the change in the location of slack generator. Network operators supervising different regions of the interconnection might not be aware of the slack bus change and hence there could be discrepancies in decision making, which can provoke an impact on regional power transactions. Therefore, our main objective in this paper is to develop a new clustering method as well as new network equivalent that overcomes the limitation of the GSF-based methods.

Our work in this paper includes our previous work [? ] and its enhancements. The rest of this paper is organized as follows. Section 7.1 gives an introduction to all the basic concepts that are of interest in the development of techniques discussed in subsequent sections. We introduce in Section 7.2, the concept of average electrical distance (AED) and discuss a relationship between AED and GSF. Also, the relevance of our work in the context of social network analysis is given in Section 7.2.2. Section 7.3 gives an introduction to the $k$-means algorithm for clustering. Section 7.4 presents our AED-based $k$-means clustering method. Section 7.5 presents the AED-based $k$-means++ clustering method. The new method uses a seeding technique [? ] for initialization of centroids. We call this augmented algorithm as AED-based $k$-means++ algorithm. We also incorporate in this method silhouette analysis to determine the number $k$ of clusters to be given as input to the clustering method. The resulting AED-based $k$-means++ method yields clustering which is $O(logk)$ competitive. Section 7.6 presents how we use clustering to develop a power network equivalent suitable for market analysis. To demonstrate the efficacy of our approach for clustering and equivalencing, rest of Section 7.6 is concerned with experimental and comparative evaluation of our network equivalence method applied on the 300-bus system. In section **??**, conclusions are presented.

## 7.1 Preliminaries

In this section we introduce the basic concepts of Laplacian matrix of a graph, electrical distance and generation shift factor.

### *7.1.1 Laplacian matrix of a graph*

Consider a graph $G = (V, E)$ with vertex set $V = \{0, 1, \ldots, n\}$. Edge $e \in E$ connecting vertices $i$ and $j$ is denoted by $(i, j)$. We assume there are no loops on any vertices and there are no parallel edges connecting the vertices. In this paper, the terms, vertices and nodes, as well as links and edges, will be used interchangeably. Let an edge $(i, j)$ be assigned a weight $w_{ij}$, a positive real number. If there is no edge connecting $i$ and $j$ then $w_{ij} = 0$. Two vertices $i$ and $j$ are adjacent if there is an edge $(i, j)$. A vertex $j$ is incident on vertex $i$ if there is an edge connecting $i$ and $j$. The degree of a vertex $i$ denoted by $deg(i)$ is the sum of the weights of the edges incident on $i$.

The Laplacian matrix, $Y = [y_{ij}]$ of $G$ is an $(n + 1) \times (n + 1)$ matrix defined as follows:

$$y_{ij} = \begin{cases} -w_{ij}, & \text{if } i \neq j \\ deg(i), & \text{if } i = j \end{cases} \tag{7.1}$$

As an example, a graph $G$ and its adjacent matrix are shown in Fig. **??**(a) and **??**(b). Note that $y_{ij} = y_{ji}$. It can be seen that the sum of all the elements in any row and the sum of all the elements in any column are both equal to zero. So, $Y$ is singular and has no inverse. To handle this singularity problem of $Y$, two different approaches are adopted, namely, the eigenvalue approach and the determinant approach.

In the eigenvalue approach, the pseudo-inverse $Y^+$ of $Y$ is used. The properties of $G$ are studied in terms of the elements of $Y^+$. This approach is quite popular among mathematicians. See [**? ?** ]. In this paper, we follow the determinant approach which is popular in the electrical engineering community. In this approach, we first remove a row and the corresponding column from the Laplacian matrix, $Y$. Let us assume that the vertex labelled $o$ called the datum node or slack node is removed. The resulting matrix denoted by $Y(o)$ is called a reduced Laplacian matrix. The reduced Laplacian matrix $Y(o)$ of $Y$ in Fig. **??**(b) is shown in Fig. **??**(c). It can be shown that the matrix $Y(o)$ is non-singular and it has several other properties. See for example, [**?** ].

In all discussions in this paper, we will use $Y = [y_{ij}]$ to denote the reduced Laplacian of the network. We wish to draw attention to [**?** ] where the authors investigate the impact of topology on power flow using spectral graph theory.

### *7.1.2 Electrical Distance*

Consider an electrical network $N$ represented by the graph $G$. The admittance of the edge $(i, j)$ in $N$ serves as the weight $w_{ij}$ in $G$. Each edge $(s, t)$ in $G$ is associated with two variables, voltage, $v_{st}$ and current $i_{st}$. See Fig. **??**. Then by Ohm's law, we get

$$\frac{i_{st}}{v_{st}} = w_{st}, \text{ the admittance of } (s, t). \tag{7.2}$$

In electrical engineering literature, the reduced Laplacian matrix, $Y$ is called the node-to-datum matrix of $N$ with vertex $o$ as the datum vertex. Datum vertex is also known as the slack vertex. Let $Z = [Z_{ij}]$ be the inverse of the reduced Laplacian matrix. This matrix is called Z-bus ($Z_{bus}$) matrix in power engineering literature. Also, the ground is usually used as the slack vertex.

Suppose we now connect a current source of value $i_{s,t}$ across nodes $(s, t)$. See Fig. **??**. Let $v_{s,t}$ be the voltage across $s$ and $t$. Then the electrical distance between $s$ and $t$, denoted as $r_{s,t}$ is defined as

$$r_{s,t} = \frac{v_{s,t}}{i_{s,t}}. \tag{7.3}$$

We now proceed to show how to evaluate $r_{s,t}$ across all pairs of nodes $s$ and $t$. Note that definition of $r_{s,t}$ does not require that $s$ and $t$ be connected by edge $(s, t)$ in the network $N$. Suppose we now connect a current source of value $i_s$ across the vertices $o$ and for each $s \in \{1, 2, \ldots, n\}$, as shown in Fig. ??. Note that the current flows from node $o$ to node $s$. Let $v_s$ denote the voltage from node $s$ to node $o$. If we let $V = \begin{bmatrix} v_1 \\ \vdots \\ v_n \end{bmatrix}$ and $I = \begin{bmatrix} i_1 \\ \vdots \\ i_n \end{bmatrix}$, then the matrix $Z$ represents the relation between $V$ and $I$ as

$$\begin{bmatrix} v_1 \\ \vdots \\ v_n \end{bmatrix} = Z \begin{bmatrix} i_1 \\ \vdots \\ i_n \end{bmatrix} \tag{7.4}$$

So,

$$Z_{ss} = \left. \frac{v_s}{i_s} \right|_{i_j=0, j \neq s} \tag{7.5}$$

$$Z_{st} = \left. \frac{v_s}{i_s} \right|_{i_j=0, j \neq t} \tag{7.6}$$

Note that $Z_{ij}$ is a complex number denoted by $(R_{ij} + jX_{ij})$.

It follows from (7.5) that $r_{s,o} = Z_{ss}$, for all $s$. It can be shown that for all $i$ and $j$

$$r_{ij} = Z_{ii} + Z_{jj} - 2Z_{ij}. \tag{7.7}$$

In power engineering literature, electrical distance $r_{st}$ is called Thevenin resistance/impedance between the nodes $s$ and $t$, denoted by $Z_{th,st}$. Thus,

$$Z_{th,st} = r_{st} = Z_{ss} + Z_{tt} - 2Z_{st}. \tag{7.8}$$

Also, in chemistry literature electrical distance is referred to as resistance distance. See [? ].

### *7.1.3 Generation Shift Factor*

Given a power network with two or more interconnected areas, in power market analysis, a simpler equivalent network is needed which preserves the flows across the lines (edges) connecting different areas. In this context, the concept of GSF [? ] was introduced and used in determining power network equivalents.

Given a network $N$ represented by graph $G$. Consider a line connecting two nodes $u$ and $v$. Suppose we inject a current of unit value at node $i$ i.e. connect a current source of unit value between node $i$ and the slack node $o$. Then the current that flows through the line $(u, v)$ is called the generation shift factor of $i$ with respect to $(u, v)$, denoted as $g_{uv,i}$. To find a formula for $g_{uv,i}$ consider (7.4). Then,

$$v_u = z_{u1}i_1 + z_{u2}i_2 + \ldots + z_{ui}i_i + \ldots + z_{uu}i_u, \tag{7.9}$$

$$v_v = z_{v1}i_1 + z_{v2}i_2 + \ldots + z_{vi}i_i + \ldots + z_{vv}i_v. \tag{7.10}$$

If $i_j = 0$ for all $j \neq i$ and $i_i = 1$, we get $v_u = z_{ui}$ and $v_v = z_{vi}$. Then the current flowing through line $(u, v)$ is given by

$$i_{uv} = \frac{z_{ui} - z_{vi}}{c_{uv}}, \tag{7.11}$$

where $c_{uv}$ is the admittance of line $(u, v)$. Thus the GSF of $i$ with respect to $(u, v)$ is

$$g_{uv,i} = \frac{z_{ui} - z_{vi}}{c_{uv}}. \tag{7.12}$$

## 7.2 Average Electrical Distance

Average Electrical Distance (AED) is defined as the electrical distance of a specific bus with respect to a transmission line or a tie-line connecting different operating zones. It can also be viewed as the relative electrical distance of a bus w.r.t. a line. The AED, $d_{uv,i}$, is defined as

$$d_{uv,i} = \left| \frac{Z_{th,ui} - Z_{th,vi}}{2} \right|, \tag{7.13}$$

where $Z_{th,ui}$ is the electrical distance between buses $u$ and $i$. See Fig **??**. Using (7.8), we get

$$d_{uv,i} = \left| \frac{(Z_{uu} - 2Z_{ui} + Z_{ii}) - (Z_{vv} - 2Z_{vi} + Z_{ii})}{2} \right|, \tag{7.14}$$

$$= \left| \frac{\bar{Z}_{uu} - \bar{Z}_{vv}}{2} - (\bar{Z}_{ui} - \bar{Z}_{vi}) \right|. \tag{7.15}$$

where $Z_{ui}$ is the corresponding $(u, i)$ element in the bus impedance matrix shown in (7.16).

$$Z = \begin{bmatrix} Z_{11} & \cdots & Z_{1i} & \cdots & Z_{1n} \\ \vdots & \ddots & \vdots & \ddots & \vdots \\ Z_{u1} & \cdots & Z_{ui} & \cdots & Z_{un} \\ \vdots & \ddots & \vdots & \ddots & \vdots \\ Z_{n1} & \cdots & Z_{ni} & \cdots & Z_{nn} \end{bmatrix}. \tag{7.16}$$

In (7.16), the diagonal elements of the impedance matrix represent the Thevenin impedance at each corresponding bus. For real-time analysis, it is required to execute calculations of electrical distance at short intervals which can be achieved through simplification of electrical distances. Since transmission lines usually have a high $X/R$ ratio (see Fig. **??**), the resistances of the lines can be neglected when compared to the high reactances of lines. Thus, the impedances in (7.14) can be simplified as shown in (7.17).

$$X_{th,ui} = \bar{X}_{uu} - 2\bar{X}_{ui} + \bar{X}_{ii}, \tag{7.17}$$

where elements in $\bar{X} = [\bar{X}_{ij}]$ represent the approximation of elements in $Z$ i.e. $Z_{ij} \approx \bar{X}_{ij}$. Then, AED defined in (7.13) can be rewritten as

$$d_{uv,i} = \left| \frac{X_{th,ui} - X_{th,vi}}{2} \right| = \left| \frac{\bar{X}_{uu} - \bar{X}_{vv}}{2} - (\bar{X}_{ui} - \bar{X}_{vi}) \right|. \tag{7.18}$$

In previous studies [? ? ], GSF-based bus clustering methods have been used to analyse the impact of injections from groups of buses on the power flows of different transmission lines. In these GSF-based methods, buses that have similar contributions to the power flows on lines of interest are grouped together based on GSFs. But GSF does not take into account the impact of injection on buses $u$ and $v$. As shown below, AED is indeed a measure that captures the impact of injection at $u$ and $v$. This important characteristic of AED can be explained by analysing the relationship between AED and GSF. GSFs can be calculated using elements of $\bar{X}$ as shown in (7.19).

$$g_{uv,i} = \frac{\bar{X}_{ui} - \bar{X}_{vi}}{x_{uv}}. \tag{7.19}$$

Similarly, the sum of GSFs of bus $u$ and bus $v$ with respect to tie-line $uv$ is given by

$$g_{uv,u} + g_{uv,v} = \left|\frac{\bar{X}_{uu} - \bar{X}_{vv}}{x_{uv}}\right|. \tag{7.20}$$

Comparing (7.18)-(7.20), we can see that $d_{uv,i}$ enhances $g_{uv,i}$ by adding an additional term capturing the impact of injection at buses, $u$ and $v$, on the power flow across the tie-line, $uv$.

In the rest of the chapter, we discuss our improved clustering method based on AED and compare the results with the existing GSF-based clustering method.

### *7.2.1 Calculation of AED*

Algorithm given below to determine AED for each bus in the network with respect to the tie-lines of interest includes the following main steps:

*Algorithm 1: Calculation of AED*

1 *Creation of bus impedance matrix.* According to the system data, bus admittance matrix is first developed. Then, bus impedance matrix, shown in (7.16), is created by calculating the inverse of bus admittance matrix.

2 *Calculation of Thevenin impedance.* Using the elements of bus impedance matrix obtained in Step 1, the thevenin impedance for each pair of buses are calculated according to (7.17).

3 *Calculation of AED.* After calculating the Thevenin impedances, AEDs between buses and tie-lines of interest are calculated using (7.18). The results of AEDs are used to create a matrix as shown in Fig. **??**. In this matrix, each row corresponds to a tie-line and each column corresponds to a bus in the system. Thus, an element in the matrix corresponds to AED from a bus to a tie-line in the system.

■

### *7.2.2 Implications and relevance for social network analysis*

In the graph representation of a social network, link weights are all unity. Different types of metrics/measures are defined to determine certain properties of links or nodes. For example, a measure called PageRank is used to rank the nodes in terms of their importance [**?** ]. As another example, the betweenness measure of a link is used to determine the importance of a link. A link $e$ is considered more important than another link $e'$, if the fraction of the total number of messages that flow through $e$ is greater than that for $e'$. In view of the connection between random walk and current flow in a resistance network [**?** ], this fraction is in fact equal to the current through the link when a unit current is injected at a node. Taking advantage of this connection in [**?** ], a measure similar to GSF is used to determine the betweenness measures of links. For a detailed discussion of many of these measures, see [**?** ].

The concept of role discovery in networks was first studied in sociology [**? ?** ]. In this context, roles considered are social roles. Thus role discovery has become an important topic in social network analysis. Recently role discovery has been studied in other settings such as online social networks, technological networks, biological networks, web graph etc.

In [? ], a comprehensive review of literature on role discovery in network has been given. This paper discusses the problem of identifying clusters in a network such that all nodes in each cluster are equivalent in some sense. Two types of equivalence are considered: graph-based equivalence and feature-based equivalence. Several challenges that arise in the application of role discovery in non-static network such as dynamic and streaming graphs are also discussed in [? ].

Our work in this paper is about clustering in a power network and its application in deriving a simplified approximate equivalent network that preserves flows along certain lines. The GSF and AED are measures that are defined for each node with respect to certain lines. If we set the line weights to unity, then these measures in the context of social networks capture the fraction of total messages that flow through a link when messages arrive (or injected) at a node. So the work presented in this paper is relevant to social network studies. For example, a problem of interest is to determine clusters such that the total flow carried by inter-cluster links is optimized. Once such clusters are identified, we can determine simplified approximate equivalent network as explained in Section 7.6 that can be used to predict the flows across the clusters. Further discussion of these ideas is given in Section ??.

## 7.3 $k$-means algorithm

$k$-means algorithm is one of the most popular clustering techniques in unsupervised learning tasks. Given a set of nodes or buses, this algorithm has been efficiently used to partition a network into $k$ clusters [? ]. This is based on the optimal placement of centroid for the respective cluster in a network [? ].

In this algorithm, initially the network is divided into $k$ clusters with each cluster defined by a reference bus (centroid). Remaining buses are then partitioned and assigned appropriately to the clusters based on the closeness of each bus to $k$ reference buses. Then cluster adjustments are made with the calculation of new centroids. These centroids act as new reference points for the next partitioning of all the buses. These adjustments naturally produce error whose minimum corresponds to “Voronoi configuration" [? ] which result in reference locations at the centroid of the clusters. The error measure or potential function is the sum of all the variances and is given as shown in (7.21).

$$\phi = min \sum_{j=1}^{k} \sum_{i=1}^{n_j} |x_{ij} - \mu_j|^2, \tag{7.21}$$

where $k$ is the total number of clusters; $n_j$ is the number of buses belonging to the $j^{th}$ cluster, $x_{ij}$ represents $i^{th}$ bus in the $j^{th}$ cluster, $\mu_j$ is the centroid in the $j^{th}$ cluster and the term $|x_{ij} - \mu_j|$ represents the distance between $x_{ij}$ and $\mu_j$.

The process becomes iterative in order for the clusters to reach a local minimum which is dependent on the initial selection of the reference buses. The $k$-means algorithm keeps on adjusting the centroids after each partition making it more dynamic to the changes. The $k$-means algorithm is explained in algorithm 2.

*Algorithm 2: k-means algorithm*

1 *Selecting initial cluster centroids.* Cluster formation is initialized by selecting $k$ centroids, i.e., $\mu_1, \mu_2, \cdots, \mu_k$ in the network. These centroids act as initial reference points for the buses to be assigned to an appropriate cluster.

2 *Grouping buses into clusters.* For the selected $k$ centroids, based on the Euclidean distance, a bus is assigned to a cluster which has its centroid closest to the bus.

3 *Recalculating centroid positions.* After all the buses are assigned to respective clusters, the new centroid of each cluster is recalculated as shown in (7.22).

$$\mu_j = \frac{1}{n_j} \sum_{i=1}^{n_j} x_{ij} \tag{7.22}$$

4 *Evaluating objective function in (7.21).* After all buses are grouped into the clusters in Step 2, the potential function in (7.21) is evaluated.

5 *Iterations of algorithm.* Steps 2-4 are repeated until the centroid of each cluster ceases to change its position with further iterations.

■

## 7.4 AED-based $k$-means bus clustering method

In this section, we discuss our AED-based improved clustering method that uses $k$-means algorithm for power system network equivalence. This method uses a simple iterative technique known as Lloyd's algorithm for finding a locally minimal solution [? ]. Further it utilizes AED as a measure of distance between the buses in the system. Integration of AED makes $k$-means algorithm more relevant to the power system network study. This is because AED gives a measure of distance of a bus with respect to a tie-line. This algorithm proves to be sufficiently accurate for the independent analysis done by various utilities on their networks.

### *7.4.1 AED-based $k$-means algorithm*

With reference to the power system network equivalence, it is preferred to incorporate a measure that can reflect the true distance from a power system network perspective. AED presented in Section 7.2 is one such measure. In the network while determining the clusters, we replace the actual distance term in the variance calculation with the AED measure. Specifically, in (7.21) we replace the location of the bus $x_{ij}$ with $d(x_{ij})$ which represents the AED of the $i^{th}$ bus in the $j^{th}$ cluster with respect to set of tie-lines and $d(\mu_j)$ represents the AED-based measure of the centroid in the $j^{th}$ cluster with respect to the tie-lines. If the number of tie-lines is greater than 1, $d(x_{ij})$ is replaced with the average of AEDs considered for the given set of tie-lines. The updated potential function is shown in (7.23).

$$\phi = min \sum_{j=1}^{k} \sum_{i=1}^{n_j} |d(x_{ij}) - d(\mu_j)|^2, \tag{7.23}$$

This improves the $k$-means algorithm when applied in power system setting as compared to general distance used in the classical algorithm.

## 7.5 AED-based $k$-means++ bus clustering method

In this section, we introduce AED-based improved $k$-means++ algorithm which can be used for clustering of large power system networks.

### *7.5.1 $k$-means++ algorithm*

Although the results showed improvements as compared to other methods used for clustering power system networks, the AED-based improved $k$-means clustering method may deliver inconsistent results for large power system networks comprising of a large data set. This is due to the fact that $k$-means algorithm uses random centroids for initialization and thus achieves different results for each simulation. To address this problem, a seeding technique was proposed in [? ] which selected the first centroid position at random and then initialized the remaining centroids by sampling probabilistically, proportional to the squared distance of the nearest centroid. This made an improvement in the $k$-means algorithm which helps to achieve a clustering which is $O(logk)$ competitive. This is achieved by considering a potential function that satisfies the following relation for any set of buses,

$$\mathbb{E}[\phi] \leq 8(\ln\ k + 2)\phi^*, \tag{7.24}$$

where $\phi^*$ is the potential function corresponding to the set of cluster centroids in the network. The resulting augmented $k$-means algorithm is called $k$-means++ algorithm. In our study, we modify our previous AED-based $k$-means algorithm by incorporating the seeding technique to obtain a much improved AED-based $k$-means++ algorithm for bus clustering.

We would like to point out that $k$-means++ algorithm, due to its initialization process, produces starting centroids uniformly distributed for different iterations as compared to $k$-means algorithm starting centroids. This is illustrated in [? ].

### 7.5.2 AED-based $k$-means++ algorithm

Different from commonly used $k$-means++ algorithm, the improved AED-based algorithm groups the buses in a power system into various clusters based on the closeness between buses and the centroid of each cluster in terms of AEDs. The objective of the improved AED-based $k$-means++ algorithm is also to minimize the same potential function, $\phi$, as shown in (7.23).

To achieve the objective described in (7.23) with the initial seeding as shown in (7.24), the improved AED-based algorithm, shown in algorithm 3, includes the following main steps:

*Algorithm 3: AED-based k-means++ algorithm*

1 *Cluster initialization:* Cluster formation is initialized by selecting one centroid $\mu_1$, chosen uniformly at random in the network. This centroid acts as initial reference point for the buses to be assigned to an appropriate cluster. Those buses that are closer to $\mu_1$ are later assigned to the same cluster.

2 *Determining cluster centroids.* Given the centroids, $\mu_1, \ldots, \mu_{j-1}$, a new centroid, $\mu_j$, is chosen and each bus, $i$, is selected with probability

$$\frac{D(i)^2}{\sum_{i=1}^{n} D(i)^2},$$

where $D(i) = \min|d(uv, i) - d(uv, \mu_r)|$, where $r = 1, \ldots, j-1$.

3 Step 2 is repeated until we get all the centroids.

4 *k-means algorithm.* Proceed as with the standard $k$-means algorithm (Algorithm 2) with AED used as distance measure as discussed in Section 7.4.

■

### *7.5.3 Silhouette value analysis*

An important problem in the application of $k$-means algorithm is to determine appropriate value of $k$. This problem has been extensively studied in mathematical statistics literature. See [? ? ]. The authors in [? ] identified certain best performing methods. In [? ], authors determined through extensive simulation studies that all the best performers do quite well in selecting the appropriate number of clusters to be selected. In our work we use silhouette value analysis proposed in [? ] which is also among the best performers.

Silhouette value analysis is a graphical partitioning technique [? ] allowing an appreciation of the relative quality of clusters. In our study, the silhouette value analysis is used to enhance the quality of clusters identified by the improved AED-based $k$-means++ clustering algorithm. The main steps of the silhouette value analysis that are incorporated into the improved AED-based $k$-means algorithm are explained below:

*Algorithm 4: Silhouette value analysis algorithm*

Consider that in a network with $k$ clusters, a bus $i \in \{1, 2, \cdots, n\}$ is assigned to a cluster $j \in \{1, 2, \cdots, k\}$. Let $n_j$ be the number of buses in cluster $j$ and $k$ is the arbitrarily selected number of clusters. Clusters neighbouring $j$ are represented by $m \in \{1, 2, \cdots, k-1\}$ such that $m \neq j$; these are all the clusters other than $j$.

1 *Evaluating closeness between buses in a cluster.* In this step, the average closeness between the buses in cluster $j$ is evaluated by calculating AED measure, $ac_{ij}$, with respect to the tie-lines in the network. This is shown in (7.25).

$$ac_{ij} = \frac{1}{n} \sum_{\substack{r=1 \\ r \neq i}}^{n_j} |d(uv, i) - d(uv, r)| \tag{7.25}$$

2 *Evaluating closeness between each bus and clusters.* In this step, the minimum of average closeness of a bus $i$ with respect to each cluster $m \neq j$ is evaluated which

is given by $eb_{im}$.

$$eb_{im} = \frac{1}{n_m} \sum_{r=1}^{n_m} |d(uv,i) - d(uv,r)|, \; m = 1, \ldots, k-1; \; m \neq j \tag{7.26}$$

where $n_m$ is the number of buses in cluster $m$.

3 *Calculating average silhouette coefficient of all the clusters.* The silhouette coefficient of a bus indicates whether its placement is in an appropriate cluster. Silhouette coefficient ($s_{im}$) of bus $i$ can be calculated as

$$s_{im} = \frac{eb_{im} - ac_{ij}}{\max(ac_{ij}, eb_{im})}, \; m = 1, \ldots, k-1; \; m \neq j \tag{7.27}$$

The average of silhouette coefficients, $s_{im}$, of buses is evaluated as $s_i$. The average silhouette coefficient, $s_i$, of all the buses in the whole network is evaluated to give a perspective of average closeness of all the buses to their neighbouring clusters. The coefficient is in a range $[-1, +1]$, where $+1$ indicates that buses are far away from their closest neighbouring clusters; while $-1$ indicates that the buses are closer to their neighbouring clusters.

4 *Selecting value of $k$ based on silhouette value analysis.* Steps 1, 2 and 3 are repeated for different values of $k$ and the one with average silhouette coefficient closest to $+1$ is selected.

■

### *7.5.4 Flowchart*

The proposed AED-based bus clustering method integrates the improved AED-based $k$-means++ algorithm and silhouette value analysis to group buses for network equivalence of large power system networks. The flowchart shown in Fig. **??** describes this bus clustering method.

## 7.6 Power network equivalencing based on AED-based $k$-means++ clustering method

### *7.6.1 Power network equivalents based on aggregation of buses in a cluster*

The given power system network is divided into various sub-networks governed by local utilities and connected by several tie-lines. Power system operators employ various approximation methods to quickly analyse the behaviour of power system. To replicate the scenario, we employ a similar methodology that divides a given sub-network into smaller areas. This allows us to identify the tie-lines connecting the smaller areas. Further our AED-based improved clustering method is then used to identify appropriate clusters within each smaller area from which we obtain equivalent network. The equivalent network includes each cluster represented by an equivalent bus with a combined generation and load for that cluster connected directly to it. This equivalent bus is connected to the other equivalent buses through the tie-lines. A sample aggregation is illustrated in Fig. **??**. In Fig. **??**(a), a part of the network is shown with two identified clusters connected through a tie-line. Each cluster can be approximated by considering a single aggregated bus without any change in relevant information. As a result, we obtain a simple approximated network with each aggregated bus representing its respective cluster. This is shown in Fig. **??**(b).

### *7.6.2 Case Studies using Tie-lines*

In this section, we first demonstrate in Section 7.6.2 the efficacy of the proposed AED-based improved $k$-means++ clustering method by comparing it with our previous clustering method [**?** ] (Section 7.4) on the IEEE 39-bus system. Then in Section 7.6.2, we use IEEE 300 bus system to show the superiority of the proposed method when compared to the widely used GSF-based clustering method [**? ? ? ?** ].

*39-bus system (Algorithm 3 and method of Section 7.4)*

The IEEE 39-bus system is a standard test system composed of 39 buses with 10 generators and 18 loads connected as shown in Fig. **??** [**? ?** ]. The net generation and load capacity is 5266.69 MW and 5222.80 MW, respectively. In our study, we consider the system to be divided into two areas interconnected with four tie-lines in order to analyse the impact of any injection change in generation/load zones on designated transmission line flows. In Fig. **??**, area 1 comprises of 24 buses while area 2 consists of 15 buses. Bus 31 is chosen as slack bus.

**Table 7.1:** Comparison of clusters identified by two different AED-based clustering methods

| **Tie-Line 25-26 & Tie-Line 17-18** | | | |
|---|---|---|---|
| **Clusters identified by AED-based *k*-means algorithm** (Section 7.4) | | **Clusters identified by proposed AED-based improved *k*-means++ algorithm** (Algorithm 3) | |
| Clusters | Buses | Clusters | Buses |
| SA 11 | 26,28,29,38 | SA 11 | 26,28,29,38 |
| SA 12 | 27 | SA 12 | 27 |
| SA 13 | 10,11,12,13,14,15,16,17, 19,20,32,33,34,35,36 | SA 13 | 10,11,12,13,14,15,16,17, 19,20,32,33,34,35,36 |
| SA 21 | 25,37 | SA 21 | 25,37 |
| SA 22 | 1,2,30,39 | SA 22 | 1,2,30 |
| SA 23 | 18 | SA 23 | 39 |
| SA 24 | 3,4,5,6,7,8,9,31 | SA 24 | 3,18 |
| | | SA 25 | 4,5,6,7,8,9,31 |

In our study, the two tie-line scenario is used to compare the proposed method with the method of Section 7.4. In this scenario, any two tie-lines out of four are utilized to connect the two areas in the system. Under this scenario, the clusters are identified using the two methods which are based on average AEDs of each bus with respect to the two tie-lines connected. The two clustering methods follow different algorithms and hence the clusters obtained using the two methods are different as can be observed in Table 7.1. This may affect the accuracy of tie-line flows in equivalent networks when compared to the tie-line flows in the original network. The comparison of accuracy of tie-line flows in the equivalent network is demonstrated using tie-line flow analysis.

Further, we also analyse the quality of clusters in the equivalent networks based on the similarity of buses in each cluster.

***Tie-line Flow Analysis*** **(Algorithm 3 and method of Section 7.4)** The tie-line flow analysis is based on the comparison of accuracy of net tie-line flows in the equivalent networks with those in the original network. The equivalent networks are created using Algorithm 3 and method of Section 7.4. Different cases with combinations of two tie-lines are studied. In this study, the tie-line flows in the original network are calculated using GSFs and those in the equivalent networks are calculated using average GSFs for each cluster.

Table 7.2 shows the comparison of net tie-line flows under different tie-line combination cases. It can be observed from Table 7.2 that the net tie-line flows in the equivalent networks created using the proposed method are more accurate than those in the equivalent networks created using our AED-based $k$-means clustering method of Section 7.4. For instance, in cases 1, 4, 5 and 6, the net flows in the tie-lines in equivalent network obtained using AED-based $k$-means++ method are more accurate as compared to the net flows in equivalent network obtained using AED-based $k$-means method. For cases 2 and 3, the net flows in the equivalent networks obtained using the two methods are almost similar. Next we present a study involving the quality of clusters which explains the tie-line flow analysis on the basis of cluster formations and similarity of buses in each cluster.

***Cluster Quality Analysis*** We analyse the quality of clusters identified using Algorithm 3 and method of Section 7.4. In this study, the cluster quality analysis is carried out in terms of the similarity of buses in clusters. The similarity is measured by the average of standard deviation of the AEDs in each of the clusters identified by the algorithm in [**?** ] and the $k$-means++ algorithm of this paper. The standard deviation of the buses in a cluster can be defined as

**Table 7.2:** Comparison of net tie-line power flows in the original network and AED-based equivalent networks for 39 bus system

| | | Original Network | AED-based Equivalent Networks | | | |
|---|---|---|---|---|---|---|
| | | | **AED-based $k$-means algorithm** (Section 7.4) | | **AED-based $k$-means++ algorithm** (Algorithm 3) | |
| Case No. | **Tie-Line Combination** | Flow (MW) | Flow (MW) | % deviation | Flow (MW) | % deviation |
| Case 1 | TL25-26/ TL17-18 | 41.30 | 41.50 | 0.48% | 41.34 | 0.10% |
| Case 2 | TL25-26/ TL4-14 | 35.78 | 35.81 | 0.09% | 35.75 | 0.09% |
| Case 3 | TL25-26/ TL6-11 | 41.50 | 40.50 | 2.40% | 40.49 | 2.43% |
| Case 4 | TL17-18/ TL4-14 | 10.67 | 19.73 | 84.90% | 18.85 | 76.66% |
| Case 5 | TL17-18/ TL6-11 | 23.58 | 40.52 | 71.82% | 32.76 | 38.93% |
| Case 6 | TL4-14/ TL6-11 | 32.81 | 32.67 | 0.43% | 32.77 | 0.12% |

$$\sigma_j = \sqrt{\frac{1}{n_j}\sum_{i=1}^{n_j}(d_{ij} - \mu_j)^2} \tag{7.28}$$

where $\sigma_j$ represents the standard deviation of AEDs in $j^{th}$ cluster; $d_{ij}$ indicates the AED of $i^{th}$ bus in $j^{th}$ cluster; $\mu_j$ indicates the mean of AEDs in $j^{th}$ cluster. In (7.28), a smaller value of standard deviation indicates that the AEDs of the buses tend to be closer to the mean of the cluster, i.e. the buses are closer to each other.

We analyse the cluster quality based on (7.28), the results of which are shown in Fig. ??. The figure compares the average of standard deviation of the clusters identified by the AED-based improved $k$-means++ clustering method with those identified with our previous method. In Fig. **??**, for each case of combinations of tie-lines, gray bars indicate the average of standard deviations of AEDs for the clusters obtained using AED-based improved $k$-means++ algorithm; black bars correspond to the average of standard deviations of AEDs for the clusters obtained using previous AED-based algorithm.

It can be observed from Fig. **??** that for each set of two tie-lines, the similarity of buses in clusters created using proposed AED-based $k$-means++ algorithm is clearly more as compared to the buses in clusters created using previous AED-based method. Based on similarity of buses in the clusters, the created equivalent network has net tie-line flows very similar to the original network which can be observed from Table 7.2. Thus, modifying the clustering method by replacing our method of Section 7.4 with the proposed AED-based improved $k$-means++ algorithm provides much accurate results for network clustering schemes.

***300-bus system***

The IEEE 300-bus system is a test system developed by the IEEE Test Systems Task Force in 1993 [**?** ]. It is composed of 300 buses with 69 generators and 195 loads connected through 409 transmission lines as shown in Fig. **??**. Similar to IEEE 39-bus system, in order to analyse the impact on designated transmission line flows, the system is divided into two major areas interconnected using four tie-lines. In Fig. **??**, area 1 comprises of 111 buses with total load of 11824.31 MW; area 2 consists of 189 buses and total load of 11701.54 MW. Bus 7049 is chosen as slack bus.

To demonstrate the efficacy of our Algorithm 3, we compare it with the widely used GSF-based clustering method. We use different two tie-line scenarios in the 300-bus system and the two methods, based on average AEDs and average GSFs respectively, are used to identify clusters to obtain equivalent networks using $k$-means++ algorithm. Further, to validate the use of $k$-means++ algorithm, we compare Algorithm 3 with the AED-based method of Section 7.4 that uses $k$-means algorithm. In this study, we use different two tie-line scenarios in the 300-bus system for clustering. These methods yield different clusters for the same network and in order to compare the two clustering methods, we analyse the accuracy of tie-line flows in the equivalent networks. We also analyse the quality of clusters in these equivalent networks in terms of similarity of buses in each cluster.

***Tie-line Flow Analysis* (Algorithm 3, method of Section 7.4 and GSF-based clustering method)** In this section, we compare the net tie-line flows in the equivalent networks with those in the original 300-bus network. In order to study the flows, we consider the cases in which different combinations of two tie-lines connect the areas in the network. The results are shown in Table 7.3 and Table 7.4 with different combinations of two tie-lines. The net tie-line flows in the equivalent networks in Table 7.3 are obtained using average GSFs for cluster identification. It can be observed that for each of the cases, the net tie-line flow in the equivalent network created using our proposed method is more accurate as compared to the tie-line flow in equivalent network created using the GSF-based method that uses $k$-means++ algorithm. Also, from Table 7.4, it can be observed that the tie-line flows in the AED-based equivalent network using $k$-means++ algorithm are better as compared to the equivalent network that uses $k$-means algorithm. Further, cluster quality analysis is done in order to compare the methods based on the similarity of buses in each of the cluster obtained in equivalent networks.

***Cluster Quality Analysis* (Algorithm 3 and GSF-based clustering method)** In this section, we analyse the quality of clusters identified using the proposed method (Algorithm 3) and GSF-based method in terms of similarity of buses. Here, the similarity of buses refers to the degree of change in AEDs or GSFs in a cluster with respect to a set of tie-lines. The similarity of buses in a cluster is decided using the standard deviation of buses given by (7.28). Based on (7.28), we obtain results as shown in Fig.

**Table 7.3:** Comparison of net tie-line power flows in the original network and those in GSF and AED-based equivalent networks obtained using Algorithm 3 for 300 bus system

| | | **Original Network** | **GSF-based equivalent network** | | **AED-based equivalent network** (Algorithm 3) | |
|---|---|---|---|---|---|---|
| **Case No.** | **Tie-Line Combination** | Flow (MW) | Flow (MW) | % deviation | Flow (MW) | % deviation |
| Case 1 | TL19-87/ TL8-14 | 448.09 | 375.31 | 16.24% | 392.85 | 12.33% |
| Case 2 | TL19-87/ TL4-16 | 1051.79 | 1019.24 | 3.09% | 1032.31 | 1.85% |
| Case 3 | TL19-87/ TL62-144 | 55.34 | 156.84 | 183.41% | 57.93 | 4.68% |
| Case 4 | TL8-14/ TL62-144 | 450.86 | 391.79 | 13.10% | 487.01 | 8.02% |
| Case 5 | TL4-16/ TL62-144 | 994.46 | 490.70 | 50.66% | 973.19 | 2.14% |

**??**. In this figure, for each combination of two tie-lines, grey bars indicate the average of standard deviations of AEDs for the clusters obtained using AED-based improved $k$-means++ algorithm; black bars correspond to the average of standard deviations of GSFs for the clusters obtained using widely used GSF-based clustering method.

It can be observed from Fig. **??** that for each set of two tie-lines, buses in clusters created based on AEDs are more similar than those in clusters created based on GSFs since the average of standard deviations of AEDs in clusters for each set of two tie-lines is smaller than the average of standard deviations of corresponding GSFs. Based on the similarity and closeness of buses in the clusters, the created equivalent network has net tie-line flows very similar to that of the original network. It can be observed from Table 7.3, that the net tie-line flows in the equivalent network of 300-bus system

**Table 7.4:** Comparison of net tie-line power flows in the original network and the AED-based equivalent networks obtained using the Algorithm 3 and method of Section 7.4

| | | **Original Network** | **AED-based Equivalent Networks** | | | |
|---|---|---|---|---|---|---|
| | | | **AED-based $k$-means algorithm** (Section 7.4) | | **AED-based $k$-means++ algorithm** (Algorithm 3) | |
| Case No. | **Tie-Line Combination** | Flow (MW) | Flow (MW) | % deviation | Flow (MW) | % deviation |
| Case 1 | TL19-87/ TL8-14 | 448.09 | 292.39 | 28.08% | 392.85 | 12.33% |
| Case 2 | TL19-87/ TL4-16 | 1051.79 | 978.73 | 6.95% | 1032.31 | 1.85% |
| Case 3 | TL19-87/ TL62-144 | 55.34 | 89.87 | 62.39% | 57.93 | 4.68% |
| Case 4 | TL8-14/ TL62-144 | 450.86 | 324.26 | 28.08% | 487.01 | 8.02% |
| Case 5 | TL4-16/ TL62-144 | 994.46 | 922.42 | 7.24% | 973.19 | 2.14% |

created by bus clustering method using AED-based improved $k$-means++ algorithm are more accurate than those in the equivalent network created by GSF-based bus clustering method. Similar results comparing AED-based $k$-means algorithm [? ] and the proposed $k$-means++ algorithm are shown in Table 7.4.

# CHAPTER 8

## Adavanced technique of power system restoration

A power system subjected to a power outage needs to be quickly restored to an optimal system operating configuration such that it can be re-synchronized to the grid. The complexity of the power system requires such restoration process to be subject to steady state and dynamic constraints of the network including those related to the generation, transmission and distribution, and load.

Though historically negligible and infrequent, power system outages across the US for the last 15 years are on the rise at an alarming rate [? ]. The outages are mainly caused from disruptions on the distribution system, both in terms of the duration and frequency of outages. While not very frequent, any damage to the transmission system can result in major power outages that can affect large numbers of customers and can cause major economic disruptions [? ].

Power system operators have to deal with the most important task of system restoration following a disruption. The formalism of such restoration process can be highly complex involving a large number of generation, transmission and distribution, and load constraints. Such complexities warrant the operators to employ off-line solution plans to re-synchronize the newly formed islands post disruption. Therefore in practice, power system restoration should be achieved optimally according to different objectives such as maximizing generation capacity and quickly re-energizing major transmission corridors in order to minimize the impact of blackout and recover the load. These considerations make the power system restoration a multi-objective and multi-stage non-linear integer programming problem [? ]. For such a problem, several approaches have been proposed, which can be categorized as: heuristics-based methods [? ? ? ? ] which require more time to solve this combinatorial optimization problem and may not be adequate for real-time operation; expert systems (ES) [? ? ? ? ] require specialized software which make the process time-consuming for the operators. Additionally, mathematical programming (MP) [? ], soft computing [? ] and combinations of above approaches [? ? ? ] are some approaches that may not be considered reliable in terms of solution accuracy at specific and crucial times.

### 8.1 NERC requirements for system restoration

Due to the concerns related to increasing frequency and severity of power outages in an interconnected power system network, North American Electric Reliability Corporation (NERC) elevated the standard of compliance for restoration by adopting revised Emergency Operations and Preparedness (EOP) reliability standards [? ? ]. The critical importance of having advanced analytics and techniques that can be applied to real-world restoration planning and real-time decision support has been recognized and is becoming more significant for the power community.

The revisions carried out by NERC are deemed important for reliability of the North American bulk power system. The NERC standards EOP-005-2 [? ] and EOP-006-2 [? ] proposed to have a definite procedure for Blackstart and required Generator Operators (GOP) to meet the requirements for the Transmission Operators (TOP). Thus, the operators must be able to identify the Blackstart capabilities so that generation utilization can be maximized and an optimal start-up sequence can be initiated. On the hind sight, most power system operators rely on off-line restoration plans that only deal with certain contingencies and outages. The power network planners and operators have found it challenging to address NERC's elevated standards regarding restoration at planning stage, let alone meet the demands in real time. This issue has become more serious as recent changes in generation mix have prompted operators to reassess Blackstart needs. Even though NERC has revised the standards to provide enhanced reliability, it still remains a long standing challenge to meet these standards for the power industry.

## 8.2 Efforts to meet NERC requirements

In order to overcome the challenge for power system operators to meet the NERC standard regarding restoration, several methods have been proposed to provide optimal solutions [? ? ]. Most of the proposed solutions are limited to a theoretical discussion with very few extending the findings and applying them to a practical real-time situation. Out of those, two major efforts in this area are carried out by Power System Engineering Research Center (PSERC) and Electric Power Research Institute (EPRI).

1 *PSERC's methodology:* PSERC's effort follows a practical approach with an adaptive strategy procedure for power system restoration [? ]. The procedure is governed by a strategy module which centrally controls four major operation modules: (1) Generation Capability Optimization; (2) Transmission Path Search; (3) Constraint Checking; (4) Distribution System Restoration. The restoration process with central strategy module is illustrated in Fig. 8.1.

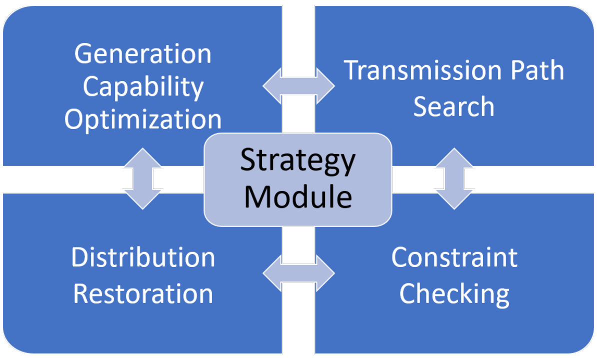


**Fig. 8.1:** Illustration of PSERC's restoration process

In this methodology, PSERC adopted a goal oriented restoration process involving a different problem formulation for each of the modules. The overall objective is to maximize the total number of transmission lines energized along with the feeders for all the time intervals and in addition allowing the increase of overall system generation capacity for start-up power requirements as shown below in (8.1).

$$\max \quad \sum_{t=1}^{N_T} \left[ \sum_{l=1}^{N_L} (\omega_l^t \cdot L_l^t) + \sum_{i=1}^{N_B} (\omega_i^t \cdot P_i^t) \right]. \tag{8.1}$$

$s.t.$ Critical Min. & Max. Time Intervals

Start-up Power Requirement

Flow capacity of transmission lines.

where $N_T$ is the total number of time intervals, $N_L$ is the total number of transmission lines, $N_B$ is the total number of buses and for the time interval $t$, transmission line $l$ and bus $i$, $\omega$ represents the respective weighting factors, $L$ is the status of lines and $P$ is the active power. The objective function in (8.1) is subject to physical constraints such as flow capacity of transmission lines, generation limits with other start-up power requirements. In addition, the model also considers the minimization of de-energized load for the start-up period.

2 *EPRI's methodology:* EPRI developed tools to provide decision support to system restoration planning citing that the system reliability is directly affected by the efficiency of system restoration [**?** **?** ]. On-line restoration process after a blackout requires the operators to adapt to actual outage scenarios and available resources. In order to cater to the on-line restoration process, EPRI developed two tools: (1) *System Restoration Navigation (SRN)*: This was intended to be used for offline planning at the initial stage and further on for dispatcher training and online decision support for power system restoration; and (2) *Optimal Blackstart Capability (OBC)*: This was designed to assist system restoration planners in evaluating system Blackstart capabilities and determining the optimal locations and amounts for additional Blackstart resources.

The methodologies proposed by PSERC and EPRI, although designed to address the elevated system restoration requirements, could not address the issue for large scale power systems and the changing dynamics of real-time operation. The methods are subject to the limitations of dynamic programming (DP) which have been highlighted and addressed upon in this study.

In this chapter the key ideas and associated algorithms are introduced that have made a significant breakthrough in development of system restoration technique. They have not only been used in improving the effort and time of planning but has also made the real-time application very possible. The proposed method is based on Approximate Dynamic Programming (ADP) which addresses the key limitations of DP and uses the structural analysis to reduce the solution space. This allows our method to create a feasible restoration plan of a large-scale power system along with completions of sophisticated simulation tests including steady state AC power flow analysis, frequency dynamic stability analysis and electromagnetic transients analysis in a significantly shorter duration of time when compared to other existing platforms. Currently, the work is being used to integrate the solver engine and automated techniques into a software package that are designed for off-line system restoration planning. Also based on this study, the work is to be extended further so that it can be used for real-time applications.

In this chapter, the challenges of application of DP in real world scenarios with NP-hard nature are highlighted in Section 8.3 and have been addressed with the introduction of ADP-based backward thinking. Section 8.4 proposes ADP-based technique with the simplification of solution space based on structural analysis that significantly reduces the complexity of the problem. Section 8.5 presents the integrated tool developed using ADP-based technique that uses a strategy to divide the problem into various subproblems in order to evaluate overall optimal solution to the original problem. In Section 8.6, the integrated tool is used to illustrate system restoration on IEEE 118-bus test system. The efficacy of restoration process is illustrated by comparing restoration plans with different sequences and priorities. Our restoration process is further validated by developing a restoration plan on the 2000-bus synthetic test system. In Section **??**, conclusions are drawn and the feedback of the integrated tool from the users/community is mentioned.

## 8.3 Approximate dynamic programming-based technique

The advanced system restoration technique has taken an unconventional approach which is based on dynamic programming (DP). The DP approach allows recursive optimization that includes backward induction process and provides a systemic way to address a multi-stage non-linear integer programming problem. However, DP still faces the challenge of the curse of dimensionality which can be addressed by using ADP approach.

### *8.3.1 What are the limitations of dynamic programming?*

The inherent nature of non-linear integer programming problems presents three curses of dimensionality which challenge the development of this technology. These three curses of dimensionality are: (1) size of *state space*; (2) the size of *action space* or *feasible region*; and (3) size of *outcome space*. These curses act as major limitations to any dynamic programming model since the number of variables and stages increases rapidly and with that the number of calculations required and hence the computational effort. It is due to these curses of dimensionality that PSERC and EPRI could only address small scale problems, possibly localized and could not address large scale real-time problems. Consequently, EPRI's tool has been used for training and restoration drills while PSERC's model works as a research grade solution. Moreover, both the tools only concern steady state stability.

### *8.3.2 Why is approximate dynamic programming needed?*

The limitations of DP due to the curses of dimensionality cause the model to fall short when dealing with real-time problems. In order to overcome such limitations, ADP-based modeling framework offers strategies for tackling the curses of dimensionality in large, multi-period, stochastic optimization problems.

As the algorithm steps forward in time, it may take many iterations before the costs incurred in later time periods are correctly transferred to the earlier time periods. To overcome this, the ADP algorithm can also be used with a double pass approach consisting of a forward pass and a backward pass. In the forward pass, decisions simulated moving forward in time, remembering the trajectory of states, decisions, and outcomes. Then it is followed by a backward pass strategy that determines a decision, given the available information at the current state, updating the value functions moving backwards in time using the trajectory information [? ].

For ADP, the principle of optimality is determining a sequence of optimal decisions or choices at each stage which is defined by a policy or decision function. This sequence of sub-problems is solved recursively as a natural form of Bellman equation as shown in (8.2).

$$V_t(S_t) = \max_{x \in \mathcal{X}} \Big[ C_t(S_t, x_t) + \mathbb{E}\{V_{t+1}(S_{t+1}|S_t, x_t)\} \Big], \tag{8.2}$$

where each possible state $S_t$ maps to a decision $x_t$ for each stage at time $t$ in the planning horizon. The state space $\mathcal{S}$ determines the evaluation of value function $V_t(S_t)$ for all states within a reasonable time along with the addition of decision space $\mathcal{X}$.

## 8.4 Proposed ADP with solution space reduction

Different from the perspectives provided by the existing theories of power system analysis and techniques of optimizations, our solution space reduction technology is developed based on graph theory and advanced complex network techniques. The technique is useful in identification of critical components in a weighted network, and it also highlights the relation between global performance of power grids and localized interactions, and successfully addresses the long-standing real-world power system problem. In addition to the complex networks techniques, we use additional information about the strength of the links to incorporate the electro-magnetic properties, transient behavior and laws of physics underlying the power grid.

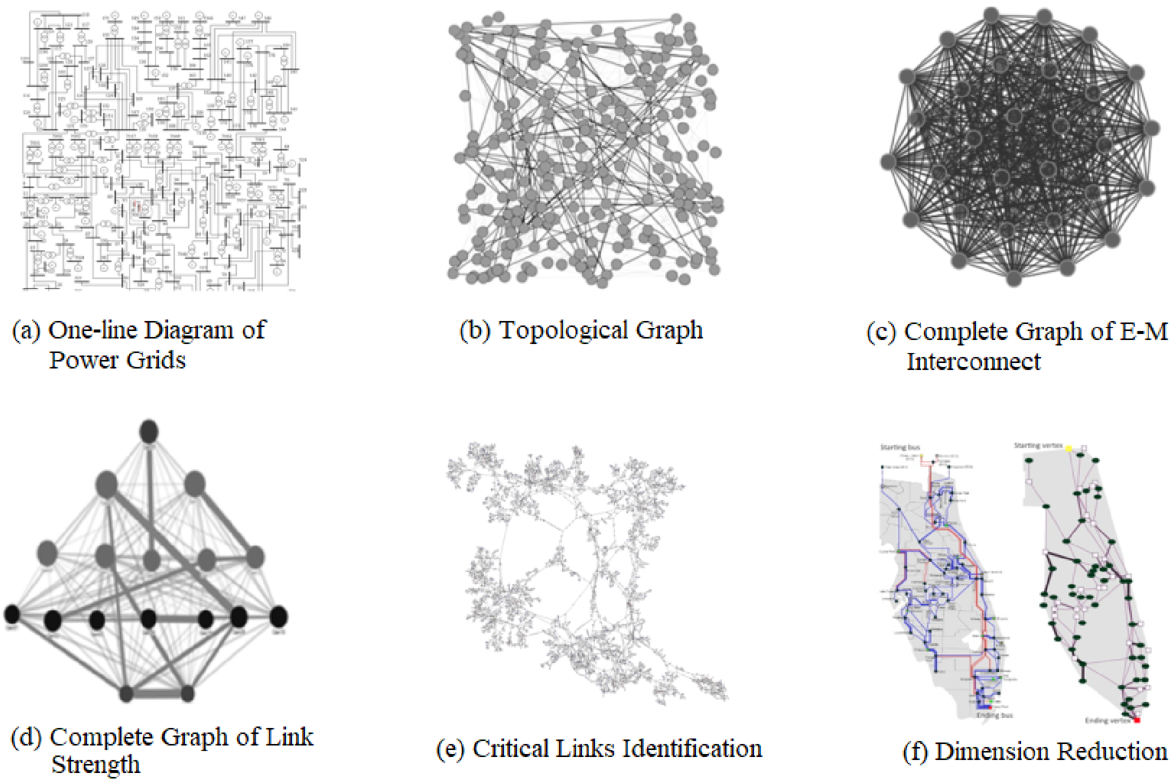

(a) One-line Diagram of Power Grids

(b) Topological Graph

(c) Complete Graph of E-M Interconnect

(d) Complete Graph of Link Strength

(e) Critical Links Identification

(f) Dimension Reduction

**Fig. 8.2:** Illustration of Solution Space Reduction

Our solution space reduction technology shown in Fig. 8.2 is based on four key algorithms:

1 *Topological representation:* Our first algorithm considers a power system network, shown in 8.2(a), and produces a corresponding topological graph representation to allow structural and criticality analyses. The graph representation of a power system network utilizes vertex-edge diagrams, where each bus is represented by a node and the connection between buses by an edge/link. This is illustrated in Fig. 8.2(b);

2 *Complete graph and link strength determination:* Oue second algorithm generates a complete graph representing electro-magnetic links between all the nodes, shown in Fig. 8.2(c), and estimates link strength or weights of the edges/links in the complete graph for a given problem, illustrated in Fig. 8.2(d). Due to the difference in link weights in finite identical complete graphs, there could be infinite number of graphs distinctively different from each other that may change the performance of power grids. Thus a simple representation of link strength can be used as the "link-weight" of edge;

3 *Structural analyses and criticality identification:* Our third algorithm uses criticality and structural analyses to find the winning probabilities of possible solutions and determine the categories of granularity as illustrated in Fig. 8.2(e), in which various critical components can be distinguished. The most significant part of the reduction process is the criticality identification based on the weighted graph. This involves algorithms primarily based on planarity test of the weighted structure to characterize the set of planar graphs; and planarization which involves removal of a certain number of vertices so that the graph becomes planar ensuring a minimal impact on the criticality of the graph. This is shown in Fig. 8.3;

4 *Reduced space solution:* The fourth algorithm solves the optimization problem in the reduced solutions space by either avoiding lower winning probability options or selecting high winning probability options based on link strength information. This results in a condensed solution space with critical components, as illustrated

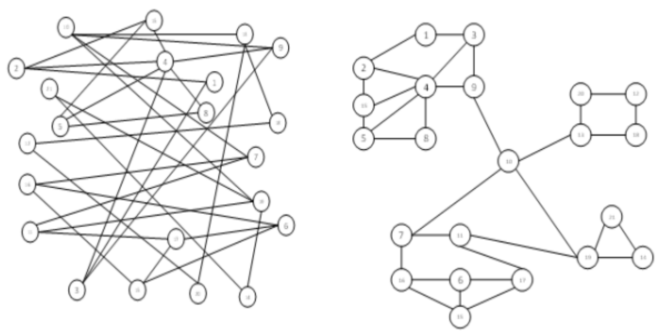

**Fig. 8.3:** Critical components identification

in Fig. 8.2(f).

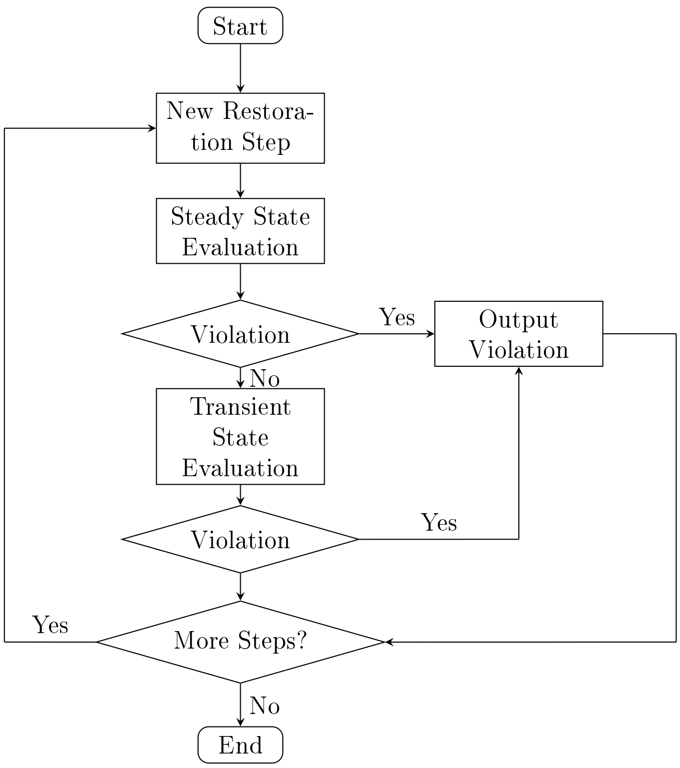


**Fig. 8.4:** Restoration process involving transient state evaluation.

### *8.4.1 Why is solution space reduction required?*

The advanced algorithm with reduced solution space can carry out all stability analyses to allow feasibility studies, as illustrated using a flowchart in Fig. 8.4 and it can be applied to most optimization problems with different objective functions. The aforementioned algorithms and structural analysis have been integrated to address the real-world restoration problems and incorporated into an analytical tool, named Brightstart®, that has been tested, validated and used at ISO New England, Southwest Power Pool and the associated transmission owners (TOs).

### 8.5 Integrated tool for system restoration

The development of the integrated tool with a number of integrated automated analytics allows it to be NERC compliant with standard power system models. This tool still follows the standard model of restoration and the optimization problem presented here is similar to the existing models involving automated modeling, path searching, simulation and feasibility studies. However it simplifies the analysis with the application of ADP based formulation with involvement of complex networks science and graph theory based solution space reduction technique. Further, the solution is based on an algorithm which uses an optimal strategy to obtain restoration path by dividing the problem into various sub-problems.

Further the model can be utilized for real-time scenarios due to its capability to carry out steady-state, transient and dynamic stability analyses as opposed to only steady-state analysis in the existing models. Such a model formulation of optimal decision in each backward induction step is similar to Bellman equation as shown in (8.3) below.

$$V(X_0) = \sup_{(U_t)_{t=0}^{N_T}} \left[ \sum_{t=0}^{N_T} \left( \sum_{j=1}^{N_G} G_j(U_j) + \sum_{i=1}^{N_D} D_i(U_i) + \sum_{k=1}^{N_L} L_k(U_k) - f_c(U_c) \right) \right], \tag{8.3}$$

where

$$U_t = \{u^t_{g,j}, u^t_{d,j}, u^t_{l,k}, P^t_{g,j}, V^j_{set}, P^t_i, Q^t_i, Q^t_{shunt,s}\},$$

$$U_j = \{X_t, u^t_{g,j}, t, \omega^g_j, P^{min}_{g,j}, P^{max}_{g,j}, T^{min}, T^{max}, j, P^t_{g,j}, R_j, V^j_{set}\},$$

$$U_i = \{X_t, u^t_{d,i}, t, \omega^d_i, P^{min}_i, P^{max}_i, P^t_i, Q^{min}_i, Q^{max}_i, Q^t_i\},$$

$$U_k = \{X_t, u^t_{l,k}, t, \omega^l_k\}, \ and \ U_c = \{N^t_{GS}, N^t_{DS}, N^t_{LS}, t\}.$$

where $P$, $Q$ represent the active and reactive power respectively, associated with the generators in the network, $R_j$ is the ramping rate of generator $j$, $u$ is the decision variable for various sub-problems and $\omega$ represents the weight associated with various elements in the system. The above objective function is subject to constraints similar to those of the PSERC model in (8.1).

In order to obtain a solution to the Bellman's type equation in (8.3), the following algorithm is used to select the most probable/optimal set of elements and state path at each stage of restoration:

*Step 1:* The problem in (8.3) is divided into a set of overlapping sub-problems;

*Step 2:* An optimal strategy, $\pi^* = \arg\max_\pi V^\pi(x_0)$, is constructed which is used to generate the choice at the current restoration stage, such that the solution space is reduced on the basis of the importance of the state sequence and an optimal path of restoration;

*Step 3:* This strategy, $\pi^*$, is used to find the sub-problem solutions at all stages for the overall optimal solution of the original problem described by (8.3).

Since the essence of ADP is to replace the true value function with the statistical approximation, based on the algorithm mentioned above, the problem function in (8.3) can be framed as an objective function for each sub-problem as shown in (8.4).

$$\begin{aligned} V(X_s) = & \sup_{(U_t)_{t=s}^{N_T}} \left[ \sum_{t=s}^{N_T} \left( \sum_{j=1}^{N_G} G_j(X_t, U_t) \right.\right. \\ & \left.\left. + \sum_{i=1}^{N_P} D_i(X_t, U_t) + \sum_{k=1}^{N_L} L_k(X_t, U_t) - f_c(U_t) \right) \right], \end{aligned} \tag{8.4}$$

where $X_s$ and $U_s$ represent the state at stage $s$ and the decision that optimizes the value of the subsequent stages, respectively. Equation (8.4) can be rewritten in Bellman equation form as shown in (8.5).

$$V(X_s) = \overset{sup}{U_s}\Big(T(X_s, U_s) + V(X_{s+1})\Big), \tag{8.5}$$

where $T(X_s, U_s)$ represents the elements of (8.4) for $t = s$. The dimensionality of the problem can be reduced if the important states of transition function, $S(X_t, U_t) = X_{t+1}$, to the global optimal value can be percepted and quantified by an associated weight $a_s^{ij}$. Hence the optimal decision can also be obtained based on the weights. Further with the assumption of a perception function based on weights, the Bellman equation in (8.5) can be approximated as

$$V(X_s) = \overset{sup}{U_s}\Big(F\{V(X_s)\} \cdot T(X_s, U_s) + V(X_{s+1})\Big), \tag{8.6}$$

where $F\{V(X_s)\} = a_s^{ij}$ is the assumed perception function with $i \in X_s, j \in X_{s+1}$.

The reduction in dimensionality as a result of approximation on the basis of assumed perception function makes the process of restoration explicit. This improves the quality of the restoration path without concerning associated voltage violations. The advantages of using solution space reduction based on approximation is illustrated in the next section using an IEEE 118-bus test system and further validated using 2000-bus synthetic test system.

## 8.6 Illustration of system restoration

This section demonstrates the restoration process using the integrated tool on IEEE 118-bus test system [? ] and a bigger 2000-bus synthetic test grid system [? ]. The capability of the tool is highlighted by specifying a Blackstart unit in these systems and carrying out feasible restoration plan. The feasibility of the restoration plan is validated based on steady-state analysis, transient analysis and frequency dynamics of the system.

### *8.6.1 IEEE 118-bus system*

We demonstrate the restoration process on IEEE 118-bus system illustrated in Fig. 8.5. In this system, there are 54 generator units and 99 load units with a peak demand of 4242 MW. For this study, the generator at bus 12 can be assumed to be the Blackstart unit and for demonstration of restoration process, the location of nuclear generator station is assumed to be located at bus 77.

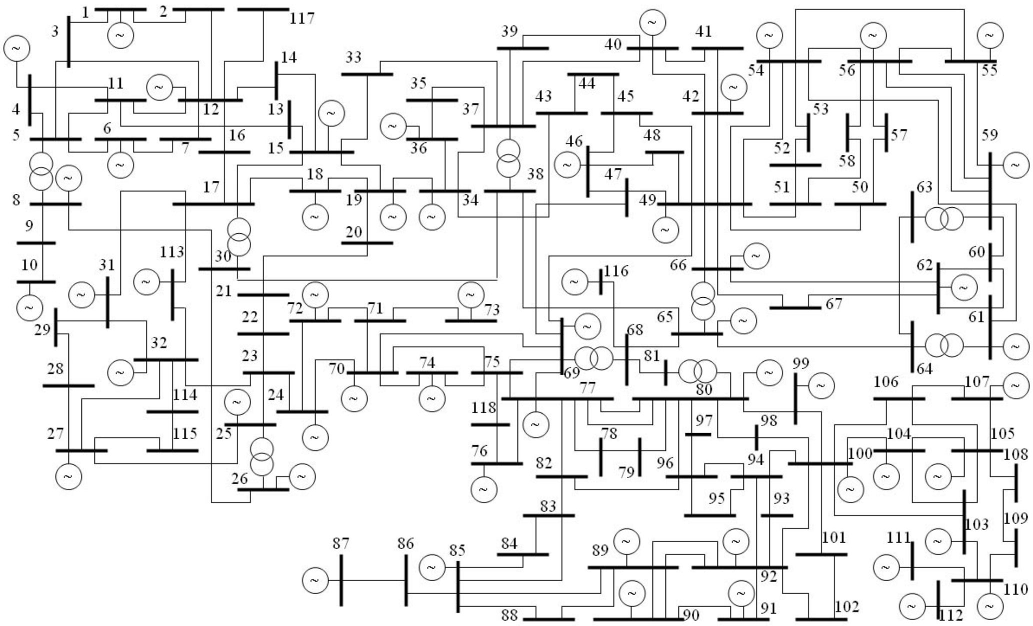


**Fig. 8.5:** IEEE 118 bus system

### *Generation restoration*

One of the critical requirements after a system blackout is the assurance of reliable shutdowns of nuclear generators. Therefore it is imperative to have a feasible restoration plan for expeditious restoration of off-site AC power sources to the nuclear station.

In this study, we simulate a restoration scenario using different restoration plans devised using our proposed tool. The tool is used to create a critical restoration path from the Blackstart unit at Bus 12 to the nuclear station assumed to be located at bus 77 in our test system. We test 3 different plans to restore the system: Restoration Plan I generally renders priority to the final outcome without focusing on the criticality of the path; Restoration Plan II is based on the simple distance rule; and Restoration Plan III uses an alternative restoration path based on our ADP algorithm with solution space reduction. Plan I and Plan II show steady-state and transient violations for different cases while Plan III avoids such steady-state and transient violations based on alternative restoration path as shown in Table 8.1.

**Table 8.1:** Restoration Plan III

| Sequence No. | Bus No. | Bus (From) | Bus (To) | Type | Bus (From) | Bus (To) | Output (MW) |
|---|---|---|---|---|---|---|---|
| 1 | 12 | Txxxxxxh | Txxxxxxh | Gen | | | 47 |
| 2 | 12 | Txxxxxxh | Sxxxxxxd | Branch | 12 | 11 | |
| 3 | 11 | Sxxxxxxd | Sxxxxxxd | Load | | | 70 |
| 4 | 11 | Sxxxxxxd | Oxxxe | Branch | 12 | 11 | |
| 5 | 12 | Txxxxxxh | NxE | Branch | 12 | 16 | |
| 6 | 16 | NxE | NxE | Load | | | 25 |
| 7 | 16 | NxE | Sxxxxxxn | Branch | 16 | 17 | |
| 8 | 17 | Sxxxxxxn | Sxxxxxxn | Load | | | 11 |
| 9 | 17 | Sxxxxxxn | Dxxxxxk | Branch | 17 | 31 | |
| 10 | 31 | Dxxxxxk | Dxxxxxk | Load | | | 21.5 |
| 11 | 31 | Dxxxxxk | Dxxxxxxe | Branch | 31 | 32 | |
| 12 | 32 | Dxxxxxxe | Dxxxxxxe | Load | | | 7.37 |
| 13 | 32 | Dxxxxxxe | Cxxxxxxr | Branch | 32 | 33 | |
| 14 | 23 | Cxxxxxxr | Cxxxxxxr | Load | | | 7 |
| 15 | 23 | Cxxxxxxr | Txxxxxn | Branch | 23 | 24 | |
| 16 | 24 | Txxxxxn | Txxxxxn | Load | | | 13 |
| 17 | 24 | Txxxxxn | Pxxxxxxh | Branch | 24 | 70 | |
| 18 | 70 | Pxxxxxxh | Pxxxxxxh | Load | | | 8.25 |
| 19 | 70 | Pxxxxxxh | Sxxxxxxt | Branch | 70 | 75 | |
| 20 | 75 | Sxxxxxxt | Sxxxxxxt | Load | | | 2.94 |
| 21 | 75 | Sxxxxxxt | Txxxxr | Branch | 75 | 77 | |
| 22 | 77 | Txxxxr | Txxxxr | Load | | | 3.81 |

### *Ideal restoration plan*

As discussed earlier, Restoration Plan I prioritizes restoration of off-site power sources to the nuclear power station without any specific rules, hence it may be seen as a pure vanilla case. The restoration path starts with energization of Blackstart unit at bus 12 and after 27 sequences, the off-site power sources to the nuclear power station at bus 77 is restored. This restoration plan shows no steady-state violations, however, when

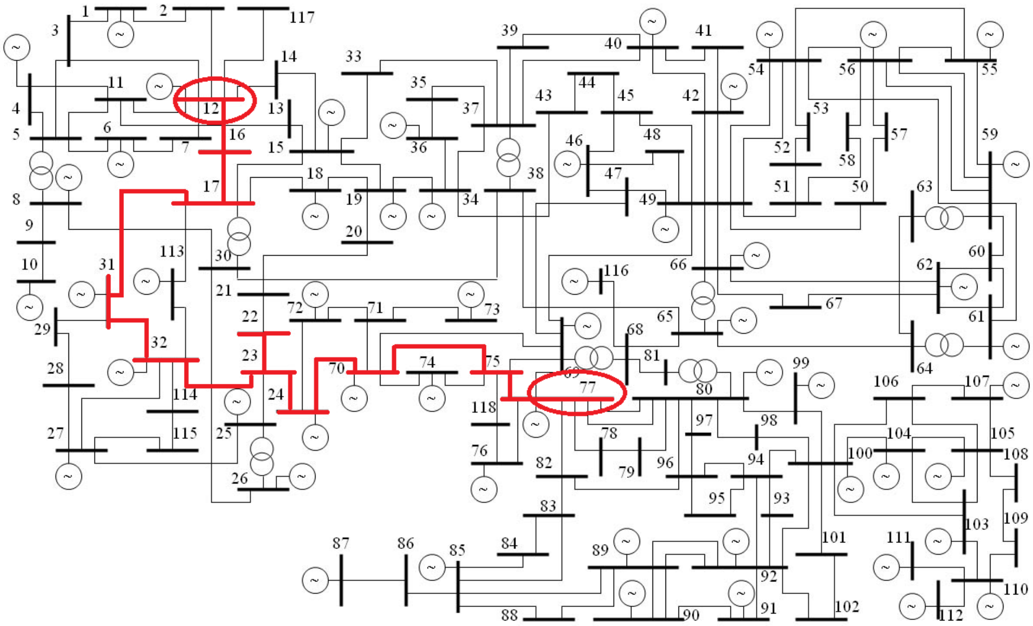


**Fig. 8.6:** Restoration Plan III on IEEE 118-bus system

subject to worst-case switching transients, it may show transient voltage violations at certain locations in the path. Restoration Plan II on the other hand follows most existing restoration plans in utilities which are manually created by operators based on the simple distance rule, which selects restoration paths using minimum distance. Although this rule may work in several simple cases, it does not guarantee feasibility for all complicated systems. For example, in our test case restoration plans created by simple distance rule generate a quick path with only 10 sequences but it also shows voltage violations which may cause instability issues. Hence, considering the real-time dynamics of a power system Plan I and Plan II may not be feasible.

**Table 8.2:** Comparison of Restoration Plans

| Restoration Plans | Blackstart Unit | Restored Bus | No. of Sequences | Steady-state Violations | Transient Violations |
|---|---|---|---|---|---|
| Restoration Plan I | 12 | 77 | 27 | No | Yes |
| Restoration Plan II | 12 | 77 | 10 | Yes | - |
| Restoration Plan III | 12 | 77 | 22 | No | No |

Our tool is then used to create an alternative Restoration Plan III which utilizes the ADP algorithm with backward induction along with solution space reduction. This plan reduces the dimensionality of the problem and using the perception function, it can reach an optimal decision by avoiding use of any risky branches in the restoration path that can cause transient over-voltage violations. This plan, shown in Fig. 8.6, takes 22 sequences to successfully restore bus 77 in our test system. This makes Restoration Plan III more robust and ideal for real-time scenarios. The comparison of the three plans based on voltage violations is illustrated in Table 8.2.

### *8.6.2 2000-bus synthetic test system*

We further check the validity of our integrated tool and demonstrate the restoration process on a bigger and more complex 2000-bus synthetic test grid system which is overlayed on the geographic footprint of the state of Texas, USA served by Electrical Reliability Council of Texas (ERCOT) [**?** ]. The system on the Texas map is shown in Fig. 8.7. In this system eight major geographic areas are identified which comprise of a total 1500 substations. The system is considered to operate at two nominal voltages, 345 kV and 115 kV.

#### *Generation restoration*

In the system, we consider generator at Bus 5262 located in Zone 1 as the Blackstart unit and assume a nuclear generator station in Zone 1 at Bus 6216. We devise a restoration plan for the nuclear generator station using Restoration Plan III which is based on our ADP algorithm with solution space reduction. The Restoration Plan III does not show any steady-state and transient violations and thus shown to be better than Restoration Plan I and Restoration Plan II in Section 8.6.1 and illustrated in Table 8.2.

The restoration plan for the nuclear generator starting from the Blackstart unit at Bus 5262 utilizes 369 sequences to reach the target generator at Bus 6216. The restoration

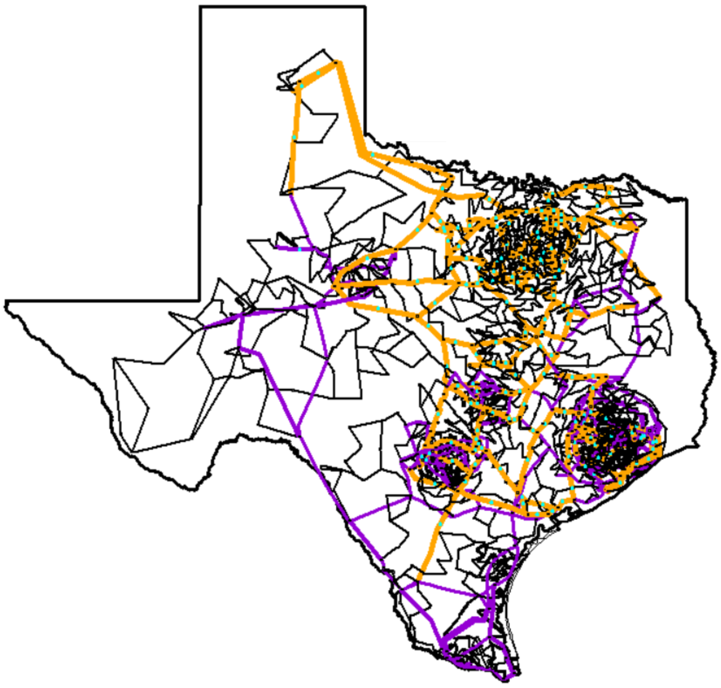

**Fig. 8.7:** 2000-bus synthetic grid test case [**?** ]

plan model based on solution space reduction takes approximately 4 minutes to simulate and is illustrated in Table 8.3.

**Table 8.3:** Restoration plan for 2000-bus synthetic test system

| Sequence No. | Bus No. | Bus (From) | Bus (To) | Type | Bus (From) | Bus (To) | Output (MW) |
|---|---|---|---|---|---|---|---|
| 1 | 5262 | Gxxxxe3 | Gxxxxe3 | Gen | | | 390.249 |
| 2 | 5263 | Gxxxxe4 | Gxxxxe1 | Transf | 5263 | 5260 | |
| 3 | 5317 | Gxxxx10 | Gxxxx20 | Branch | 5317 | 5401 | |
| 4 | 5401 | Gxxxx20 | Gxxxx21 | Transf | 5401 | 5402 | |
| 5 | 5402 | Gxxxx21 | Gxxxx21 | Load | | | 65.97 |
| 6 | 5405 | Sxxxxxxl1 | Bxxxxxd0 | Branch | 5045 | 5120 | |
| 7 | 5120 | Bxxxxxd0 | Bxxxxxd1 | Transf | 5120 | 5121 | |
| 8 | 5121 | Bxxxxxd1 | Bxxxxxd1 | Load | | | 76.66 |
| 9 | 5317 | Gxxxy1 | Wx20 | Branch | 5317 | 5388 | |
| 10 | 5388 | Wx20 | Wx21 | Transf | 5388 | 5389 | |
| 11 | 5389 | Wx21 | Wx21 | Load | | | 87.46 |
| ⋮ | | | | | | | |
| 361 | 6214 | Mxxx8 | Mxxx8 | Gen | | | 14.89 |
| 362 | 6215 | Mxxx9 | Mxxx4 | Transf | 6215 | 6210 | |
| 363 | 6210 | Mxxx4 | Mxxx5 | Transf | 6210 | 6211 | |
| 364 | 6211 | Mxxx5 | Mxxx6 | Transf | 6211 | 6212 | |
| 365 | 6212 | Mxxx6 | Hxxxx1 | Branch | 6212 | 6020 | |
| 366 | 6020 | Hxxxx1 | Hxxxx1 | Load | | | 16.53 |
| 366 | 6215 | Mxxx9 | Mxxx9 | Gen | | | 16.53 |
| 367 | 6216 | Mxxx10 | Mxxx4 | Transf | 6216 | 6210 | |
| 368 | 6212 | Mxxx6 | Kxxx0 | Branch | 6212 | 3014 | |
| 369 | 6216 | Mxxx10 | Mxxx10 | Gen | | | 22.002 |

# CHAPTER 9

## Conclusion and Future Research Directions

### 9.1 Conclusion

Self-healing will play a frontline role in managing the costs of deploying and maintaining mobile cellular networks of the future. However, the path towards satisfying the quality of experience requirements of these future networks is fraught with challenges. These challenges stem primarily from the technologies to be employed in these networks such as network densification, millimeter spectrum utilization and massive multiple input multiple output solutions among others.

The challenges which will result from these technologies include: 1) unpredictable noise variance in the network, 2) spatio-temporal variability of network data, 3) sparsity of data, and 4) increased probability of parametric miscofiguration. An in-depth review of the state-of-the-art solutions for self-healing shows that these solutions are not yet capable of adapting to these challenges. Therefore, self-healing solutions for future mobile cellular networks will be required to address these challenges in order for them to be effective. This dissertation attempts to address these challenges for future mobile cellular networks.

To address the challenge of detecting spatio-temporal outages in variable noise environment, this dissertation presents an entropy field decomposition based outage detection solution that is robust to noise distribution. The proposed solution is demonstrably better at detecting both coverage holes and outages compared to the state-of-the-art solutions.

The entropy field decomposition based outage detection solution relies on complete network coverage information. However, in the very likely event that only sparse network coverage information is available, this dissertation presents another solution that utilizes the hidden feature extraction capabilities of deep neural networks to detect network outages. This alternative solution performs much better than other state-of-the-art solutions in highly sparse network information environments even when noise distribution is variable.

Additionally, in order to address the challenge of proactively avoiding partial outages due to parametric misconfiguration, this dissertation presents a comprehensive framework for resolving conflicts between self-organizing network functions. The proposed framework combines heuristic, analytical and machine-learning based outage avoidance methodologies under one all-encompassing umbrella.

The proposed partial outage avoidance and SON coordination framework is leveraged to develop an analytical solution for conflict avoidance between coverage and capacity optimization and load balancing functions with results showing that such a solution can perform better than state-of-the-art solutions if the user requirements are known.

## 9.2 Future Research Direction

The future research directions opened up by this dissertation include the development of outage diagnosis and compensation solutions for millimeter wave ultra-dense heterogeneous networks that will form the backbone of future mobile cellular networks. Another potential area of research opened up by this study is the use of the proposed outage avoidance framework proposed in this dissertation to develop coordination solutions that will address the idiosyncrasies of millimeter wave cell communication networks including the limited directional coverage, low cell sojourn time per user and higher data rate requirements.

## List of Key Symbols

| | |
|---|---|
| $P_{r,u}^{c}$ | Received power by user $u$ from cell $c$ |
| $P_{r_{out}}^{t}h$ | Received power threshold for outage |
| $P_{r_{ch}}^{t}h$ | Received power threshold for coverage hole |
| $P_{t}^{c}$ | Transmit power of cell $c$ |
| $G_u$ | User equipment antenna gain |
| $G_u^c$ | Channel gain |
| $b$ | Pathloss constant |
| $\epsilon_u^c$ | Shadowing in dBm |
| $d_u^c$ | Distance of user $u$ from cell $c$ |
| $beta$ | Pathloss exponent |
| $\hat{\boldsymbol{P}}_{\boldsymbol{t}}$ | Subset of cell transmit powers |
| $\boldsymbol{P_t}$ | Set of cell transmit powers |
| $\boldsymbol{P_r}$ | Set of downlink received powers |
| $\boldsymbol{P_{r_{out}}}$ | Set of downlink received powers with outage |
| $\zeta_l$ | Combined spatio-temporal coordinate |
| $\mathcal{H}$ | Hamiltonian function of an interacting field |
| $\mathcal{Z}$ | Partition function |
| $\boldsymbol{\vartheta}$ | Field transformation of input signal |
| $\mathcal{D}$ | Information propagator |
| $\boldsymbol{j}$ | Information source |
| $\mathcal{H}_o$ | Hamiltonian function of non-interacting field |
| $V$ | Signal interaction terms |
| $\tilde{V}$ | Field interaction terms |
| $\boldsymbol{\sigma^2_{P_t}}$ | Transmit power covariance |

| | |
|---|---|
| $\boldsymbol{\mathcal{N}}$ | Noise covariance |
| $\boldsymbol{\mathcal{A}}$ | Adjacency matrix |
| $\boldsymbol{\mathcal{Q}}$ | Information field interaction matrix |
| $\boldsymbol{a_k}$ | Eigenmode amplitudes for information field reconstruction |
| $\boldsymbol{j_k}$ | Eigenmode amplitudes for information source |
| $\varphi$ | Eigenmode of information field |
| $\lambda$ | Eingenvector of information field |
| $\boldsymbol{P_{r_{norm}}}$ | Set of downlink received powers without outage |
| $\boldsymbol{P_{r_{RT}}}$ | Set of real-time downlink received powers |
| $\mathcal{O}$ | Computational complexity notation |
| $\boldsymbol{A}$ | Weight matrix for independent component analysis |
| $\mu_i^{(t)}$ | $i$-th mean at time $t$ for k-means clustering |
| $\boldsymbol{S_i^{(t)}}$ | $i$-th set of points at time $t$ for k-means clustering |
| $\hat{y}_j^{(l)}$ | Output of $j$-th neuron of layer $l$ |
| $\boldsymbol{w_j^{(l)}}$ | Weights of $j$-th neuron of layer $l$ |
| $\boldsymbol{x_j^{(l)}}$ | Inputs of $j$-th neuron of layer $l$ |
| $b_j^{(l)}$ | Bias of $j$-th neuron of layer $l$ |
| $E$ | Loss of deep neural network |
| $P_{r,u_{t-\Delta t}}^c$ | Received power by user $u$ from cell $c$ before an outage |
| $P_{r,u_t}^c$ | Received power by user $u$ from cell $c$ after an outage |
| $d_{u_{t-\Delta t}}^c$ | Distance of user $u$ from cell $c$ before an outage |
| $d_{u_t}^c$ | Distance of user $u$ from cell $c$ after an outage |
| $\mathcal{C}$ | Set of all cells in the network |
| $\hat{\mathcal{C}}$ | Set of outage affected cells in the network |
| $\mathcal{U}$ | Set of all users in the network |
| $\varrho$ | Functional margin of SVM algorithm |
| $\mathfrak{A}$ | Difference in the number of user between cell A and B |
| $\mathfrak{B}$ | Difference in the cell A $\Leftrightarrow$ cell B handovers |

| | |
|---|---|
| $\mathfrak{C}$ | Ratio of users switching between cell A and cell B due to handovers |
| $\mathfrak{a}$ | Load offset between cell A and Cell B |
| $\mathfrak{b}$ | Handover offset between cell A and Cell B |
| $\mathfrak{c}$ | Intercell distance between cell A and cell B handovers |
| $\eta_u^c$ | Physical resource blocks allocated to user $u$ at cell $c$ |
| $\omega_B$ | Bandwidth per physical resource block |
| $\hat{\tau}_u$ | Desired user throughput |
| $\mathbb{U}$ | Set of all active users |
| $\gamma_u^c$ | SINR of user $u$ at cell $c$ |
| $\hat{\mathbb{U}}$ | Set of all active satisfied users |
| $N_b^c$ | Total physical resource blocks at cell $c$ |
| $\kappa$ | Thermal noise |
| $\varpi$ | Network coverage threshold |
| $P_{th}^c$ | Downlink Rx power threshold |
| $\eta_{th}^c$ | Cell load threshold |
| $\alpha$ | User association exponent |
| $\mu$ | Antenna gain constant |
| $\Omega$ | Objective value for CLASS solutions |
| $\psi_u^c$ | Vertical angle between user $u$ and cell $c$ |
| $\psi_{tilt}^c$ | Antenna tilt of cell $c$ |
| $\phi_u^c$ | Horizontal angle between user $u$ and cell $c$ |
| $\psi_{azi}^c$ | Azimuth of cell $c$ |
| $P_{CIO_{dB}}$ | Cell individual offset of cell $c$ |

## Bibliography


[1] M. Kent *et al.*, "Dynamic modeling of loads in stability studies," *IEEE Trans on PAS*, vol. 88, pp. 756–763, 1969.

[2] F. Harary, "Graph theory," *Addison-Wesley, New York*, 1969.

[3] R. Graham and L. Lovasz, "Distance matrix polynomials of trees," *Advances in Math.*, vol. 28, pp. 60–88, 1978.

[4] J. Plesnik, "On the sum of all distances in a graph or digraph," *Journ. of Graph Theory*, pp. 1–21, 3 1984.

[5] Z. Mihalić, D. Veljan, D. Amić, S. Nikolić, D. Plavšić, and N. Trinajstić, "The distance matrix in chemistry," *Journal of Mathematical Chemistry*, vol. 11, no. 1, pp. 223–258, 12 1992.

[6] R. Merris, "Laplacian matrices of graphs: a survey," *J. Linear Algebra and its applications*, vol. 197, no. 1, pp. 143–176, 1 1994.

[7] R. Graham, A. Hoffman, and H. Hosoya, "On the distance matrix of a directed graph," *Journ. Graph Theory*, vol. 1, pp. 85–88, 1977.

[8] D. J. Klein and M. Randić, "Resistance distance," *Journal of Mathematical Chemistry*, pp. 81–95, 1993.

[9] B. Zhou and N. Trinajstić, "On resistance-distance and kirchhoff index," *Journal of Mathematical Chemistry*, vol. 283, no. 46, 6 2009.

[10] D. Babic, D. Klein, I. Lukovits, S. Nikolić, and N. Trinajs, "Resistance-distance matrix: A computational algorithm and its application," *Int. Journ. Quantum Chemistry*, vol. 90, no. 1, pp. 166–176, 12 2001.

[11] H. Zhang and Y. Yang, "Resistance distance and kirchhoff index in circulant graphs," *Int. Journ. Quantum Chemistry*, vol. 107, no. 2, pp. 330–339, 9 2006.

[12] J. Palacios, "Resistance distance in graphs and random walks," *Int. Journ. Quantum Chemistry*, vol. 81, no. 1, pp. 29–33, 11 2000.

[13] P. Hines and S. Blumsack, "A centrality measure for electrical networks," in *41st annual Hawaii Int. Conf. on System Sci.*, 2008.

[14] A. Barrat, M. Barthelemy, R. Satorras, and A. Vespignani, "The architecture of complex weighted networks," in *Nat. Academy of Sci. of USA*, vol. 101, no. 11, 3 2004, p. 3747–3752.

[15] S. Boccaletti, V. Latora, Y. Moreno, M. Chavez., and D. Hwang, "Complex networks: Structure and dynamics," *Phy. Report*, vol. 424, p. 175–308, 2 2006.

[16] M. Newman, "Analysis of weighted networks," *Phy. Rev. E*, vol. 70, no. 5, pp. 175–308, 11 2004.

[17] P. Hines, S. Blumsack, E. C. Sanchez, and C. Barrows, "The topological and electrical structure of power grids," in *43rd annual Hawaii Int. Conf. on System Sci.*, 2010.

[18] P. Lagonotte, J. Sabonnadiere, J. Leost, and J. Paul, "Structural analysis of the electrical system: Application to secondary voltage control in france," *IEEE Trans. Power Syst.*, vol. 4, 5 1989.

[19] P. Crucitti, V. Latora, and M. Marchiori, "A topological analysis of the italian electric power grid," *Physical Review E.*, vol. 338, no. 1, pp. 92–97, 7 2004.

[20] J. Undrill, J. Casazza, E. Gulachenski, and L. Kirchmayer, "Electromechanical equivalents for use in power system studies," *IEEE Trans. Power App. Syst.*, vol. 90, pp. 2060–2071, 1971.

[21] S. Lee and F. Schweppe, "Distance measures and coherency recognition for transient stability equivalents," *IEEE Trans. Power App. Syst.*, vol. 92, no. 5, pp. 1550–1557, 1973.

[22] R. Podmore, "Identification of coherent generators for dynamic equivalents," *IEEE Trans. Power App. Syst.*, vol. 97, no. 4, pp. 1344–1354, 1978.

[23] V. Sankaranarayanan, M. Venugopal, S. Elangovan, and R. Dharma, "Coherency

identification and equivalents for transient stability studies," *Elect. Power Sys. Res.*, vol. 6, pp. 51–60, 1983.

[24] W. Mittlestadt, "Proposed algorithms for approximate reduced dynamic equivalents," *BPA Internal Memorandum*, 1973.

[25] F. Wu and N. Narsimhamurthi, "Coherency identification for power system dynamic equivalents," *IEEE Trans. on Circuits and Syst.*, vol. 30, no. 30, pp. 140–147, 3 1983.

[26] M. A. Pai and R. P. Adgaonkar, "Electromechanical distance measure for decomposition of power systems," *Int. Journ. of Electric Power and Energy Systems*, no. 4, 1984.

[27] R. Belhomme and M. Pavella, "A composite electromechanical distance approach to transient stability," *IEEE Trans. on power systems*, 1991.

[28] R. Belhomme, M. Pavella, and Y. Xue, "Electromechanical distances for identifying contingency propagation in transient stability studies," in *IFAC Int. Symp. on power systems and power plant control*, 1989, pp. 940–945.

[29] R. Belhomme, H.Zhao, and M. Pavella, "Power system reductino techniques for direct transient stability methods," *IEEE Trans. on Power Systems*, pp. 723–729, 1993.

[30] D. Wang and X. Wang, "Study on electromechanical distance of electrical power system," in *Power and Energy Engineering Conference (APPEEC)*, 3 2010.

[31] H. Liu, A. Bose, and V. Venkatasubramanian, "A fast voltage security assessment method using adaptive bounding," 5 1999.

[32] E. Nobile and A. Bose, "A new scheme for voltage control in a competitive ancillary service market," 6 2002.

[33] J. Zhong, E. Nobile, A. Bose, and K. Bhattacharya, "Localized reactive power markets using the concept of voltage control areas," *IEEE Trans. on Power Systems*, no. 3, 2004.

[34] M. Javadi *et al.*, "A study of reactive power margins in power system following

severe generation imbalance," in *IEEE PES General Meeting*, 2015.

[35] A. Abed, "Wscc voltage stability criteria, under-voltage, load shedding strategy, and reactive power reserve monitoring methodology," 1999, p. 191.

[36] Z. Feng, W. Xu, C. Oakley, and S. Mcgoldrich, "Experiences on assessing alberta power system voltage stability with respect to the wscc reactive power criteria," 1999, p. 1297.

[37] T. Cutsem, "A method to compute reactive power margins with respect to voltage collapse," *IEEE Trans. on power systems*, no. 1, 1991.

[38] C. Parker, I. Morrison, and D. Sutanto, "Application of an optimization method for determining the reactive margin from voltage collapse in reactive power planning," *IEEE Trans. on power systems*, no. 13, p. 1473, 1998.

[39] K. Visakha *et al.*, "An approach for evaluation of transmission charges based on desired and deviations of power contracts in open access," in *6th Int. Conf. on APSCOM*, 2003.

[40] L. Willis, J. Finncy, and G. Raman, "Computing the cost of unbundled services," *IEEE Computer Applications in Power*, p. 16, 1996.

[41] D. Shirmohmmadi, C. Rajagopalan, E. Alward, and C. Thomas, "Cost of transmission transactions: An introduction," *IEEE Trans. on power systems*, no. 3, p. 1546, 1991.

[42] J. Bialek, "Topological generation and load distribution factors for supplement charge allocation in transmission open access," *IEEE Trans. on power systems*, no. 3, p. 1185, 1997.

[43] Y. Ni, P. Wei, and F. Wu, "Power transfer allocation for open access using graph theory, fundamentals and applications in systems without loop flow," *IEEE Trans. on power systems*, vol. 15, no. 3, 2000.

[44] M. Enns and J. Quada, "Sparsity-enhanced network reduction for fault studies," *IEEE Trans. on Power Syst.*, vol. 6, no. 2, pp. 613–621, 5 1991.

[45] X. Cheng and T. Overbye, "Ptdf-based power system equivalents," *IEEE Trans. on*

*Power Syst.*, vol. 20, no. 4, pp. 1868–1876, 7 2005.

[46] D. Shi and D. Tylavsky, "A novel bus-aggregation-based structure preserving power system equivalent," *IEEE Trans. on Power Syst.*, vol. 30, no. 4, pp. 1977–1986, 7 2015.

[47] H. Oh, "A new network reduction methodology for power system planning studies," *IEEE Trans. on Power Syst.*, vol. 25, no. 2, pp. 677–684, 5 2010.

[48] H. Dommel, "Digital computer solution of electromagnetic transients in single and multiphase networks," *IEEE Trans on PAS*, vol. 88, no. 4, pp. 388–399, 1969.

[49] A. Morched and V. Brandwajn, "Transmission network equivalents for electromagnetic transients studies," *IEEE Trans on PAS*, vol. 102, no. 9, pp. 2984–2994, 1983.

[50] H. Su, K. Chan, L. Snider, and T. Chung, "A parallel implementation of electromagnetic electromechanical hybrid simulation protocol," in *IEEE Int. Conf. DRPT*, 4 2004.

[51] Y. Zhang, W. Wu, B. Zhang, and A. Gole, "A decoupled interface method for electromagnetic and electromechanical simulation," in *IEEE Electrical Power and Energy Conf.*, 4 2011.

[52] W. W. B. Z. Y. Zhang, A.M. Gole and H. Sun, "Development and analysis of applicability of a hybrid transient simulation platform combining tsa and emt elements," *IEEE Trans on Power Syst.*, vol. 28, no. 1, pp. 357–366, 2013.

[53] P. Kundur, "Power system stability and control," McGraw-Hill, 1994.

[54] D. Povh, "Modeling of facts in power system studies," *IEEE Power Eng. Soc. Winter Meeting*, vol. 2, pp. 1435–1439, 2000.

[55] L. Gyugyi, "Power electronics in electric utilities: Static var compensators," *Proc. of IEEE*, vol. 76, no. 4, pp. 483–494, 1988.

[56] C. W. G. 31-01, "Modeling of static var systems (SVS) for system analysis," *Electra*, vol. 51, 1977.

[57] C. T. F. 38-01-02, *Static Var Compensator*, 1986.

[58] I. S. S. C. W. Group, "Static var compensator models for power flow and dynamic performance simulation," *IEEE Trans on Power Syst.*, vol. 9, no. 1, pp. 229–240, 1994.

[59] L. Gyugyi, "Fundamentals of thyristor-controlled static var compensators in electric power system applications," *IEEE Symp. on Application of Static Var Systems for System Dynamic Performance*, no. 87, 1987.

[60] Y. Ma, A. Huang, and X. Zhou, "A review of STATCOM on the electric power system," in *IEEE International Conference on Mechatronics and Automation (ICMA)*. IEEE, 2015.

[61] B. Singh, K. Al-Haddad, R. Saha, and A. Chandra, "Static synchronous compensators (STATCOM): A Review," *IET Power Electronics.*

[62] L. Gyugyi, "Unified power-flow control concept for flexible ac transmission systems," in *Proc. Inst. Electr. Eng. Part C: Gener., Transmiss. Distrib.*, vol. 139, no. 4, 1992, pp. 323–331.

[63] K. Sen and E. Stacey, "UPFC-unified power flow controller: theory, modeling and applications," *IEEE Transactions on Power Delivery*, vol. 13, no. 4, pp. 1453–1460, 1998.

[64] K. Padiyar, *HVDC Power Transmission Systems: Technology and System Interactions.* New York/Chichester, U.K.: Wiley, 1990.

[65] N. Flourentzou, V. Agelidis, and G. Demetriades, "VSC-based HVDC power transmission systems: An Overview," *IEEE Trans on Power Electronics*, vol. 24, no. 3, pp. 592–602, 2009.

[66] J. Undrill and A. Turner, "Construction of power system electromechanical equivalents by modal analysis," *IEEE Trans on PAS*, vol. 90, no. 5, 1971.

[67] R. Tewerson, *Sparse Matrices.* New York: Academic Press, 1973.

[68] A. Brameller, R. Allan, and Y. Hamam, *Sparsity: Its Practical Application to Systems Analysis.* London: Pitman Publishing, 1976.

[69] W. Tinney and J. Walker, "Direct solutions of sparse network equations by optimally ordered triangular factorization," *Transactions of the IEEE*, vol. 55, no. 11, pp. 1801–1809, 1967.

[70] P. Dimo, *L'analyse Nodale des Reseaux D'energie.* Paris: Eyrolles, 1971.

# Appendix A

The dowlink received power based on standard exponential pathloss model with Gaussian distributed shadowing for user $u$ associated with cell $c$ is:

$$P_{r,u}^{c} = P_{t}^{c} G_{u} G_{u}^{c} \epsilon_{u}^{c} a \left(d_{u}^{c}\right)^{-\beta}$$

Due to the randomness of $\epsilon_{u}^{c}$, the coverage constraint of user $u$ i.e. $C_{u} := P_{r,u}^{c} \geqslant P_{th}^{c}$ becomes a function of $\epsilon_{u}^{c}$ such that for user $u$, the coverage constraint will be satisfied with some probability i.e. $Pr(P_{r,u}^{c}(\epsilon_{u}^{c}) \geqslant P_{th}^{c})$. We can then calculate the minimum value of $\epsilon_{u}^{c}$ above which the coverage constraint for an individual user will be satisfied.

$$\begin{aligned} &Pr(P_{t}^{c} G_{u} G_{u}^{c} \epsilon_{u}^{c} a \left(d_{u}^{c}\right)^{-\beta} \geqslant P_{th}^{c}) \\ &Pr(\epsilon_{u}^{c} \geqslant \frac{P_{th}^{c}}{P_{t}^{c} G_{u} G_{u}^{c} a \left(d_{u}^{c}\right)^{-\beta}}) \end{aligned} \quad (9.1)$$

Based on the assumption that $\epsilon_{u}^{c}$ has a Gaussian distribution, the value of $\epsilon_{u}^{c}$ inside the parentheses in (9.1) gives the Z-score below which the coverage constraint of an individual user will be violated. If $p$ gives the probability $Pr(\epsilon_{u}^{c} \geqslant \frac{P_{th}^{c}}{P_{t}^{c} G_{u} G_{u}^{c} a (d_{u}^{c})^{-\beta}})$, we can remodel the event that a user is inside the coverage of its serving cell as a Bernoulli variable with probability $p$.

The consequence of modeling $Pr(P_{r,u}^{c} \geqslant P_{th}^{c})$ as a Bernoulli random variable is that the network coverage $C$ can be modeled as a Binomial random variable with chance of success $p$ per user. Thus the probability of having $\varpi * |\mathbb{U}|$ users or more in coverage can be given as:

$$Pr(k \geqslant \varpi * |\mathbb{U}|) \geqslant \sum_{i=\varpi*|\mathbb{U}|}^{|\mathbb{U}|} \binom{|\mathbb{U}|}{i} p^i (1-p)^{|\mathbb{U}|-i} \tag{9.2}$$

If the desired value for $Pr(k \geqslant \varpi * |\mathbb{U}|) \to 1$, and $\varpi \to 1$, then

$$\lim_{\substack{\varpi \longrightarrow 1 \\ Pr(k \geqslant \varpi * |\mathbb{U}|) \longrightarrow 1}} p = 1$$

In such a scenario, we can substitute the probability $p$ with the indicator function 1(.), thus giving us the following formulation for constraint (i):

$$\frac{1}{|\mathbb{C}|} \sum_{\mathbb{C}} \frac{1}{|\mathbb{U}_c|} \sum_{\mathbb{U}_c} 1 \left( P^c_{r,u} \geqslant P^c_{th} \right)$$

# Appendix B

The simplified form of the SINR function in antenna tilts is given as:

$$\gamma_u^c = \frac{10^{\mu\left(\left(\psi_u^c - \psi_{tilt}^c\right)^2 + x_u^c\right)}}{\kappa + 10^{\mu\left(\left(\psi_u^i - \psi_{tilt}^i\right)^2 + x_u^i\right)}}$$

The expression for antenna gains expressed as a function of tilts is given as:

$$G_u^c = 10^{\mu\left(\left(\psi_u^c - \psi_{tilt}^c\right)^2 + x_u^c\right)}$$

We treat $x_u^c$ and $\mu$ as constants and assign then unit value and -1.2 respectively which gives us the resulting function of $\psi_{tilt}^c$:

$$f(\psi_{tilt}^c) = 0.0631 * 10^{-1.2\left(\psi_u^c - \psi_{tilt}^c\right)^2}$$

Taking derivative of $f(\psi_{tilt}^c)$ gives us:

$$f'(\psi_{tilt}^c) = 0.0631 l_n(10) * 10^{-1.2\left(\psi_u^c - \psi_{tilt}^c\right)^2} * (2.4(\psi_u^c - \psi_{tilt}^c))$$

Taking the second derivative:

$$f''(\psi_{tilt}^c) = 0.3634 l_n(10) * 10^{-1.2\left(\psi_u^c - \psi_{tilt}^c\right)^2} [(\psi_u^c - \psi_{tilt}^c) l_n(10) - 0.417]$$

For a function to be convex, the second derivative has to be non-negative which is only possible in the range $[(\psi_u^c - \psi_{tilt}^c) \leqslant -0.4254, (\psi_u^c - \psi_{tilt}^c) \geqslant 0.4254]$. Hence, the antenna gain function is a non-convex function and by extension, the SINR expression with antenna gain is non-convex.